2

MACH REFLECTION, MACH DISC, AND THE ASSOCIATED NOZZLE FREE JET FLOWS

BY

I-SHIH CHANG

THESIS

Submitted in partial fulfillment of the requirements
for the degree of Doctor of Philosophy in Mechanical Engineering
in the Graduate College of the

Urbana, Illinois

157

MACH REFLECTION, MACH DISC, AND THE ASSOCIATED NOZZLE FREE JET FLOWS

BY

I-SHIH CHANG

Mech. Eng., Taiwan Provincial Taipei Institute of Technology, 1965
M.S., University of Kansas, 1969

THESIS

Submitted in partial fulfillment of the requirements
for the degree of Doctor of Philosophy in Mechanical Engineering
in the Graduate College of the
University of Illinois at Urbana-Champaign, 1973

Urbana, Illinois

MACH REFLECTION, MACH DISC, AND THE ASSOCIATED NOZZLE FREE JET FLOWS

I-Shih Chang, Ph.D.
Department of Mechanical and Industrial Engineering
University of Illinois at Urbana-Champaign, 1973

The numerical method involving both the method of integral relations and the method of characteristics has been applied to investigate the steady flow phenomena associated with the occurrence of Mach reflection and Mach disc from nozzle flows. The solutions of triple-shock intersection have been presented in detail. The regime where Mach configuration appears is defined for the inviscid analysis. The method of integral relations originally developed for the blunt body problem is modified and extended to the attached shock wave and to the internal nozzle flow problems. This method, together with the method of characteristics, is adopted to study Mach reflection from two-dimensional overexpanded nozzle flows whereas the axisymmetric underexpanded nozzle flows with Mach disc are studied by using the method of characteristics exclusively. The reflected shock configuration, as well as the accompanying flow field including the Mach stem height in two-dimensional cases and the Mach disc radius in axisymmetric jet flow, is established through the consideration that the central core flow downstream of the Mach configuration should reach a state which is equivalent to choking for a uniform one-dimensional flow. In the axisymmetric underexpanded nozzle study, it is found that the rotationality resulting from the entropy difference must be considered. The numerical results are compared with the experimental data of Love and Grigsby for the axisymmetric gas jet. An approximate method based on the idea of matching the interacting force between the streams has also been developed for quick estimation of Mach stem height in overexpanded nozzle flows. This simple analysis seems to yield reasonable results even outside of its applicable flow regime.

ACKNOWLEDGMENT

The author wishes to express his sincere gratitude to his thesis adviser, Dr. W. L. Chow, for his helpful suggestions and guidance throughout the course of this investigation and for his financial support under Research Grant NGL 14-005-140 from the National Aeronautics and Space Administration, Lewis Laboratory, Cleveland, Ohio, which not only made the completion of this thesis possible, but provided the author with the opportunity of pursuing the advanced study.

He is indebted to his colleague, Dr. L. D. Howlett, for supplying the information on the solution of nozzle flow by the method of integral relations. Special thanks are due Mrs. June Kempka for her assistance in preparing the final manuscript.

The author is obliged to his family in Taiwan for their trust, patience, and encouragement.

He would also like to acknowledge the healthful discussions with his colleagues and jogging mates during daily workouts in the gymnasium. Their friendship has made the stay at the University of Illinois at Urbana-Champaign a very pleasant period of his life.

NOMENCLATURE

a,b,c,d	coefficients defined in Eq. (39)
$A,B,C,D,$ E,F,G	functions, see APPENDIX A and Eqs. (24) and (25)
$A_1,B_1,C_1,$ D_1,E_1,F_1	functions, see APPENDIX B and Eqs. (35) and (36)
C_v	specific heat at constant volume
H_2,H_{3a},H_{4a}	distances defined in Fig. 33
I	incident shock
L	reference length (here maximum body height above the centerline of symmetry)
M	Mach number
M^*	Mach number based on speed of sound at critical condition
MS	Mach shock
n	dimensionless coordinate normal to the body surface measured from the surface
N	number of divisions on the starting characteristic line
P	dimensionless pressure
q	dimensionless magnitude of velocity
R	reflected shock, dimensionless radius of curvature of body surface
r	dimensionless radial coordinate in the axisymmetric method of characteristics
s	dimensionless coordinate along the body surface measured from the shock attached point; entropy per unit mass
SL	slipline
T	triple point
u,v	dimensionless velocity along horizontal and vertical direction in internal flow, see Fig. 13b
v_n,v_s	dimensionless velocity normal and parallel to the body surface

$\vec{V}$	velocity vector
V	dimensionless velocity
X,Y	dimensionless horizontal and vertical coordinate for flow inside a nozzle, see Fig. 13b
$\overline{X},\overline{Y}$	dimensionless horizontal and vertical coordinate for supersonic flow over an arbitrary body, see Figs. 12 and 13a
Y_e	dimensionless nozzle exit height above centerline of symmetry
Y_o	dimensionless Mach shock height above centerline of symmetry
z	parameter defined in Eq. (32)
∇	del vector operator
R	dimensionless shock radius of curvature
$(\tilde{})$	dimensional quantity

GREEK LETTERS

α	Mach angle
γ	ratio of specific heats ($\gamma = 1.4$ here for air)
δ	deflection angle
ε	dimensionless shock layer thickness measured normal to the body surface
θ	angle from axis of symmetry to surface tangent; flow angle in the method of characteristics
κ	angle from normal to centerline to shock tangent
λ	angle defined in Eq. (51)
ρ	dimensionless density
σ	shock wave angle
ϕ	$P/(\rho^{\gamma})$, see APPENDIX A
ω	Prandtl-Meyer function; Crocco number = q/q_{max}, see APPENDIX A

SUBSCRIPTS

o	stagnation state; starting place at triple point; condition on body surface in the method of integral relations
1,2,3,4	region 1, 2, 3, and 4, see Fig. 12; integration step
∞	freestream condition
a	ambient condition
c	centerline of symmetry
e	nozzle exit
f	free-jet boundary
i	incident wave; integration step index
ℓ	lower part of slipline
max	maximum state
Md	Mach disc
MS	Mach shock
n	normal to streamline coordinate
n3,n4	extreme cases of σ_3 = 90 degrees or σ_4 = 90 degrees at triple point
P-M	Prandtl-Meyer expansion
r	reflected wave; reference state
rℓ	limit of regular reflection
s	streamline direction
s_o	body surface
sk	imbedded shock wave
sℓ	sonic condition after shock
t	throat
u	upper side of slipline
w	wall condition
I,II	characteristics of family I or family II
ε	conditions just behind the shock wave

LIST OF FIGURES

		Page
Figure 1a	Pattern of Regular Reflection	62
Figure 1b	Pattern of Mach Reflection	62
Figure 2a	Regular Reflection produced from Two-Dimensional Overexpanded Nozzle Flow	62
Figure 2b	Mach Reflection produced from Two-Dimensional Overexpanded Nozzle Flow	62
Figure 3	Mach Disc produced from Axisymmetric Underexpanded Nozzle Flow	63
Figure 4	Triple Shocks Intersection of Mach Reflection from Nozzle Flows	64
Figure 4a	Limiting Case of Triple Shocks Intersection ($\sigma_4 = 90°$)	65
Figure 4b	Limiting Case of Triple Shocks Intersection ($\sigma_3 = 90°$)	65
Figure 5	Triple-Point Solutions, M_3 vs. δ_2	66
Figure 6	Triple-Point Solutions, M_4 vs. δ_2	67
Figure 7	Triple-Point Solutions, P_3/P_2 vs. δ_2	68
Figure 8	Triple-Point Solutions, P_4/P_1 vs. δ_2	69
Figure 9	Triple-Point Solutions, δ_3 vs. δ_2	70
Figure 10a	Regions of Regular and Mach Reflection, δ_2 vs. M_1	71
Figure 10b	Jet Deflection Angle δ_2 vs. Pressure Ratio P_2/P_{o1}	72
Figure 11	Oblique Reflection of Shock Wave from the Central Plug at a Nozzle Exit	73
Figure 12	Detailed Figure for Mach Reflection from Two-Dimensional Overexpanded Nozzle Flow	74
Figure 13a	Isolated Region for Upper Part of Slipline (External Flow)	75
Figure 13b	Isolated Region for Lower Part of Slipline (Internal Flow)	75

Page

Figure 14 Plot of Eq. (28) for Attached Shock Wave, $\left.\frac{d\varepsilon}{ds}\right|_{\varepsilon \to 0}$ vs. θ 76

Figure 15 Plot of Eq. (29) for Attached Shock Wave, $\left.\frac{d\kappa}{ds}\Big/\frac{d\theta}{ds}\right|_{\varepsilon \to 0}$ vs. θ. 77

Figure 16 Plot of Eq. (30) for Attached Shock Wave, $\left.\frac{1}{R}\Big/\frac{d\theta}{ds}\right|_{\varepsilon \to 0}$ vs. θ 78

Figure 17 Plot of Eq. (31) for Attached Shock Wave, $\left.\frac{dv_{so}}{ds}\Big/\omega_\infty \frac{d\theta}{ds}\right|_{\varepsilon \to 0}$ vs. θ. 79

Figure 18 Z vs. V_{so} from Eq. (32) 80

Figure 19 Roots of F/ε from Eq. (24) and the Equations given in APPENDIX A 81

Figure 19a Illustration of Applicability of the One-Strip Method of Integral Relations for Weak Attached Shock Wave . 82

Figure 19b Illustration of Inapplicability of the One-Strip Method of Integral Relations for Strong Attached Shock Wave 82

Figure 20 Detailed Figure for the Solution of Slipline Point for Eqs. (43) through (48) 83

Figure 21 Illustration of the Dependence of Sonic Condition in Region 4 on the P-M Fan Location 84

Figure 22 In-Scale Plot of Two-Dimensional Mach Reflection Pattern ($M_1 = 3.0$, $\delta_2 = 25°$) 85

Figure 23 In-Scale Plot of Two-Dimensional Mach Reflection Pattern ($M_1 = 3.0$, $\delta_2 = 30°$) 86

Figure 24 Velocity Distribution along Slipline for $\delta_2 = 25°$, and $\delta_2 = 30°$ at $M_1 = 3.0$ 87

Figure 25 Mach Stem Height Y_o/Y_e vs. δ_2 for Two-Dimensional Overexpanded Nozzle Flow 88

Page

Figure 26 Mach Stem Location $|x_e|/Y_e$ vs. δ_2 for Two-Dimensional Overexpanded Nozzle Flow 89

Figure 27 P-M Fan Position Y_{p-M}/Y_e vs. δ_2 for Two-Dimensional Overexpanded Nozzle Flow 90

Figure 28 P-M Fan Location $(x_{p-M} + |x_e|)/Y_e$ vs. δ_2 for Two-Dimensional Overexpanded Nozzle Flow 91

Figure 29 P-M Fan Range $\Delta\omega$ vs. δ_2 for Two-Dimensional Overexpanded Nozzle Flow 92

Figure 30 Central Core Throat Height Y_t/Y_e vs. δ_2 for Two-Dimensional Overexpanded Nozzle Flow 93

Figure 31 Central Core Throat Location $(x_t + |x_e|)/Y_e$ vs. δ_2 for Two-Dimensional Overexpanded Nozzle Flow 94

Figure 32 Speed on the Upper Side of Slipline at Throat M^*_{ut} vs. δ_2 for Two-Dimensional Overexpanded Nozzle Flow . . 95

Figure 33 Control Volume and Coordinates used in the Approximate Method for Estimating Mach Stem Height and Location. 96

Figure 34 Velocity Profiles in the Asymptotic Downstream Flow from the Approximate Method for Different Pressure Ratios at $M_1 = 1.92$ 97

Figure 35a Intersection of Two Compression Waves of the Same Family 98

Figure 35b Coalescence of the Compression Waves of the Same Family into Stronger Shock Waves 98

Figure 36 First Step along the Slipline for Axisymmetric Underexpanded Flow 99

Figure 37 Characteristic Net Layout behind the Reflected Shock Wave 99

Figure 38 Determination of the Flow Properties in Front of the Reflected Shock 100

Figure 39 Determination of Flow Properties and Coordinates at the Intersection Point of Reflected Shock and Free Jet Boundary 100

Page

Figure 40 Ambient-to-Nozzle Stagnation Pressure Ratio, P_a/P_{oe}, Free Jet Mach Number, M_f, and Initial Free Jet Inclination Angle at Nozzle Lip, θ_f, vs. Nozzle Exit-to-Ambient Pressure Ratio, P_e/P_a 101

Figure 41a Dependence of the Sonic State on the Location of Mach Disc without Entropy Gradient at $M_e = 2.0$, $P_e/P_a = 6.39$, N = 20 102

Figure 41b Comparison of Analysis with and without Vorticity at $M_e = 2.0$, $P_e/P_a = 6.39$, N = 20 103

Figure 42 In-Scale Characteristic Wave Pattern in Physical Scale at $M_e = 1.5$, $P_e/P_a = 5.0$, N = 30 104

Figure 43 Free Jet Boundaries and Shock Wave Patterns at Different Pressure Ratios for $M_e = 1.5$ 105

Figure 44 Free Jet Boundaries and Shock Wave Patterns at Different Pressure Ratios for $M_e = 2.5$ 106

Figure 45 Distributions of Various Flow Properties at $M_e = 2.0$, $P_e/P_a = 3.195$ 107

Figure 46 Distributions of Various Flow Properties at $M_e = 3.0$, $P_e/P_a = 5.0$ 108

Figure 47 Coordinates of the First Trace of Imbedded Shock Wave, X_{sk} and r_{sk}, vs. P_e/P_a 109

Figure 48 Coordinates of the Maximum Radius of the Imbedded Shock Wave, X_{sk} (at $r_{sk_{max}}$) and $r_{sk_{max}}$, P_e/P_a . . . 110

Figure 49 Coordinates of the Maximum Height of the Free Jet Boundary, x_f (at $r_{f_{max}}$) and $r_{f_{max}}$, vs. P_e/P_a 111

Figure 50 Location and Radius of Mach Disc, X_{md} and r_{md}, vs. P_e/P_a 112

Figure 51 Location and Radius of Throat, X_t and r_t, vs. P_e/P_a 113

Figure 52 Incident Flow Conditions, M_1 and θ_i, and Deflection Angle δ_2 at Triple Point vs. P_e/P_a 114

LIST OF TABLES

Page

Table 1 Triple-Point Solutions, $M_1 = 1.6$ 115

Table 2 Triple-Point Solutions, $M_1 = 1.8$ 116

Table 3 Triple-Point Solutions, $M_1 = 1.92$ 117

Table 4 Triple-Point Solutions, $M_1 = 2.0$ 118

Table 5 Triple-Point Solutions, $M_1 = 2.2$ 119

Table 6 Triple-Point Solutions, $M_1 = 2.4$ 120

Table 7 Triple-Point Solutions, $M_1 = 2.6$ 121

Table 8 Triple-Point Solutions, $M_1 = 2.8$ 122

Table 9 Triple-Point Solutions, $M_1 = 3.0$ 123

Table 10 Triple-Point Solutions, $M_1 = 3.2$ 124

Table 11 Triple-Point Solutions, $M_1 = 4.0$ 125

Table 12 Triple-Point Solutions, $M_1 = 5.0$ 126

Table 13 Triple-Point Solutions, $M_1 = 10.0$ 127

Table 14 Actual Results of Iteration from Approximate Method for Estimating Mach Stem Height, $M_1 = 1.92$, $P_{o1}/P_a = 3.67$ 128

Table 15 Actual Results of Iteration from Approximate Method for Estimating Mach Stem Height, $M_1 = 1.92$, $P_{o1}/P_a = 3.54$ 129

Table 16 The Effect of Changing the Number of Divisions on the Initial Characteristic Line on the Calculated Mach Disc Result 130

TABLE OF CONTENTS

Page

1. INTRODUCTION 1

2. LITERATURE REVIEW 6

3. TRIPLE POINT AND FLOW REGIME FOR MACH REFLECTION 12

4. FUNDAMENTAL EQUATIONS 18

5. MACH REFLECTION FROM OVEREXPANDED TWO-DIMENSIONAL NOZZLE FLOW. 19

5.1 BASIC DESCRIPTION OF THE FLOW FIELD 19
5.2 THE METHOD OF INTEGRAL RELATIONS 21
5.3 SUPERSONIC FLOW OVER TWO-DIMENSIONAL ARBITRARY BODY . . . 21
5.4 FLOW INSIDE A TWO-DIMENSIONAL NOZZLE BY THE METHOD OF INTEGRAL RELATIONS 28
5.5 THE METHOD OF CHARACTERISTICS 30
5.6 THE CALCULATION OF INTERACTING FLOW FIELD 31
5.7 RESULTS AND DISCUSSIONS 36
5.8 APPROXIMATE METHOD FOR ESTIMATING MACH STEM HEIGHT . . . 40

6. MACH DISC FROM UNDEREXPANDED AXISYMMETRIC NOZZLE FLOW 46

6.1 BASIC DESCRIPTION OF THE FLOW FIELD 46
6.2 THE METHOD OF CHARACTERISTICS 47
6.3 THE CALCULATION OF INTERACTING FLOW FIELD 50
6.4 RESULTS AND DISCUSSIONS 53

7. CONCLUDING REMARKS 60

FIGURES AND TABLES 61

REFERENCES 131

APPENDIX A FUNCTIONS FOR EQS. (24) AND (25) OF TWO-DIMENSIONAL EXTERNAL FLOW 134

APPENDIX B FUNCTIONS FOR EQS. (35) AND (36) OF TWO-DIMENSIONAL INTERNAL FLOW 136

APPENDIX C CHARACTERISTIC EQUATIONS FOR NUMERICAL CALCULATION OF A STEADY SUPERSONIC FLOW FIELD 137

VITA 144

1. INTRODUCTION

The study of supersonic flow necessarily involves the considerations of normal or oblique shock waves since almost any irregularities will produce one or more shock waves in high speed flow field. Although the appearance of these waves can be explained and taken into account in many of the flow situations, one of the unsatisfactory and yet unanswered areas involving their reflection and mutual interaction with the flow field is "Mach Reflection" or irregular reflection. This type of phenomenon was originally observed by E. Mach [1]* and later brought to public attention by von Neumann [2]. The role of shock wave interactions in the determination of the overall flow field can perhaps be best appreciated by quoting von Neumann's remark:

> "No situation involving two or more shocks can be fully understood without solving such problem, and a majority of the practically or theoretically significant situations involve several shocks."

When an oblique shock I is generated within a supersonic flow field, such as shown in Fig. 1a, it must be reflected from the lower wall, and the flow behind the incident shock must undergo a change of streamline angle δ after this reflection. If this angle δ is less than δ_{max} corresponding to the flow Mach number M_2, the reflection of the incident wave is regular--both the incident and the reflected waves I and R are straight and intersect with the solid wall. On the other hand, if δ is larger than the maximum allowable turning angle for the flow Mach number M_2, a completely different situation appears (see Fig. 1b). Somewhere along the incident wave a triple point T occurs. A reflected

---

*Numbers in brackets refer to entries in REFERENCES.

curved shock R and a strong curved Mach shock MS (Mach stem in two-dimensional problem) appear at this triple point. The flow behind the Mach shock is subsonic; the flow behind the shock wave R may be subsonic or supersonic. A slipline also emanates from this point indicating the discontinuity in entropy. This type of shock pattern is named Mach Reflection; its configuration also fully illustrates the complication of the flow field arising from the multiple interaction of curved shocks. It should be mentioned that the incident shock remains, nevertheless, to be straight for the case shown in Fig. 1b for uniform incident flow.

Mach reflection also occurs within the overexpanded and underexpanded two-dimensional nozzle flow field. As it is well known that for slightly overexpanded nozzle flow, an oblique shock which is generated from the corner of the nozzle will be regularly reflected from the centerline (Fig. 2a). If the nozzle is highly overexpanded, i.e. higher back pressure, the shock can no longer be regularly reflected and a Mach reflection pattern such as shown in Fig. 2b appears.

In both overexpanded and underexpanded axisymmetric nozzle flows the irregular reflection patterns occur as well and have appearances essentially similar to those of the two-dimensional counterparts. Referring to Fig. 3 (an underexpanded axisymmetric nozzle): If the back pressure is much lower than the jet pressure at the nozzle exit, the compression waves resulting from the reflection of expansion waves from free jet boundary coalesce into an incident shock wave inside the jet and the Mach disc eventually appears.

Mach reflection also takes place in many other flow situations such as the transient flow field within a shock tube, steady flow field

within diffusers and nozzles and the transient shock interaction resulting from simultaneous explosion of two charges. Close to a wall in boundary layer-shock wave interactions, Mach reflection has often been observed.

The Mach reflection study finds its application in many military systems. The flash appearing in the issuing gas jet at the muzzle of a gun or at the exit of a rocket motor is often attributed to the Mach reflection phenomenon. The investigation of recoilless and noiseless rifles is closely related to the jet structure and shock interaction problem in supersonic flow. Since Mach reflection would generally result in a higher pressure on the reflecting surface than regular reflection, the maximization of the damage effect in conjunction with Mach reflection was studied and utilized in the atomic bomb explosion at Nagasaki and at Hiroshima, Japan, during World War II [3]. Rocket motors, missiles, jet engines, and other propulsive devices flying at very high altitudes, for example, always have Mach configuration associated with them. The relaxation and radiation behind the Mach shock are so intense that they could be detected by a modern electronic device (e.g., an infrared detector [4]). The thorough study of the Mach reflection problem would, therefore, be helpful in the search and detection of these flying objects.

Problems in the design of rocket motors, jet engines or turbine blades cannot be fully understood without a knowledge of exhaust plume flow field of a gas jet which, in turn, relies on the study of Mach reflection in high speed flow.

Academically, the solution of Mach reflection problem is of high interest. It not only provides useful information concerning multiple

shock wave pattern, but it fills the gap existing in the theoretical nozzle analysis when the back pressure outside the nozzle is at off-design condition.

The present investigation is restricted to the inviscid study of Mach reflection and the associated flow field of steady two-dimensional overexpanded and axisymmetric underexpanded nozzle flows. The experience gained in the study of ejector flow problems at the University of Illinois at Urbana-Champaign [5] suggested that the problem at hand belongs to the category of inviscid interaction between multi-streams as long as the central core flow is distinct while the viscous effects (such as prevailing along the slipline or along the jet boundary) can at most contribute to a modifying influence to the flow pattern within this flow regime. It is thus believed that the shock configuration as well as the accompanying flow field (such as Mach stem height or Mach disc radius) can be established under the consideration that the central core flow behind the Mach shock should eventually assume a state which is equivalent to "choking" in the uniform one-dimensional flow. Also, previous studies of shock wave-viscous layer interaction [6] established the conviction that the shock structure can only be modified within the rarefied flow regime. Therefore, the Rankine-Hugoniot shock relation for air flow can be applied with confidence for the triple point in the study of Mach reflection.

It is pertinent to point out that, in most of the overexpanded flow situations under the present investigation, the back pressure is so high that the flow would separate from the nozzle wall. It would produce a Mach reflection pattern with non-uniform approaching flow conditions. It is believed that these modifications of the flow field, due to the

viscous interaction, can be examined only after the flow models for Mach reflection with uniform approaching flows and their methods of analysis are successfully developed and established. The present investigation is, therefore, restricted to the inviscid flow field only; even the possible influences of the viscous effects are well recognized.

2. LITERATURE REVIEW

Although Ernst Mach (1838-1916) did not bring forth theoretical solutions, his observation and discovery of experimental facts in compressible fluid flow and ballistic research have been the inspiration and foundation for many theoretical studies in gas dynamics. Among his various findings in physical science, the irregular reflection pattern of shock wave interaction was first observed by him in 1875 and was later named "Mach reflection" in honor of his excellent experimental contribution [1]. By igniting two electric spark gaps simultaneously to produce two intersecting blast waves in the physical laboratory at the University of Prague, Mach was able to visualize a trace of triple point of forked shockwaves (die gegabelte Verdichtungsstösze) on a flat plate covered with a thin sheet of soot. The intersecting wave phenomenon of the irregular reflection configuration in a supersonic air jet exhausting from a high pressure reservoir to low pressure surroundings was also discovered by Mach using the then already-known schlieren technique, and the first schlieren photograph of Mach configuration from nozzle flow was published in 1889.

It was much later (during World War II) when von Neumann brought this subject into general attention. The importance of study of production, equilibrium, and interaction of shock waves in the science of fluid dynamics was emphasized by von Neumann. In his expository paper [2] he elucidated the basic difference between regular reflection and Mach reflection and questioned the effect of viscosity and heat conduction as an essential part in the study of Mach configuration because of good agreements between the theoretical regular reflection analysis using

the conventional inviscid nonheat-conducting shock theory of Rankine-Hugoniot and the experimental results. Because of considerable discrepancy between theoretical analysis and experimental evidence in Mach reflection for weak incident shock, he surmised that there might be some other unknown discontinuities existing in nature other than the well known discontinuities such as shock wave, density discontinuity (slipline), and Prandtl-Meyer angular expansion and compression in the ideal fluid analysis.

The early studies of regular reflection and Mach reflection of shocks were carried out by Bleakney and Taub. They were mainly concerned with transient flow situations within the shock tube. Excellent agreement was obtained between the theoretical and experimental results for regular reflection of shocks [7]. On the other hand, Mach reflection has been observed for weak incident shock strengths and wave angles where the three-shock theory for the triple point predicts no non-trivial solution. However, experimental results did support the three-shock theory when the incident wave of Mach reflection is strong.

The Mach configuration is also viewed by Taub [8] as shocks with singularity at triple point where the tangent to shock is discontinuous. He proved rigorously that the locus behind the singular point on shock should be a slipline in inviscid analysis. He also gave the expressions for curvature of the shock and the derivative of pressure behind the shock at triple point singularity in terms of flow variables along the shock so that the geometric properties of the shock configuration near singular point for the pseudo-stationary flow could be determined.

Fletcher, et al., [9] reviewed the case of pseudo-stationary Mach reflection of a nearly glancing incident shock using linearized theory.

With their own interferometrical experimental results they showed the adequacy of the linearized theory in handling the pseudo-stationary Mach reflection of shock waves at nearly glancing incidence.

By using the method of power series expansion of the flow variables, Clutterham and Taub [10] gave the numerical results of flow variables near triple point in table form and used them to determine the trace of the triple point (called world line) and to construct approximately the Mach configuration in the neighborhood of the triple point for pseudo-stationary flow.

In response to the above mentioned discrepancy between inviscid triple shock theory and experiment for weak incident shock, Sternberg [11] took the effect of viscosity into consideration and introduced a non-Rankine-Hugoniot shock wave zone (incomplete shock wave) at the intersection of the three shock waves based on the reason that for weak incident shock the wave was thicker and that this finite shock zone was able to support some difference in pressure and flow angle. The conditions of equality of pressure and of flow angle across the slipline were then abandoned. With the aid of experimental results from a shock tube, he found that the height of this two-dimensional non-Rankine-Hugoniot shock zone for weak incident shock was several times greater than the thickness of Rankine-Hugoniot shock wave. Using the results found from Busemann electric tank analogy for two-dimensional subsonic flow in distorted hodograph plane, he discovered the reflected and Mach shocks were so strongly curved at the triple point that the shock wave angles between theory and experiment could not be compared accurately because the region involved was too small to be visible by the present experimental method. The introduction of non-Rankine-Hugoniot shock

wave zone necessarily seems to make theoretical analysis insurmountable for weak incident shock wave.

The supersonic gas jet has been studied by many researchers after World War II. The formation of shock wave in a two-dimensional supersonic gas jet was examined by Pack [12] using the method of characteristics. The origin and position of shock wave imbedded inside a free jet boundary for underexpanded nozzle flow were located based on the reason that the trace of shock was the result of intersection of compression waves of the same family. He observed that for two-dimensional gas jet, the regular reflection still existed at rather high pressure ratio where Mach reflection pattern already appeared in the axisymmetric jet. However, he did not go further to treat the irregular reflection problem. Some experimental investigations have been performed by Ladenburg, et al., [13], using interferometric study, for the axisymmetric gas jet from an orifice instead of a well designed nozzle.

By introducing a one-dimensional fictitious nozzle extension, Adamson and Nicholls [14] employed the pressure distribution on the centerline of the flow behind an axisymmetric orifice based on the method of characteristics to find the location of the first Mach shock. This Mach shock was assumed to exist at the end of this fictitious nozzle extension where the ambient pressure would be produced behind the normal shock. The analysis is very simple but it is not very helpful in the determination and understanding of the overall flow field. Eastman and Radtke [40], however, employed a different speculation that the location of the normal Mach shock wave coincided with the point of "minimum" pressure behind the imbedded shock wave.

The criterion of sonic condition at the throat in the interacting

flow field was used earlier by Chow and Addy [5] in the study of the mutual interactions between primary and secondary streams of a supersonic ejector system. A similar idea has been adopted by Ashratov [15] to find the Mach disc radius of a jet leaving an overexpanded axisymmetric nozzle flow. By using a one-dimensional approach for the entire core flow and applying the method of characteristics for the supersonic flow above the slipline, he was able to determine, iteratively, the Mach disc radius which agreed well with experimental data. The theoretical results were given for $M = 2.8$ and $M = 3.2$.

Love and Grigsby [16] made an extensive experimental investigation on the axisymmetric jets exhausting from sonic and supersonic nozzles into still air and into supersonic stream. Some theoretical considerations were also given in their report but were not complete as far as Mach configuration study was concerned. Their experimental data are to be compared here with the numerical solutions.

The method of integral relations plays an essential role in the approximate solution of fundamental hydrodynamics equations. Traugott [17] carried out a one-strip analysis of integral method of Belotserkovskii [18] for supersonic flow over arbitrary blunt axisymmetric bodies. The higher order approximation using the gradient method to evaluate the flow variables across the shock layer was also mentioned and was different from the higher approximation scheme used by Belotserkovskii. His one-strip analysis [17] is to be modified and applied in this study for solving supersonic flow over arbitrary two-dimensional body with attached shock wave.

South and Newman [19] used the method of integral relations to solve real gas flow problems. They found that this method was generally applicable to supersonic flow past a pointed body with weak attached shock

wave. The effect of the surface flow properties propagating normal to the boundary surface rather than propagating along characteristic curve was found to be self-compensated in the method of integral relations. They also gave the stability criterion for determining the step size of integration in hyperbolic domain.

The method of integral relations has also been adopted to solve the nozzle flow problem. Liddle and Archer [20] gave the equations for one- and two-strip analysis derived from continuity, energy, and irrotationality relations. Howlett [21] used the one-strip analysis originating from continuity, energy, and normal momentum equations to investigate nozzle flows. His analysis is utilized for solving two-dimensional central core flow for the present study.

3. TRIPLE POINT AND FLOW REGIME FOR MACH REFLECTION

The Mach configuration is characterized by the mutual interaction of several shock waves. This distinguished feature is manifested through the appearance of a triple point where shocks of different strengths intersect each other. The flow condition in the neighborhood of this triple point has the dominant effect on the downstream flow field because of the necessary existence of subsonic flow behind the Mach shock. The study of the equilibrium of flow variables near this triple point is, therefore, indispensable in the investigation of Mach reflection.

For nozzles operating under the condition where Mach configuration occurs, a triple point T accordingly appears (see Figs. 1b, 2b, 3, and 4). The shock MS belongs to strong shock family and becomes a normal shock on the centerline while the reflected shock R can be weak or strong and is also curved. The strengths of reflected shock and of Mach shock in the immediate vicinity of triple point T are determined locally by the fact that the pressure is continuous and the flow angles are the same across the slipline which results from the entropy differences in state 3 and state 4 for this inviscid analysis. Upon combining oblique shock relations [22], the flow regions 3 and 4 at point T for an arbitrary incident shock (arbitrary γ, M_1, and δ_2) can be solved from the following equations:

$$\frac{P_3}{P_2} = \frac{2\gamma}{\gamma + 1} M_2^2 \sin^2 \sigma_3 - \frac{\gamma - 1}{\gamma + 1} \tag{1}$$

$$\frac{P_4}{P_1} = \frac{2\gamma}{\gamma + 1} M_1^2 \sin^2 \sigma_4 - \frac{\gamma - 1}{\gamma + 1} \tag{2}$$

$$\tan \delta_3 = \frac{2}{\tan \sigma_3} \frac{M_2^2 \sin^2 \sigma_3 - 1}{M_2^2(\gamma + \cos 2\sigma_3) + 2} \tag{3}$$

$$\tan \delta_4 = \frac{2}{\tan \sigma_4} \frac{M_1^2 \sin^2 \sigma_4 - 1}{M_1^2(\gamma + \cos 2\sigma_4) + 2} \tag{4}$$

$$\delta_3 + \delta_4 = \delta_2 \tag{5}$$

$$P_3 = P_4 \tag{6}$$

The solutions are found from Newton-Raphson's method for simultaneous nonlinear algebraic equations by numerically evaluating partial derivatives [29]. These equations have trivial solutions corresponding to $M_2 = M_3 = M_4$, and three shocks merge into one shock which is of no interest and is discarded. The nontrivial solutions are plotted in Figs. 5, 6, 7, 8, and 9.

It is interesting to note that the state behind the reflected shock may be subsonic or supersonic near the triple point. The condition when sonic flow behind the reflected shock occurs can be determined, in addition to Eqs. (1) through (6), for any given M_1 and γ from the following equations:

$$\tan \delta_2 = \frac{2}{\tan \sigma_2} \frac{M_1^2 \sin^2 \sigma_2 - 1}{M_1^2(\gamma + \cos 2\sigma_2) + 2} \tag{7}$$

$$M_2^2 = \frac{(\gamma + 1)^2 M_1^4 \sin^2 \sigma_2 - 4\left(M_1^2 \sin^2 \sigma_2 - 1\right)\left(\gamma M_1^2 \sin^2 \sigma_2 + 1\right)}{\left[2\gamma M_1^2 \sin^2 \sigma_2 - (\gamma - 1)\right]\left[(\gamma - 1) M_1^2 \sin^2 \sigma_2 + 2\right]} \tag{8}$$

$$\sin^2 \sigma_3 = \frac{1}{4\gamma M_2^2}\left\{(\gamma + 1) M_2^2 - (3 - \gamma) + \sqrt{(\gamma + 1)\left[(\gamma + 1) M_2^4 - 2(3 - \gamma) M_2^2 + (\gamma + 9)\right]}\right\} \tag{9}$$

These solutions are also given in Figs. 5, 6, 7, 8, and 9 and are labeled $M_3 = 1$.

Two extreme cases are of interest: One is $\sin \sigma_4 = 1.0$, which implies that Mach shock is a normal shock at triple point; that is, $\delta_2 = \delta_3$, $\delta_4 = 0$ and is a pseudo-regular-type reflection as shown in Fig. 4a. The other case is $\sin \sigma_3 = 1.0$, which indicates that the shock between state 2 and state 3 is a normal shock (see Fig. 4b). This is the physical limit where a solution to the triple point exists under the condition of fixed M_1 and γ.

The solutions to these two extreme circumstances are easily found from solving Eqs. (1) through (8) with additional restriction of $\sin \sigma_4 = 1.0$, $\delta_4 = 0$, or $\sin \sigma_3 = 1.0$, $\delta_3 = 0$ for the specified value of γ and M_1 and are shown in Figs. 5, 6, 7, 8, and 9 identified with $\sigma_4 = 90$ degrees and $\sigma_3 = 90$ degrees, respectively. It should be noted that for $M_1 < 1.484\left(\sqrt{(\gamma + 3)/2}\right.$ as given in [42]) with $\gamma = 1.4$, no triple point solution is possible for this nozzle flow, and for $M_1 < 2.406$, M_3 will be subsonic regardless of the value of δ_2.

The numerical values of triple-point solutions together with their two extreme cases for various Mach numbers are tabulated in Table 1 through Table 13 where 1, 2, 3, and 4 refer to the different states at triple point as shown in Fig. 4, DELTA is the deflection angle in degrees, SIGMA is the wave angle in degrees, M is the Mach number, P2/P01 is the ratio of pressure at state 2 to the stagnation pressure at state 1, and (P4/P1)* is the ratio of the pressure at state 4, when expanding to sonic condition, to the pressure at state 1.

In order to study the flow field associated with Mach reflection,

it is also necessary to identify the regime where Mach reflection occurs. It is well known, according to [7], that for an incident shock wave striking a horizontal lower wall (see Fig. 1a), regular reflection would occur if the turning angle δ associated with the incident shock is less than some limiting value $\delta_{r\ell}$. The relations between flow Mach number M_1, $\delta_{r\ell}$, and wave angles are

$$\tan \delta_{r\ell} = \frac{2}{\tan \sigma_i} \frac{M_1^2 \sin^2 \sigma_i - 1}{M_1^2(\gamma + \cos 2\sigma_i) + 2} \tag{10}$$

$$\tan \delta_{r\ell} = \frac{2}{\tan \sigma_r} \frac{M_2^2 \sin^2 \sigma_r - 1}{M_2^2(\gamma + \cos 2\sigma_r) + 2} \tag{11}$$

$$M_2^2 = \frac{(\gamma + 1)^2 M_1^4 \sin^2 \sigma_i - 4\left(M_1^2 \sin^2 \sigma_i - 1\right)\left(\gamma M_1^2 \sin^2 \sigma_i + 1\right)}{\left[2\gamma M_1^2 \sin^2 \sigma_i - (\gamma - 1)\right]\left[(\gamma - 1) M_1^2 \sin^2 \sigma_i + 2\right]} \tag{12}$$

$$\sin^2 \sigma_r = \frac{1}{4\gamma M_2^2}\left\{(\gamma + 1) M_2^2 - 4 + \sqrt{(\gamma + 1)\left[(\gamma + 1) M_2^4 + 8(\gamma - 1) M_2^2 + 16\right]}\right\} \tag{13}$$

The solutions are given in Fig. 10a for $\gamma = 1.4$.

Since M_2 must be greater than one in order that there may be a reflected shock, the upper limit is thus tentatively established under the condition of the sonic state behind the incident shock and is marked as curve $\delta_{s\ell}$ in Fig. 10a.

If the two extreme results, δ_{n3} and δ_{n4}, from triple-point solution are also plotted in Fig. 10a, there is some overlapping area below curve $\delta_{r\ell}$ where both regular and Mach reflections are possible and some empty area between curve $\delta_{s\ell}$ and curve δ_{n3} where regular

reflection is impossible. The empty area between curve $\delta_{s\ell}$ and curve δ_{n3} above regular reflection limit, curve $\delta_{r\ell}$, is, perhaps, due to the limitation of the inviscid assumption. For this lower Mach number regime ($M_1 \simeq 1.0$), Sternberg [11] discarded the criterion of equality of pressure and of flow angle across the slipline and introduced a non-Rankine-Hugoniot shock at the triple point with the viscous effect considered. From an electric tank experiment, he was able to find the solution to the Mach reflection problem. Moreover, Mölder [23] proposed a smooth curving shock pattern for the case where neither regular nor Mach reflection is theoretically possible.

In the overlapping portion both two-shock and three-shock theories predict nontrivial solutions. Whether two-shock theory or three-shock theory should be used depends, at least, on the boundary conditions. As indicated in Fig. 11, if a plug with a particular shape shown were inserted at the exit of a two-dimensional nozzle giving a two-shock theory pattern, the removal of this very plug might arouse a Mach configuration from dormancy under the same ambient pressure. Hypothetically, this plug could be used to control the appearance of Mach configuration. For the problem shown in Fig. 1b, the experimental evidence of Mölder [23] shows that at $M_1 = 2.8$, the transition from regular to Mach reflection occurs at the limiting case of three-shock theory rather than that of two-shock theory and that the Mach shock is a normal shock during this transition. Therefore, the steady Mach reflection produced from nozzle flow of this study is confined to the domain between curve δ_{n3} and curve δ_{n4} in the present analysis.

The relation between jet deflection angle at nozzle exit δ_2 and

the ratio of ambient pressure-to-nozzle stagnation pressure P_2/P_{o1} is given in Fig. 10b for various Mach numbers. For convenience of reference, the region specified in Fig. 10a is also plotted here. At high Mach numbers the flow is relatively sensitive in the sense that a very small change in ambient pressure results in tremendous variation in the jet deflection angle δ_j at the nozzle exit.

4. FUNDAMENTAL EQUATIONS

For a steady inviscid gas flow, without shock discontinuity inside the region considered, the conservation equations in vector form are:

Continuity:

$$\nabla \cdot (\tilde{\rho}\vec{\tilde{V}}) = 0 \tag{14}$$

Momentum:

$$\tilde{\rho}(\vec{\tilde{V}} \cdot \nabla)\,\vec{\tilde{V}} = -\nabla\tilde{P} \tag{15}$$

Energy:

$$(\vec{\tilde{V}} \cdot \nabla)\left[\frac{\tilde{P}}{\tilde{\rho}^{\gamma}}\right] = 0 \tag{16}$$

where the equation of state for ideal gas has been tacitly used and $(\tilde{\ })$ indicates dimensional quantity.

The first two equations simply mean that mass and momentum are conserved. The last equation states the entropy is constant along the streamline under the above assumptions. Of course the entropy can change across the streamlines in the case of flow behind curved shock wave.

The vector form of the fundamental equations shown above give concise expression for the conservation principle without referring to any particular coordinate system. For different physical problems, the conservation equations have different forms for specific coordinate systems used which can be derived from the vector form through vector analysis and coordinate transformation.

The fluid considered in this study is assumed both thermally and calorically perfect with $\gamma = 1.4$.

5. MACH REFLECTION FROM OVEREXPANDED TWO-DIMENSIONAL NOZZLE FLOW

5.1 BASIC DESCRIPTION OF THE FLOW FIELD

As shown in Fig. 12 for the case of overexpanded two-dimensional nozzle flow with a triple point shock system imbedded in the flow field, regions 3 and 4 are separated by the slipline of a yet unknown configuration. It is obvious that the two streams have to coexist so that along their common boundary they shall have the same pressure and flow direction. Region 3 is usually supersonic (although it may be subsonic close to the triple point T) while region 4 is invariably subsonic. It resembles a great deal the problem occurring within a two-dimensional ejector system [5]. It appears to be extremely attractive to approximate the lower stream by a one-dimensional treatment, especially in view of the fact that the variation of entropy seems to be insignificant. However, it has been observed that in the early part of the flow development the pressure is increasing along the slipline. A one-dimensional flow analysis for the lower stream will not be able to match such a flow condition, and a more sophisticated flow analysis is thus needed in this region near triple point.

The flow field of region 3 for the upper stream is bounded by a curved, attached shock and is to be treated as a supersonic flow past a curved body whose configuration is still unknown (see Fig. 13a). It presents itself as a part of the flow field produced by a supersonic flow past a pointed body. Although the method of characteristics will be useful when the flow is supersonic, it was originally expected that the general method of analysis for blunt body problems will be needed if the flow is subsonic behind the curved shock. The method of integral

relations developed by Dorodnitsyn and applied by Belotserkovskii [12] to fluid flow problems is thus adopted for both the upper and lower flow fields during the early part of the flow development.

From the fundamental equations the momentum equation along the streamline direction can be integrated to obtain the Bernoulli's equation. Due to different coordinate systems used, one has different sets of equations for external and for internal flow. Hence, one obtains the following two-dimensional equations in streamline coordinate system:

External Flow for Region 3 (Fig. 13a)

Continuity:

$$\frac{\partial}{\partial \tilde{n}}\left[\tilde{\rho}\tilde{v}_n \frac{\tilde{R}+\tilde{n}}{\tilde{R}}\right] + \frac{\partial}{\partial \tilde{s}}(\tilde{\rho}\tilde{v}_s) = 0 \tag{17}$$

Normal Momentum:

$$\frac{\partial}{\partial \tilde{n}}\left[\tilde{\rho}\tilde{v}_n^2 \frac{\tilde{R}+\tilde{n}}{\tilde{R}}\right] + \frac{\partial}{\partial \tilde{s}}(\tilde{\rho}\tilde{v}_n \tilde{v}_s) - \frac{\tilde{\rho}\tilde{v}_s^2}{\tilde{R}} = -\frac{\partial}{\partial \tilde{n}}\left[\tilde{P}\frac{\tilde{R}+\tilde{n}}{\tilde{R}}\right] + \frac{\tilde{\rho}}{\tilde{R}} \tag{18}$$

NOTE: These are Tollmien's equations [24] for inviscid flow.

Internal Flow for Region 4 (Fig. 13b)

Continuity:

$$\frac{\partial \tilde{\rho}\tilde{u}}{\partial \tilde{x}} + \frac{\partial \tilde{\rho}\tilde{v}}{\partial \tilde{y}} = 0 \tag{19}$$

Normal Momentum:

$$\tilde{\rho}\tilde{u}\frac{\partial \tilde{v}}{\partial \tilde{x}} + \tilde{\rho}\tilde{v}\frac{\partial \tilde{v}}{\partial \tilde{y}} + \frac{\partial \tilde{P}}{\partial \tilde{y}} = 0 \tag{20}$$

The Bernoulli relationship can be conveniently expressed by

$$\int \frac{d\tilde{P}}{\tilde{\rho}} + \frac{1}{2}\tilde{q}^2 = \text{constant along the streamline} \tag{21}$$

and the entropy equation is

$$\frac{D}{Dt}\left[\frac{\tilde{P}}{\tilde{\rho}^{\gamma}}\right]=0, \text{ where } \frac{D}{Dt} \text{ is the substantial derivative.} \qquad (22)$$

Eqs. (21) and (22) are used for both external and internal flows. Here, $(\tilde{\ })$ refers to dimensional quantities.

5.2 THE METHOD OF INTEGRAL RELATIONS

The basic procedures of applying the method of integral relations [17,18,21,25] to this study are to express the governing nonlinear continuity and momentum equations in streamline coordinates, to write them in divergence forms, and then to integrate them along the normal to streamline direction. The unknown integrands are approximated by some polynomial functions (or some other convenient continuous functions). With the aid of Leibnitz's rule for differentiation under the integral sign, the original nonlinear partial differential equations are reduced to a set of ordinary differential equations readily solvable by using a digital computer. Since the integration is a smoothing process, the overall character of the solution is preserved even though the detailed description of the flow field cannot be achieved. The accuracy of the solution depends on the number of strips of the normal direction divided.

5.3 SUPERSONIC FLOW OVER TWO-DIMENSIONAL ARBITRARY BODY

If the normalizing parameters $\tilde{q}_{max}$, $\tilde{P}_{o\infty}$, $\tilde{\rho}_{o\infty}$, and L are introduced to normalize the flow parameters in a one-strip analysis, and if the unknown integrands are approximated by linear function in normal direction

$$f(n,s) = f_o(n,s) + \frac{n}{\varepsilon}\left[f_\varepsilon(n,s) - f_o(n,s)\right] \qquad (23)$$

the nonlinear partial differential equations, Eqs. (17) and (18), for external flow can be integrated along the normal direction from the body surface to shock layer thickness ε and, after tedious mathematical manipulation, will yield:

$$\frac{d\kappa}{ds} = \frac{G + E\frac{d\varepsilon}{ds}}{F} \tag{24}$$

from normal momentum equation,

$$\frac{dV_{s_o}}{ds} = \frac{1}{B}\left[\left(D - A\frac{d\varepsilon}{ds}\right) - C\frac{d\kappa}{ds}\right] \tag{25}$$

from continuity equation, and

$$\frac{d\varepsilon}{ds} = \frac{1 + \frac{\varepsilon}{R}}{\tan(\kappa + \theta)} \tag{26}$$

which is a shock geometric relationship, see Fig. 13a.

Functions A, B, C, D, E, F, and G are complicated functions of κ, V_{s_o}, ε, γ, M_∞, θ, $d\theta/ds$, and are given in APPENDIX A. Three unknowns, κ, V_{s_o}, and ε, are left to be determined. It is interesting to note that the above two-dimensional relations can easily be deduced from Traugott's axisymmetric equations [17] by allowing the body radius to approach infinity.

5.3.1 Detached Shock Wave

If the shock wave is detached, the initial conditions for the above coupled first-order nonlinear ordinary differential equations are

$$\kappa\Big|_{s=0} = 0, \quad V_{s_o}\Big|_{s=0} = 0, \quad \varepsilon\Big|_{s=0} = \varepsilon_o \tag{27}$$

The shock stand-off distance ε_o is unknown and must be solved as part

of the solution. There are two singular points involved. One occurs at B = 0 and the other at F = 0. The singular point of B = 0 occurs at $v_{s_o} = \sqrt{(\gamma - 1)/(\gamma + 1)}$ which is the sonic condition. This singular behavior has been adequately used as the criterion for iteratively determining the correct stand-off distance ε_o for axisymmetric body [17,18,25], since the surface velocity gradient must be finite for the smooth body profile. On the other hand, some investigators [25] have questioned the applicability of the one-strip method of integral relations to two-dimensional detached shock wave problems due to the ill behavior of the second singular point F = 0. This will be discussed later.

5.3.2 Attached Shock Wave

In this study of Mach reflection, the shock wave is always attached to the triple point. A limiting case corresponding to the zero shock stand-off distance must be investigated, since the foregoing equations assume undetermined form if the condition $\varepsilon = 0$ is imposed directly into these equations. By formally using L'Hospital's rule and by noting $v_{n\varepsilon} \to 0$, $P_\varepsilon \to P_o$ at the attached point when $\varepsilon \to 0$, the coupled differential equations, Eqs. (24), (25), and (26), become

$$\left[\frac{d\varepsilon}{ds}\right]_{\varepsilon \to 0} = \frac{1}{\tan(\theta + \kappa)} \tag{28}$$

$$\left[\frac{\frac{d\kappa}{ds}}{\frac{d\theta}{ds}}\right]_{\varepsilon \to 0} = \frac{v_{s_o}^2\left[\tan^2(\theta+\kappa) - \left(\frac{1 - \frac{\gamma+1}{\gamma-1}v_{s_o}^2}{1 - v_{s_o}^2}\right)\right]}{\tan(\theta+\kappa)\left[\left(1 - \frac{\gamma+1}{\gamma-1}v_{s_o}^2\right)\left(\frac{\kappa_4}{2\gamma\rho_o} + \frac{v_{s_o}k_1k_2}{1 - v_{s_o}^2}\right) + v_{s_o}k_1k_2\tan(\theta+\kappa)\right]} \tag{29}$$

with

$$\left[\frac{\frac{1}{R}}{\frac{d\theta}{ds}}\right]_{\varepsilon \to 0} = \left[\frac{\frac{d\kappa}{d\theta}}{\frac{d\theta}{ds}}\right]_{\varepsilon \to 0} \sin(\kappa + \theta), \text{from shock geometry} \qquad (30)$$

$$\left[\frac{\frac{dV_{s_o}}{ds}}{\omega_\infty \frac{d\theta}{ds}}\right]_{\varepsilon \to 0} = \frac{v_{s_o}\left[\left(\frac{k_4}{2\gamma\phi_o} + \frac{v_{s_o} k_1 k_3}{1 - v_{s_o}^2}\right)\left(1 - v_{s_o}^2\right)\tan(\theta+\kappa) + v_{s_o} k_1 k_3\right]}{\omega_\infty\left[\left(1 - \frac{\gamma+1}{\gamma-1} v_{s_o}^2\right)\left(\frac{k_4}{2\gamma\phi_o} + \frac{v_{s_o} k_1 k_3}{1 - v_{s_o}^2}\right) + v_{s_o} k_1 k_2 \tan(\theta+\kappa)\right]} \qquad (31)$$

The parameters have the same meaning as those of APPENDIX A.

These are the equations for the initial derivatives of the unknowns ε, κ, and v_{s_o}. The initial values of κ and v_{s_o} can be found from oblique shock relations. These equations can also be interpreted as the relationships between shock curvature $1/R$ and body curvature $\frac{1}{R}\left(= -\frac{d\theta}{ds}\right)$ and surface velocity gradient dv_{s_o}/ds (or surface pressure gradient) at the attached point of shock wave on the body surface. Figures 14, 15, 16, and 17 present the behavior of these relationships both for weak and for strong shock waves. A discussion on the general strong shock relations can also be found in Reference [26]. It is noteworthy that the exact expressions for weak shock wave have been derived by Thomas [27], Taub [8], and by Lin and Rubinov [28] from different methods of analysis for uniform approaching flow, and by Mölder [23] for non-uniform incident stream with rotationality in front of curved shock wave.

5.3.3 Treatment of Singular Points

If one sets

$$B_o = \frac{\varepsilon}{2}\left(1 - v_{s_o}^2\right)^{[(2-\gamma)/(\gamma-1)]}$$

and if one uses the transformation

$$Z = v_{s_o}\left(1 - \frac{1}{3}\frac{\gamma+1}{\gamma-1}v_{s_o}^2\right) \tag{32}$$

Eq. (25) becomes

$$\frac{dz}{ds} = \frac{1}{B_o}\left(D - A\frac{d\varepsilon}{ds} - C\frac{dK}{ds}\right) \tag{33}$$

Since during the flow development v_{s_o} shall not reach the value of 1, which is the maximum velocity, one has, in fact, removed the sonic singular point through the above manipulation. The relationship between z and v_{s_o} is illustrated in Fig. 18 for $\gamma = 1.4$.

One should also note that

$$z = 0 \text{ when } v_{s_o} = 0 \quad \text{or} \quad v_{s_o} = \sqrt{3}\sqrt{\frac{\gamma-1}{\gamma+1}}$$

$$z = \frac{2}{3}\sqrt{\frac{\gamma-1}{\gamma+1}} \quad \text{when} \quad v_{s_o} = \sqrt{\frac{\gamma-1}{\gamma+1}}$$

and

$$z = \frac{2}{3}\left(\frac{\gamma-2}{\gamma-1}\right) \quad \text{when} \quad v_{s_o} = 1.$$

For a fixed value of $z > 0$, there corresponds two different positive values of v_{s_o} : one for subsonic flow and the other for supersonic flow. At sonic condition, $(dz/dv_{s_o}) = 0$. Therefore, near sonic speed, for a known value of z, the corresponding v_{s_o} cannot be determined efficiently from Newton-Raphson's method for solution of nonlinear algebraic equations. Other methods such as the bisect method or the false position method [29] will yield the solution near sonic point. At sonic condition, for $\gamma = 1.4$, $z = 0.2721655$ when $v_{s_o} = 0.408248$.

The ill behavior of the differential equation and the inaccuracy of interpolating too close or too far near sonic condition as mentioned in [17,25] have been eliminated. The singular behavior of the differential equation has changed, as a result of the transformation shown above, to the extreme behavior of the nonlinear algebraic equation which is much easier to handle. Also, because a small change in z will cause tremendous change in v_{s_o} near sonic point, a smaller integration step size should be used there. Since z is an odd function of v_{s_o}, there is another branch of solutions giving negative values of v_{s_o} which is physically unrealistic and is ignored.

By noting that in two-dimensional flow F/ε is a function of κ only when γ, M_∞, and θ are independent of κ, it also seems to be possible to use the similar treatment as before to eliminate the singularity occurring in differential equations when $F = 0$. However, because of the appearance of $d\kappa/ds$ in Eq. (25), nothing will be gained when the technique utilized above is applied to Eq. (24)--even the complexity of the function F/ε is ignored. Nevertheless, since $F/\varepsilon = f(\kappa)$, if γ, M_∞ and θ were held fixed, one can investigate, for $\varepsilon \neq 0$, when F/ε will vanish.

Figure 19 is the result of the solutions of $F/\varepsilon = 0$ for $\gamma = 1.4$. Two curves from oblique shock equations for $M_\infty = 2.0$ and $M_\infty = 5.0$ are also plotted in the same figure for comparison. The intersection of these curves with solution curves of $F/\varepsilon = 0$ at the same flow Mach number occurs at the attachment limit which is a particular solution of $F/\varepsilon = 0$ and is also one of the starting points for attached shock wave problem. Since shock is a local phenomenon, the magnitude of the velocity vector just behind the shock wave at point away from body is

independent of the surface tangent angle θ, that is, $\omega_\varepsilon = f(M_\infty,\kappa)$ only. Therefore, the flow properties just behind the shock wave can be found by tracing oblique shock polar for the corresponding free stream Mach number. Noting that the sonic state is very close to the attachment limit point on θ-κ diagram for the same free stream Mach number, one has, in general, two different categories, depending on whether the state behind the shock is supersonic or mixed type.

1. Supersonic State Downstream of Shock Wave

   Because κ will not decrease in general for the unbounded flow field and the maximum value of κ is the one when shock weakens to become a Mach wave, F/ε will not vanish for different combinations of θ and κ along shock polar as illustrated in Fig. 19a.

2. Subsonic and Supersonic Mixed State Downstream of Shock Wave

   As shown in Fig. 19b, the singular point $F/\varepsilon = 0$ will be unavoidably met for all the smoothly varying body profiles carrying flow changing from subsonic to supersonic state.

From these results the conclusion is that the one-strip method of integral relations is not suitable for solving two-dimensional blunt body with detached shock or pointed body with strong attached shock. The two-strip or multi-strip method is required and the calculation will be much more involved. This agrees with the comments made in [25]. However, for solving two-dimensional pointed body with weak attached shock, the one-strip method of integral relations is generally applicable (see also [19]) for slowly changing body profile with nearly constant value of κ such as the case in our study of Mach reflection.

In conclusion, in the one-strip method of integral relations for a

two-dimensional profile the singular point B = 0 occurs at the sonic condition and can be handled without difficulty, but the occurrence of the other singular point F = 0 will greatly restrict the applicability of the one-strip analysis.

It does not appear to be necessary to use the multi-strip analysis of the method of integral relations with the present method of approach in order to avoid the erratic behavior of $d\kappa/ds$ in the one-strip analysis. In weak incident shock regime, where subsonic flow behind the reflected shock prevails, it is believed that the triple point solutions do not provide adequate initial conditions as they do not agree with the experimental results according to [7]. Worst of all, the three-shock theory does not give any nontrivial solution while Mach configuration has been observed in actual flow situations with weak incident shock. If the multi-strip analysis is to be useful for weak incident shock wave, instead of the results from the present inviscid three-shock theory, the initial conditions at triple point must be obtained from other more sophisticated approaches, for example, Sternberg's non-Rankine-Hugoniot model.

5.4 FLOW INSIDE A TWO-DIMENSIONAL NOZZLE BY THE METHOD OF INTEGRAL RELATIONS

As mentioned previously, a one-dimensional treatment of lower part of the slipline is not adequate for solving the lower flow field close to triple point. A more detailed approach is indispensable. Referring to Fig. 13b, upon introducing the assumptions that entropy difference along the Mach shock is negligible and after the variables are non-dimensionalized by reference quantities, the integrands can be

approximated by polynomial functions given by:

$$\rho u = (\rho u)_c + [(\rho u)_w - (\rho u)_c]\,\eta^2$$

$$\rho uv = (\rho u)_c\, v_w\, \eta + [(\rho u)_w - (\rho u)_c]\, v_w\, \eta^3 \qquad (34)$$

$$\rho v^2 = (\rho v^2)_w\, \eta^2$$

where $\eta = y/y_w$.

The integration of the system of equations for internal flow will yield two ordinary differential equations as the consequence of the application of the one-strip method of integral relations. They are:

$$\frac{dq_w}{dx} = q'_w = \frac{C_1 E_1 - B_1 F_1}{A_1 E_1 - B_1 D_1} \qquad (35)$$

$$\frac{dq_c}{dx} = q'_c = \frac{A_1 F_1 - D_1 C_1}{A_1 E_1 - B_1 D_1} \qquad (36)$$

with initial conditions

$$q_w = q_w\Big|_o \qquad (35a)$$

$$q_c = q_c\Big|_o \qquad (36a)$$

where A_1, B_1, C_1, D_1, E_1, and F_1 are functions of Y_w, Y'_w, Y''_w, q_c, and q_w, and are given in APPENDIX B. The detailed derivations and discussions on singular behavior of these differential equations are given in [21]. Note that Eqs. (35) and (36) are functions of wall height, slope, and curvature.

The rotationality behind this strong Mach shock is usually very small and can be neglected, as can be seen from the results of triple point solution at $M_1 = 3.0$, for example, for

$\delta_2 = 25$ degrees $\quad \sigma_4 = 81.434$ degrees $\quad M_4 = 0.551$

$\delta_2 = 30$ degrees $\quad \sigma_4 = 86.24$ degrees $\quad M_4 = 0.491$

in comparison to the normal shock at centerline $\sigma = 90$ degrees, $M = 0.4752$. An extension of the analysis to include the vorticity can easily be made and was done [30].

5.5 THE METHOD OF CHARACTERISTICS

In the supersonic flow field the method of characteristics is a powerful tool. If the rotationality behind the curved shock wave is also considered, the fundamental equations can be solved by tracing the physical and the hodographical characteristics simultaneously in a step-by-step manner. For the two-dimensional case, the characteristic equations are (see [31,32]):

$$\left.\frac{dy}{dx}\right|_{I,II} = \tan(\theta \mp \alpha) \tag{37}$$

$$\left.\frac{1}{M^*}\frac{dM^*}{d\theta}\right|_{I,II} = \mp \tan\alpha - \left.\frac{\sin^2\alpha}{\gamma(\gamma-1)}\frac{d(s/c_v)}{d\theta}\right|_{I,II} \tag{38}$$

The last term in the second equation accounts for the vorticity behind curved shock. When derivatives are approximated by difference forms, these equations can be solved simultaneously to give the unknown quantities and, therefore, the whole flow field (see APPENDIX C).

Because of the erratic behavior of dk/ds of Eq. (24), the one-strip method of integral relations for two-dimensional blunt body problems is not suitable for the calculation of subsonic flow behind the triple point in region 3, which is contrary to the original intention of adopting this method. Although the method of characteristics could be used for all of the supersonic flow computations in region 3, the requirement of information on height, slope, and curvature of wall for quasi two-dimensional analysis in the internal flow renders Eqs. (24), (25), and (26) of the method of integral relations to be the natural

choice to match with the upper flow based on Eqs. (35) and (36) at the early part of the calculation. The method of characteristics, however, will be employed for the upper flow in conjunction with the one-dimensional treatment of central core flow after the early complications in the core flow have been resolved.

5.6 THE CALCULATION OF INTERACTING FLOW FIELD

With the results at the triple point and the relations given by Eqs. (28), (29), and (31) as the initial conditions for external flow and Eqs. (35a) and (36a) as the initial conditions for internal flow, the system of differential equations, Eqs. (24), (25), (26), (35), and (36), can be integrated numerically. The fourth-order Runge-Kutta numerical method is used in the integration. For each step of integration, one assumes that the slipline has the profile of a polynomial of third degree.

$$Y = a_i + b_i X + c_i X^2 + d_i X^3 \qquad (39)$$

where the coefficients a_i, b_i, c_i, and d_i are to be determined for each step i (see Fig. 12).

For the first step of integration, a slipline curvature $-1/R_o$ is assumed. This amounts to employing a circular arc for the first step as the slipline with radius of curvature R_o. Therefore,

$$a_1 = Y(o) = Y_o$$

$$b_1 = Y'(o) = Y'_o$$

$$c_1 = \frac{Y''(o)}{2} = \frac{Y''_o}{2} = \frac{-1}{2R_o}\left[1 + Y'^2_o\right]^{3/2}$$

where prime (') indicates the derivative taken with respect to x, and d_1 is found from solving

$$2c_1 + 6d_1 X_1 = \frac{-1}{R_o}\left[1 + \left(b_1 + 2c_1 X_1 + 3d_1 X_1^2\right)^2\right]^{3/2}$$

when an arbitrary increment x_1 is selected. One should note that Y_o is the Mach stem height having length of unity and Y'_o is known from triple point solution. R_o is yet to be determined.

For the steps thereafter, d_i is the only unknown since a_i, b_i, and c_i can be determined from the results of the previous step. In this way, the slipline would have no discontinuity in slope and curvature. For an assumed R_i, the unknown d_i can be found from

$$2c_i + 6d_i X_i = \frac{-1}{R_i}\left[1 + \left(b_i + 2c_i X_i + 3d_i X_i^2\right)^2\right]^{3/2} \qquad (40)$$

with

$$a_i = Y_{i-1}$$

$$b_i = Y'_{i-1}$$

$$c_i = \frac{-1}{2R_{i-1}}\left(1 + Y'^2_{i-1}\right)^{3/2}$$

Here x_i is the x-coordinate at the end of the ith integration step and Y_{i-1} is the Y-coordinate at the end of the i-1st integration step.

For the selected geometric configuration of the slipline in each step of the calculations, integrations of Eqs. (24), (25), (26), (35), and (36) can be carried out. In particular, Eqs. (25) and (35) would give v_{s_o} and q_w and thus the pressures across the slipline at the end of each step. The requirement of pressure matching thereby allows the determination of the correct R_i for that particular step (R_o for the

first step).

It should be mentioned that in the first step of the calculation of the lower stream, the difference in the x-coordinates of the triple point and the leg of the Mach shock is ignored for the purpose of simplification.

It is also obvious from Fig. 20 that the coordinate transformational relations between the lower and upper portions of the flow field are given by

$$Y = \bar{Y} \cos \delta_2 - \bar{X} \sin \delta_2 + Y_o \tag{41}$$

$$X = \bar{X} \cos \delta_2 + \bar{Y} \sin \delta_2 \tag{42}$$

The error analysis and the choice of step size in the numerical integration are discussed, for example, in [33,34]. The simplest way in practice to obtain good results is to integrate the same equations twice: first using reasonably small step size, then using twice larger step size and comparing the results.

The integration process is carried out until the fluid along the slipline accelerates. Thereafter, the analysis for the lower stream is replaced by a one-dimensional isentropic flow while the method of characteristics is employed for the upper flow for simplification purposes. Meanwhile, a Prandtl-Meyer expansion, which would occur as the result of reflection of the curved shock from the free jet boundary, is inserted into the flow calculation. In switching from the method of integral relations to the method of characteristics for the upper flow field, gradient method [25] can be used to recover from previous results of the method of integral relations the information needed for the method of characteristics. In all of the calculations, the reflected

shock is observed to be rather straight. The vorticity term in Eq. (38) can, therefore, be neglected.

Here one notices that another important reason for switching to the method of characteristics for the upper flow field is based upon the fact that the method of integral relations cannot handle the intersection between reflected shock and free jet in a satisfying manner.

The Prandtl-Meyer expansion zone $\Delta\omega$ is arbitrarily divided into an increment of approximately one degree each where

$$\omega(M^*) = \sqrt{\frac{\gamma+1}{\gamma-1}}\tan^{-1}\sqrt{\frac{M^{*2}-1}{\frac{\gamma+1}{\gamma-1}-M^{*2}}} - \tan^{-1}\sqrt{\frac{M^{*2}-1}{1-\frac{\gamma-1}{\gamma+1}M^{*2}}}$$

is the Prandtl-Meyer function resulting from direct integration of the two-dimensional characteristic equation, Eq. (38), when the entropy gradient term is disregarded.

In the field or along the free jet boundary where pressure is constant, the unknown flow properties are found from conventional calculation procedure by tracing characteristic curves in physical and in hodographical planes as described in APPENDIX C.

The procedure required for matching region 3 using method of characteristics and region 4 using one-dimensional analysis along the slipline needs special treatment. This scheme is similar to the study of the interaction between primary and secondary streams of supersonic ejector systems [5]. Referring to Fig. 20: If Y_r and M_r are the dimensionless reference height and Mach number, and if flow field has been calculated up to state 2 and flow variables at states 1, 2u and 2ℓ are all known, one may write for state 3

$$\frac{P_{o4}}{P_{o3}} = \frac{\left[1 - \frac{\gamma - 1}{\gamma + 1} M_{3u}^{*2}\right]^{[\gamma/(\gamma-1)]}}{\left[1 - \frac{\gamma - 1}{\gamma + 1} M_{3\ell}^{*2}\right]^{[\gamma/(\gamma-1)]}} \tag{43}$$

from equality of pressure across the slipline, and

$$\frac{Y_r}{Y_{3\ell}} = \frac{Q(M_r)}{Q(M_{3\ell})} \tag{44}$$

from constancy of flow rate for a one-dimensional nozzle flow where

$$Q(M) = \frac{1}{M}\left[\left(\frac{2}{\gamma + 1}\right)\left(1 + \frac{\gamma - 1}{2} M^2\right)\right]^{\{(\gamma+1)/[2(\gamma-1)]\}} \tag{45}$$

The characteristic equations, Eqs. (37) and (38), with entropy gradient neglected, can be written in finite difference form as

$$\frac{Y_{3u} - Y_{2u}}{x_{3u} - x_{2u}} = \tan\left(\bar{\theta}_{23}\right) \tag{46}$$

$$\frac{Y_{3u} - Y_{1u}}{x_{3u} - x_{1u}} = \tan\left(\bar{\theta}_{13} - \bar{\alpha}_{13}\right) \tag{47}$$

$$\frac{1}{\bar{M}_{13}^{*}}\left[\frac{M_{3u}^{*} - M_{1u}^{*}}{\theta_{3u} - \theta_{1u}}\right] = -\tan\bar{\alpha}_{13} \tag{48}$$

One now has five equations, Eqs. (43), (44), (46), (47), and (48) to determine five unknowns X_{3u}, Y_{3u}, M_{3u}^{*}, θ_3, and $M_{3\ell}$. The unknown $Y_{3\ell}$ is related to Y_{3u} through coordinate transformations from Eqs. (41) and (42), and P_{o4}/P_{o3} is found from triple-point solution.

An early insertion of Prandtl-Meyer expansion would cause the lower flow passing through a minimum area with subsonic Mach number, while a delayed insertion will cause the lower flow reaching sonic condition at a section with decreasing area. The correct location where the curved shock-jet boundary intersection occurs is such that

the lower stream will assume a sonic state at a minimum area location. Once this condition is met, it will be a simple matter to determine the location of the Mach stem height relative to the height of the nozzle exit section by using triangular relations (see Fig. 12)

$$Y_e = Y_{P-M} + \sqrt{(Y_{P-M} - Y_o)^2 + X_{P-M}^2}\ \frac{\sin(180^\circ - \sigma_2 - \lambda)\sin\delta_2}{\sin(\sigma_2 - \delta_2)} \qquad (49)$$

$$X_e = \frac{Y_o - Y_e}{\tan\sigma_2} \qquad (50)$$

here

$$\lambda = \tan^{-1}\left[\frac{Y_{P-M} - Y_o}{X_{P-M}}\right] \qquad (51)$$

and σ_2 is the shock wave angle corresponding to M_1 and δ_2.

5.7 RESULTS AND DISCUSSIONS

The method of analysis given above is indeed fruitful for the present study with supersonic state behind the reflected shock at the triple point. A successful calculation using double precision mode takes two to five minutes computation time on an IBM system 360/75 digital computer. Figure 21 shows the flow condition of the lower stream when the P-M expansion starts at various places for $M_1 = 3.0$ and $\delta_2 = 30$ degrees. It clearly demonstrates the dependence of sonic state of the central core flow on the location of Prandtl-Meyer expansion fan. A similar trend is found for other flow conditions. The early occurrence of P-M fan, say at $X_{P-M} = 30$ in Fig. 21, gives subsonic state, $M_t = 0.72$, at the throat ($\delta_t = 0^\circ$) for the slipline. The delayed appearance of P-M fan, say at $X_{P-M} = 40$, results in a sonic state at a position where the area is not a minimum, which contradicts the

one-dimensional isentropic flow theory. The correct position of P-M fan is therefore found by iteration (approximately at $X_{P-M} = 35.53$ for the present case). It is to be noticed that the iteration procedure is carried out only up to the state where Mach number in central core is close to 1.0 at the minimum area. The sonic state at throat cannot be reached in an exact manner since sonic point behaves as a saddle point mathematically.

All above stated discussions are based on the isentropic one-dimensional approach in central core flow after the highly non-uniform state near triple point has been solved by using quasi two-dimensional integral method. For more rigorous and accurate analysis not only the vorticity behind the curved Mach stem shock should be considered in the quasi two-dimensional integral method, but the nonisentropic effect in the continued calculation of the one-dimensional treatment must be taken into account also. In that case, the lower stream flow is not necessarily sonic at the throat. For one-dimensional nonisentropic nozzle flow, Snyder [35], Bryant [36], and Ferguson [37] showed that for nozzle efficiency less than one, the Mach number at throat of the nozzle is also less than one. On the other hand, in an irrotational quasi two-dimensional nozzle analysis [21], the "choking" condition is defined as the throat singular point which permits continuous acceleration from subsonic to supersonic flow. However, these deviations are small compared with those of [21,35] for high efficiency nozzle flow.

Figures 22 and 23 give the flow patterns for $\delta_2 = 30$ degrees and $\delta_2 = 25$ degrees, respectively, at $M_1 = 3.0$.* For $\delta_2 = 25$ degrees the

*There was a minor error in reporting the results in [38]. This has been corrected in Figs. 22, 23, and 24.

minimum area (sonic state for region 4 in one-dimensional isentropic analysis) occurs in the P-M expansion zone as shown in Fig. 22. For δ_2 = 30 degrees, however, the minimum area stands at the place where the last P-M expansion wave reflects from the free jet boundary and intersects with the slipline, since the ambient pressure is higher and the P-M zone is smaller ($\Delta\omega$ = 8.84 degrees compared with $\Delta\omega$ = 15.26 degrees for the case of δ_2 = 25 degrees) as shown in Fig. 23.

Figure 24 illustrates the velocity distribution along the slipline. The decrease in velocity along the early part of the slipline accounts for the necessity of using quasi two-dimensional analysis in region 4 near the triple point.

Figures 25 and 26 present the information of the height and the position of Mach stem for two-dimensional overexpanded nozzle flow. It is understood that at the same nozzle Mach number, it takes more computation to reach the sonic condition in central core flow for lower ambient pressure levels. These curves could be, therefore, extrapolated to the zero Mach stem height corresponding to the regular reflection pattern. For higher ambient pressure, the Mach stem is higher and stands closer to the nozzle exit plane.

The correct positions of P-M fan for various flow conditions are shown in Figs. 27 and 28. It has a trend similar to that of the Mach stem height. Figure 29 shows the range of expansion of P-M fan. Evidently at the same nozzle Mach number lower ambient pressure induces wider range of P-M expansion.

The height and location of the throat of central core flow are plotted in Figs. 30 and 31. The higher Mach stem height is associated

with higher throat height for the same nozzle exhaust condition. This indicates that for a propulsional device flying at a designed nozzle Mach number from higher pressure atmosphere to lower pressure surroundings, the Mach stem height decreases as does the throat height in the central core flow. Therefore, the mass flow rate passing through the central core is reduced and the pumping effect of this central core is reduced also. However, the higher surrounding pressure does not necessarily result in a throat position closer to the nozzle exit plane. As depicted in Figs. 22 and 23, different ranges of P-M expansion for various ambient pressure levels would affect the location of the throat significantly. This perhaps accounts for the occurrence of kinks in the curves as shown in Fig. 31.

Figure 32 reveals the values of M^* on the upper side of slipline at the place where the lower side is at sonic condition. It is interesting to note that at the throat the velocity difference on the two sides of the vortex sheet (slipline) decreases as the ambient pressure increases under the same nozzle design condition.

With the data given above, it should be fairly easy to construct a Mach reflection pattern from an overexpanded two-dimensional nozzle flow when it occurs. First of all, the nozzle exit height and Mach number are specified. For a particular ambient pressure one finds a corresponding δ_2 from Fig. 10b. The properties at triple point are found in Figs. 5 through 9 (or from Tables 1 through 13). Using this information and the data shown in Figs. 25 through 32, the appropriate location and height of Mach stem, P-M fan, and central core throat can all be laid out.

5.8 APPROXIMATE METHOD FOR ESTIMATING MACH STEM HEIGHT

For higher back pressures, state 3 at the triple point becomes subsonic and the method described previously does not yield any fruitful results, since the calculation cannot overcome the singularity corresponding to F = 0 (see Eq. (24)). However, the location of the Mach stem and its height under these situations can be determined approximately from a model emphasizing the balance of the interacting force between the two streams. As it turns out, this model can also be employed to give reasonable results even when state 3 at the triple point is supersonic.

One realizes that under this flow situation, the back pressure is relatively high that the strength of the reflected shock is not excessively strong (although it belongs to the strong shock solution) at the triple point, and it soon degenerates into a Mach wave as it extends from the triple point. It is then reasonable to assume that this variation may be expressed by (Fig. 33):

$$\sigma_r = \alpha_2 + (\sigma_3 - \alpha_2)\left(1 - \frac{\overline{Y}}{H_2}\right)^2 \tag{52}$$

where σ_3 is found from triple point solution,

α_2 is the Mach angle corresponding to M_2, and

$\overline{Y}$ and H_2 are the distances from the triple point normal to the flow as shown in Fig. 34a and are nondimensionalized by using unit nozzle exit height Y_e.

Similarly, the Mach shock profile may be approximated by

$$\sigma_{MS} = \sigma_4 + \left(\frac{\pi}{2} - \sigma_4\right)\left(1 - \frac{Y}{Y_o}\right)^2 \tag{53}$$

where Y_o is the unknown Mach stem height and is nondimensionalized

by using unit nozzle exit height, Y_e, and

σ_4 is the shock wave angle found from triple point solution.

Since the ambient pressure is relatively high such that the central core flow will not be "choked" if it expands isentropically to the ambient pressure, it is thus possible to assume that both the upper and lower streams shall expand and tend toward the final asymptotic rotational states corresponding to the uniform ambient pressure. A final balance of the flow momentum in the main flow direction associated with the control volume as shown in Fig. 34a would allow a unique determination of the Mach stem height.

From the principle of conservation of mass along stream tube, one obtains

$$\tilde{\rho}_2 \, \tilde{u}_2 \, d\bar{Y} = \tilde{\rho}_{3a} \, \tilde{u}_{3a} \, d \, Y_{3a} \tag{54}$$

and

$$\tilde{\rho}_1 \, \tilde{u}_1 \, dY = \tilde{\rho}_{4a} \, \tilde{u}_{4a} \, d \, Y_{4a} \tag{55}$$

where subscripts 3a and 4a refer to the asymptotic downstream conditions at ambient pressure for region3 and region 4, respectively.

Using the maximum velocity V_m, local stagnation conditions, and unit nozzle exit height Y_e as the nondimensionalizing parameters, one obtains from Eqs. (54) and (55),

$$\frac{d\bar{Y}}{dY_{3a}} = \frac{(P_{o2}/P_{o3})^{1/\gamma} \, (u_{3a}/V_m)}{\dfrac{u_2}{V_m}} \, \frac{P_{o3}}{P_{o2}} \tag{56}$$

and

$$\frac{dY}{dY_{4a}} = \frac{[(P_{o1}/P_{o4})(P_a/P_{o1})]^{1/\gamma} \, (u_{4a}/V_m)}{(P_1/P_{o1})^{1/\gamma} \, (u_1/V_m)} \, \frac{P_{o4}}{P_{o1}} \tag{57}$$

where P_{o3}/P_{o2} and P_{o4}/P_{o1} depend on the assumed shock profiles of Eqs. (52) and (53), and

$$\frac{u_{3a}}{V_m} = \sqrt{1 - \left[\frac{P_a}{P_{o2}} \frac{P_{o2}}{P_{o3}}\right]^{[(\gamma-1)/\gamma]}} \tag{58}$$

with similar expressions for u_{4a}/V_m, u_1/V_m, and u_2/V_m as functions of pressure ratios.

The horizontal integral momentum balance for the control volume shown in Fig. 33 gives

$$Y_o\left[\frac{P_1 - P_a}{P_{o1}}\right] - \frac{2\gamma}{\gamma - 1}\left[\int_o^{H_{4a}} \frac{P_{o4}}{P_{o1}} \left(\frac{P_a}{P_{o4}}\right)^{1/\gamma} \left(\frac{u_{4a}}{V_m}\right)^2 d\,Y_{4a}\right.$$

$$+ \int_o^{H_{3a}} \frac{P_{o3}}{P_{o2}} \cdot \frac{P_{o2}}{P_{o1}} \left(\frac{P_a}{P_{o3}}\right)^{1/\gamma} \left(\frac{u_{3a}}{V_m}\right)^2 d\,Y_{3a} - \left(\frac{P_1}{P_{o1}}\right)^{1/\gamma}$$

$$\left. \cdot \left(\frac{u_1}{V_m}\right)^2 Y_o - \frac{P_{o2}}{P_{o1}} \left(\frac{P_a}{P_{o2}}\right)^{1/\gamma} \left(\frac{u_2}{V_m}\right)^2 H_2 \cos\delta_2\right] = 0 \tag{59}$$

One now has three equations, Eqs. (56), (57), and (50), for the three unknown quantities Y_o, H_{3a}, and H_{4a} while Eqs. (52) and (53), in conjunction with the shock relations, provide the results of P_{o3}/P_{o2} and P_{o4}/P_{o1} for the corresponding stream tubes.

Since M_1 and δ_2 are given, with any initial estimate of Y_o one may find H_2 from geometric relation

$$H_2 = [1 - Y_o - X_e \tan\delta_2] \cos\delta_2 \tag{60}$$

where X_e is given in Eq. (50) (with Y_e = 1 unity). Y_o and H_2 are

subsequently divided into small divisions with each division representing the height of a stream tube. Equations (56) and (57) can be integrated numerically using a trapezoidal rule to find the unknowns H_{4a} and H_{3a} and, simultaneously, the values of two unknown integrals appearing in momentum balance equation, Eq. (59). These values are then substituted into the momentum equation and the correct Mach stem height Y_o would allow the integral momentum balance to be satisfied. This must be done in an iterative manner and is equivalent to finding the solution to a nonlinear algebraic equation. The method of false position [29] works extremely well for the present problem. Upon representing the left-hand side of Eq. (59) as the residue function $W(Y_o)$, one starts from two initial estimates of Y_o (identified as ${}^1Y_o$ and ${}^2Y_o$) such that $W({}^1Y_o)$ and $W({}^2Y_o)$ have opposite signs. The next improved approximation will be

$$ {}^3Y_o = \frac{{}^1Y_o\, W({}^2Y_o) - {}^2Y_o\, W({}^1Y_o)}{W({}^2Y_o) - W({}^1Y_o)} \qquad (61) $$

If $W({}^3Y_o) \cdot W({}^1Y_o) < 0$, one replaces ${}^2Y_o$ by ${}^3Y_o$; otherwise one replaces ${}^1Y_o$ by ${}^3Y_o$. Using Eq. (61) for the next approximation and repeating the calculation in this fashion until the criterion of accuracy is satisfied, that is, either $|{}^3Y_o - {}^1Y_o| < \varepsilon$ or $|{}^3Y_o - {}^2Y_o| < \varepsilon$, where ε is an arbitrarily small positive number, one then stops the iteration.

A flow case of $M_1 = 1.92$, $P_{o1}/P_a = 3.67$ (which is equivalent to $\delta_2 = 12.2071$ degrees) is taken as an example. The two initial estimates are ${}^1Y_o = 0.999$ and ${}^2Y_o = 0.001$ which represent two widely different Mach stem heights, and the final results are reached with three additional iterations. The actual result of all iterations based on the double

precision mode from the IBM system 360/75 digital computer using the foregoing approximate analysis is presented in Table 14 for various numbers of divisions N_{st} with which H_2 and Y_o are divided. It agrees very well with the picture given by A. Ferri [43] from schlieren photograph technique. Another example of calculation for $M_1 = 1.92$, $P_{o1}/P_a = 3.54$ (corresponding to $\delta_2 = 12.9309$ degrees) is presented in Table 15 which yields relatively lower Mach stem height in comparison with A. Ferri's experimental data of $Y_o = 0.4$. The corresponding velocity profiles in the asymptotic downstream flow are shown in Fig. 34 for a variety of pressure ratios at $M_1 = 1.92$.

Extensive calculations for two-dimensional overexpanded nozzle flows have been performed by this approximate analysis. The results of the height and the position of the Mach stem are shown in Figs. 25 and 26. In general, this approximate method gives reasonable results for flow cases with subsonic state 3 at the triple point. They also compare favorably with those from the detailed flow field analysis when state 3 at the triple point is supersonic. The cases corresponding to the two extreme solutions of the triple point are also calculated and identified as before as $\sigma_3 = 90$ degrees and $\sigma_4 = 90$ degrees. It is interesting to note that, at the extreme condition of $\sigma_3 = 90$ degrees, $Y_o/Y_e = 1$ and $X_o/Y_e \simeq 0$ for high Mach number flow ($M_1 \geq 2.5$); $Y_o < Y_e$ for Mach numbers in the range of $M_1 \simeq 1.5 \sim 2.5$; and $Y_o/Y_e \simeq 0$ for $M_1 \leq 1.5$ which was predicted before in the triple point investigation. At the other extreme of $\sigma_4 = 90$ degrees, Y_o/Y_e exhibits a maximum value in the neighborhood of $M_1 \simeq 2.75$, and X_o/Y_e has a minimum value in the vicinity of $M_1 \simeq 2.2$. It should be noted that within the region where

σ_4 = 90 degrees, the flow is within the regular reflection flow regime. Furthermore, because of the underestimation of the shock losses in this approximate analysis within this flow regime, finite Mach stem heights are obtained from these calculations. Also shown in the same figures is the line of M^*_{4a} = 1.0 indicating that the state at the triple point assumes the sonic state when it expands into the ambient pressure.

The analysis shown in this section provides an approximate method for estimating the Mach stem height in the region where M_3 can be supersonic or subsonic at the triple point. Although the detailed flow field cannot be described, this method does give useful information in the area where the method of integral relations fails to yield any detailed information. The method is simple and does not need extensive calculations. Obviously, the extension of this approximate method to the axisymmetric overexpanded nozzle flows is straightforward.

6. MACH DISC FROM UNDEREXPANDED AXISYMMETRIC NOZZLE FLOW

6.1 BASIC DESCRIPTION OF THE FLOW FIELD

For a uniform gas jet exhausting from an axisymmetric nozzle to a still medium at lower constant pressure, the flow will first follow a two-dimensional Prandtl-Meyer expansion locally at the lip of the nozzle. These expansion waves will eventually be reflected as compression waves from the constant pressure jet boundary. When the ratio of exit to ambient pressure is high, the compression waves of the same family will unavoidably intersect each other at a place where shock should originate to account for the coalescence of these waves. As the expansion and compression waves interact continuously downstream, the shock becomes stronger because of the accumulating effect of the coalescence of these reflected waves. This imbedded shock wave could be reflected from the centerline of symmetry as shown by Pack [12] for a two-dimensional gas jet. However, if the surrounding pressure is low enough, the snowballing compressive effect will result in an imbedded shock wave at downstream field so strong and curved that regular reflection from the centerline of symmetry is impossible. The configuration associated with Mach disc then comes into play.

Figure 3 shows a typical Mach configuration from axisymmetric underexpanded nozzle flow. The previous discussions for the two-dimensional overexpanded nozzle flow are applicable to this axisymmetric underexpanded problem but with several basic differences. First of all, the incident shock is no longer straight, and the flow upstream of the reflected shock (region 2) is highly nonuniform. For simplicity, the central core flow behind Mach disc can be approximated by a one-dimensional

analysis which has been used successfully in [15] for overexpanded cases. Since the incident flow in front of the Mach disc is also non-uniform and not horizontal locally at triple point, a rotation of co-ordinate as shown in Fig. 4 for triple-point solution is necessary. Furthermore, the rotationality is no longer negligible because of the rapidly changing shock strength behind the incident and the reflected shock waves. The method of characteristics will be used exclusively for the calculation of flow structure of the supersonic axisymmetric gas jet, while one-dimensional isentropic flow is applied to the central core flow immediately after the triple-point shock system is inserted into the flow field.

6.2 THE METHOD OF CHARACTERISTICS

In axisymmetric, supersonic flow field the fundamental equations, Eqs. (14), (15), and (16), in cylindrical coordinates can be solved by following characteristic curves in physical and hodographical planes simultaneously [31,32,39]. The characteristic equations are

$$\left.\frac{dr}{dx}\right|_{I,II} = \tan(\theta \mp \alpha) \tag{62}$$

$$\left.\frac{1}{M^*}\frac{dM^*}{d\theta}\right|_{I,II} = \mp \tan\alpha - \frac{\sin^2\alpha}{\gamma(\gamma-1)}\left.\frac{d(s/c_v)}{d\theta}\right|_{I,II} + \frac{\tan^2\alpha \tan\theta}{\tan\theta \mp \tan\alpha}\frac{1}{r}\left.\frac{dr}{d\theta}\right|_{I,II} \tag{63}$$

The added last term expresses the difference between axisymmetric and two-dimensional problems. Application of these equations to the field, free jet, and axis point procedures is well known and is given in APPENDIX C.

During the process of computation, the characteristic curves of the same family in physical plane are found to intersect each other. It

indicates the failure of the continuous, single-valued solution, and a shock discontinuity should accordingly be introduced into the flow field. This is where the imbedded shock wave originates. The reflected wave resulting from the intersection of the compression wave and shock wave should not be neglected since it will reflect from the free jet boundary and has the augmenting effect on the downstream shock strength. In this Mach disc problem, the accurate calculation of incident shock strength is found to be critical since all the downstream flow field, including the triple point solution, depends on it. Therefore, the region where compression wave and shock wave of the same family intersect to produce a stronger shock wave should be examined carefully and is of paramount importance. Moe and Troesch [41] are correct in stating that the calculation of the imbedded shock wave is the most complicated part of the numerical method. The simple fold-back method [16] or other simplified methods, though determining the shock position properly, will not give the appropriate shock wave strength.

As shown in Fig. 35a, I is the characteristic of family 1 and II is the characteristic of family 2. The properties at E, A, and C on characteristic curve II_{n-1} and at F on II_n are known from previous calculations. The flow variables at B are found from known properties at A and F by following characteristic curves AB of I_m and FB of II_n. Similar calculations can be formed to find point D with DC of I_{m+1} and BD of II_n. However, if the x-coordinate of D is detected to be at the upstream part of B on the characteristic II_n, it indicates waves AB and CD have intersected each other somewhere at G as shown in Fig. 35a.

Whenever waves of the same family intersect each other, extreme care should be taken to determine the flow properties at the intersection

point. As shown in Fig. 35b, there appears a slipline representing the difference in entropy between G_4 and $G_{4'}$, and a reflected wave RG accounting for the pressure difference at G_3 and $G_{4'}$. The coordinates at G are determined from geometric relations of the intersection of two straight lines, AB and CD. The flow properties (M and θ) at G_1 are established from a characteristic calculation with point A and a point between E and F. The flow Mach numbers at G_1 between waves AG and CG and at G_3 behind wave CD are obtained from linear interpolation of the flow variables at A and B and at C and D, respectively. The oblique shock wave relation is used for both compression wave and shock wave. Since compressive waves converge, one has

$$\theta_2 = \theta_1 - \delta$$

here, δ is the deflection angle found from M_1 and M_2 across the shock.

Since reflected wave RG is usually very weak, one may treat it as an isentropic wave. The Prandtl-Meyer function is then employed to find the flow angle at $G_{4'}$ from properties at G_3. The flow variables at G_4 behind the merged wave GP is determined from oblique shock relation. An iteration procedure is then necessary to determine the Mach number and flow angle at G_4 and $G_{4'}$ from the condition of equality of flow angle and pressure across the slipline GS, which is in a very similar situation as that encountered earlier in triple point solution. The shock is assumed locally straight with constant strength extending from point G up to point P where it intersects with characteristic curve II_n and replaces both points D and B in the flow field. It is to be noted that the variation of this shock strength due to wave coalescence is accounted for in this manner and the existence of the interface

GS is completely ignored afterward.

This is a systematic manner of treating the wave intersection problem since the resulting shock position and strength must be registered and recorded at all times. The flow angles at G_2 and G_3 cannot be determined from linear interpolation as was done for their Mach numbers since the local shock relation might be violated although the difference between these calculations is very minute in all of the flow cases with small characteristic grid. Furthermore, the reflected wave RG inserted into the flow field has the effect of reducing the grid size and increasing the accuracy of computation.

6.3 THE CALCULATION OF INTERACTING FLOW FIELD

Based on an idea similar to that in the two-dimensional over-expanded nozzle flow, the position of Mach disc is unknown and must be solved by an iterative fashion. The correct location and the radius of the Mach disc are determined from the considerations that as a result of the interaction between the waves and the flow fields, the corresponding uniform one-dimensional analysis will give a sonic condition at a throat downstream of the triple point.

The imbedded shock strength from the method described above is checked at every step of calculation toward downstream to see whether or not it satisfies the condition of triple point solution. When this condition is met, the central core flow is then approximated by a uniform one-dimensional treatment and the flow field including the reflected shock wave strength in the supersonic upper part of the slipline is solved by the method of characteristics. Again, the Mach disc stand-off distance is assumed to be zero as has been done in the two-dimensional case.

The very first step along the slipline is taken to be very small and to be a straight line having the slope from the triple point solution. As shown in Fig. 36, the first segment of the slipline TS has the slope tan θ where θ is found from rotation of coordinates ($\theta = \delta_4 - \theta_1$ given in Fig. 4). From the condition of equal pressure along the slipline, the flow Mach numbers M_{u1} and $M_{\ell 1}$ at the end of the first step can be solved from the following isentropic and one-dimensional equations:

$$M_{u1}^2 = \frac{2}{\gamma - 1}\left[\left(1 + \frac{\gamma - 1}{2} M_{uo}^2\right)\left(\frac{P_{u1}}{P_{uo}}\right)^{[-(\gamma-1)]/\gamma} - 1\right] \tag{64}$$

$$\frac{M_{\ell o}}{M_{\ell 1}}\left(\frac{1 + \frac{\gamma - 1}{2} M_{\ell 1}^2}{1 + \frac{\gamma - 1}{2} M_{\ell o}^2}\right)^{[\gamma+1]/[2(\gamma-1)]} - \frac{r_1^2}{r_o^2} = 0 \tag{65}$$

With

$$\frac{P_{u1}}{P_{uo}} = \frac{P_{\ell 1}}{P_{\ell o}} = \frac{P_{\ell 1}/P_{o4}}{P_{\ell o}/P_{o4}} \; ; \quad \frac{P_{\ell 1}}{P_{o4}} = \left(1 + \frac{\gamma - 1}{2} M_{\ell 1}^2\right)^{-[\gamma/(\gamma-1)]}$$

and

$$r_1 = r_o + (x_1 - x_o) \tan \theta$$

The characteristic net layout for the subsequent step-by-step calculation is shown in Fig. 37. The flow properties are known at T and S_1 from previous results. The flow variables at R_1 where characteristics of family II and the reflected shock intersect are found from solving the characteristic equations for family II and the oblique shock wave equations simultaneously as presented in APPENDIX C. This must be done in an iterative manner. One added unknown during the iteration procedure is the flow condition in front of the reflected shock wave which is

obtained through an interpolation procedure. As shown in Fig. 38, if R_1 lies inside the characteristic grid ABCD, then the Mach number and flow angle in front of the reflected shock can be approximated from linear interpolation:

$$M^*_{R_1} = \frac{\frac{M^*_a}{a} + \frac{M^*_b}{b} + \frac{M^*_c}{c} + \frac{M^*_d}{d}}{\frac{1}{a} + \frac{1}{b} + \frac{1}{c} + \frac{1}{d}} \tag{66}$$

$$\theta_{R_1} = \frac{\theta_a + \theta_b + \theta_c + \theta_d}{\frac{1}{a} + \frac{1}{b} + \frac{1}{c} + \frac{1}{d}} \tag{67}$$

Near the free jet boundary the grid can be triangular instead of quadrangular, and a corresponding modified form consisting of only three characteristic points should be used.

The need for the properties in determining the flow variables upstream of the reflected shock wave indicates one of the reasons that the characteristic net must be stored and registered. The method shown above for non-uniform approaching flow is the extension of the well known technique for determining the shock wave location shown in Fig. 17.21 [31] for uniform free stream conditions.

Figure 39 illustrates how the location where reflected shock interacts with the free jet boundary is determined. When the coordinates of the point on the reflected shock are found to lie outside of the free jet boundary, the point of intersection between the shock and the free jet is found from the intersection of two straight lines, AB and CD, as shown in Fig. 39. The flow angle in front of shock wave is found from linear interpolation between points A and B, and the Mach number is that of the free jet boundary. The oblique shock wave relations are then

employed to obtain the flow properties behind the reflected shock wave subsequently followed by a P-M expansion.

Similar to that of a two-dimensional problem, the slipline point procedures are governed by the following equations:

$$\frac{r_r^2}{r_{3\ell}^2} = \frac{Q(M_r)}{Q(M_{3\ell})} \tag{68}$$

$$\left(\frac{P_{04}}{P_{03}}\right)^{[(\gamma-1)/\gamma]} = \frac{1 - \frac{\gamma - 1}{\gamma + 1} M_{3u}^{*2}}{1 - \frac{\gamma - 1}{\gamma + 1} M_{3\ell}^{*2}} \tag{69}$$

$$\frac{r_{3u} - r_{2u}}{x_{3u} - x_{2u}} = \tan \bar{\theta}_{23} \tag{70}$$

$$\frac{r_{3u} - r_{1u}}{x_{3u} - x_{1u}} = \tan (\bar{\theta}_{13} - \bar{\alpha}_{13}) \tag{71}$$

$$\frac{M_{3u}^* - M_{1u}^*}{\bar{M}_{13}^*} = -(\theta_3 - \theta_1) \tan \bar{\alpha}_{13} + \sin^2 \bar{\alpha}_{13} \frac{1}{\gamma} \ln \left[\frac{P_{03u}}{P_{01u}}\right] + \frac{\tan^2 \bar{\alpha}_{13} \tan \bar{\theta}_{13}}{\tan \bar{\theta}_{13} - \tan \bar{\alpha}_{13}} \frac{r_3 - r_1}{\bar{r}_{13}} \tag{72}$$

where Q(M) is given in Eq. (45). The simultaneous solution of these equations will give the flow variables across the slipline.

6.4 RESULTS AND DISCUSSIONS

The analysis presented above for the underexpanded axisymmetric nozzle flow is programmed successfully on an IBM system 360/75 digital computer using double precision mode. A single successful run of the Fortran IV program takes less than four minutes computation time. For the convenience of reference, Fig. 40 illustrates the free jet Mach

numbers and pressure ratios. Also shown in the same figure is the corresponding ratio of ambient pressure to nozzle stagnation pressure at different nozzle exit to ambient pressure ratios.

Figure 41a illustrates the results of iteration for determining the Mach disc location for the case of $M_e = 2.0$, $P_e/P_a = 6.39$ ($P_a/P_{oe} = 0.02$) disregarding the effect of vorticity for N = 20 where N denotes the number of uniformly spaced waves initiated from the initial Mach line. The early insertion of the Mach disc, for example at x = 11.86, will cause the slipline bending continuously upward yielding only subsonic states in the downstream flow field. On the other hand, the insertion of the Mach disc at x = 12.025 will cause the central core flow reaching a sonic condition where the area is not a minimum. The correct location of the Mach disc for this flow situation stands at $x \simeq 12.00$. It is obvious that the flow field is very sensitive to the location of the Mach disc; a slight change in the location of the Mach disc will result in a tremendously different flow pattern downstream.

It has been mentioned previously that because of the enormous difference in stagnation pressure behind the curved imbedded incident and the reflected shock waves, the rotationality cannot be neglected in this study. Indeed, inclusion of the vorticity into the consideration results in a sizable shift in the location of the Mach disc. Figure 41b gives a comparison of the numerical results of the flows with and without vorticity for the case of $M_e = 2.0$, $P_e/P_a = 6.39$ ($P_a/P_{oe} = 0.02$) for N = 20. These results clearly demonstrate the inadequacy of the treatment ignoring the vorticity which gives a much smaller Mach disc standing farther away from nozzle exit. In all of

the following results, rotationality has been included in the considerations.

These improved calculations with vorticity, however, exhibit a somewhat unexpected phenomenon. In the determination of the sonic state in central core, the flow angle does not vanish and thus the area is not a minimum. Moving the Mach disc toward downstream will result in a steeper flow angle at sonic condition. On the other hand, no triple point solution is possible for early occurrence of the Mach disc. Presumably, this is because of small inaccuracies in the upstream numerical calculation. The reason is twofold: First, the linear interpolation used here in the characteristic grid is not accurate enough to handle the rapid change in shock strength near the triple point where the flow variables depend sensitively on the incident shock strength. Secondly, the change in stagnation properties through the variation of the entropy gradient term is based on the interpolating properties from known states, and is, therefore, dependent on the location of streamline passing through the unknown state (see APPENDIX C). When the streamline location and direction at the unknown state have different values from those found from linear interpolation, the entropy gradient term will not be calculated correctly. This influence is more pronounced at or near the occurrence of the triple point where the deflection angle of the shock changes rapidly. Taking these circumstances into consideration, the results presented for flow with vorticity will be considered as the upper limit of the location of the Mach disc.

A typical characteristic wave pattern in physical scale from the actual computation of $M_e = 1.5$, $P_e/P_a = 5.0$, $N = 30$ is given in Fig. 42.

The location and strength of the imbedded incident shock resulting from the coalescence of the compression waves are computed automatically by digital computer from the method described before whenever waves intersection occurs.

In all the calculations of this study for M_e = 1.5, 2.0, 2.5, and 3.0, the sonic state of the central core flow is reached before the appearance of the P-M fan which results from the intersection of the reflected shock with the free jet boundary. The computation is stopped at the place where the sonic state of the lower side of slipline is determined. This explains the unfinished calculation of the reflected shock and its downstream flow field which should be in a supersonic state and does not have any influence on the already established Mach disc and upstream flow field although the calculation of whole downstream field including P-M fan is well programmed and is incorporated in the same Fortran code.

Some of the free jet boundaries and shock wave patterns for M_e = 1.5 and 2.5 are shown in Fig. 43 and Fig. 44. It is evident that higher pressure ratios (P_e/P_a) for a given nozzle Mach number would result in larger Mach discs at farther downstream locations. At the same pressure ratio, however, a reduced nozzle Mach number brings Mach disc closer to the nozzle exit plane.

Figures 45 and 46 show the distributions of various flow properties for N = 30 at M_e = 2.0, P_e/P_a = 3.195 (P_a/P_{oe} = 0.04), and at M_e = 3.0, P_e/P_a = 5.0 (P_a/P_{oe} = 0.005445), respectively. All the stagnation pressures are normalized by nozzle stagnation pressure. The stagnation pressure behind the incident shock drops rapidly near the triple p

which is a consequence of the accumulated compressive effect on the gas jet. Immediately behind the reflected shock, however, the stagnation pressure increases and deviates away from the constant stagnation pressure on the upper side of slipline. All of these signify that the rotationality certainly needs to be included in the considerations.

The differences in Mach numbers and in flow angles between the states in front of the incident shock and the centerline of symmetry decrease along the flow direction and are very close to zero in front of the Mach disc. This demonstrates that the flow in the very front of Mach disc is rather uniform for the cases shown in Figs. 45 and 46. On the contrary, the differences in Mach numbers and in flow angles in front of and behind the incident shock are obviously increasing toward downstream illustrating the growth of shock strength and, eventually, reaching the state where the triple point solution is able to be satisfied.

The trace of the imbedded shock appears when the reflected compressive wave from the free jet boundary first intersects with the last P-M characteristic wave from the lip of the nozzle. In this numerical study, the position where discernible shock wave originates is given in Fig. 47 when P-M fan at the lip of the nozzle has been divided into approximately one-degree increments. The location where the imbedded shock wave has the maximum radius is shown in Fig. 48. Figure 49 gives the physical coordinates where the free jet boundary has the maximum height. Shown in the same figure are some calculated data at $P_e/P_a = 10$ from [16] using the fold-back method which agrees perfectly with the results of the present investigation. At the same pressure ratio (P_e/P_a) higher nozzle Mach numbers always produce wider gas jet profiles with maximum

width occurring farther downstream.

The Mach disc location and radius are presented in Fig. 50. Some experimental data from Love and Grigsby [16] are also shown in the same figure for comparison. Since the characteristic grid size is finite in the numerical calculations, it is, therefore, apparent that the actual Mach disc will occur earlier because of the faster growing shock strength associated with the intersection of infinite number of waves. For the same reason, the Mach disc of the numerical calculation appears shorter than the actual one does. For higher nozzle Mach number and far away from the initial characteristic line, the characteristic grid size becomes quite large which further explains the overestimation in the x-coordinate of the Mach disc location. On the other hand, at lower pressure ratios, the Mach disc is very small and the characteristic net near centerline of symmetry is usually not fine enough to produce good results near the triple point and tends to underestimate the radius of the Mach disc. Both effects are more pronounced at higher nozzle Mach numbers.

Table 16 illustrates the effect of changing the number of initial grid divisions (N) on the calculated results. The larger value of N corresponds to finer initial grid size. As indicated in the table, the use of larger N does not necessarily give better results compared with experimental data. The finer the initial grid, the more iterations are needed, and the accumulated numerical errors might aggravate the final answer. All of the calculated results show that N = 25 or 30 is a fairly good choice for the number of divisions on the initial characteristic line.

Another manner of getting more accurate results is the insertion of

extra field points into the flow field whenever the grid size is detected to be larger than a predetermined value. This will create smaller characteristic grids in downstream field without imposing a large value of N on the initial characteristic line and will probably eliminate unnecessary growth of numerical errors. However, this will somewhat complicate the programming work especially when all the wave coalescences are to be considered.

One of the salient features in most of the calculations is that the slipline tends to go upward first in the vicinity of triple point and then bends downward decreasing gradually to reach a minimum height at the throat (for example, see Fig. 42). Figure 51 shows the approximate coordinates of the throat as found from numerical results when the center core flow behind the Mach disc is close to sonic state.

Finally, Fig. 52 reveals the information necessary for finding the properties at the triple point. The results are so given that the triple point solutions of Figs. 5 through 9 (or Tables 1 through 13) can be found easily from the corresponding M_1 and δ_2 given in Fig. 52. From the computed data, it is noted that the Mach disc occurs in the very neighborhood of the limiting case of curve δ_{n4} in Fig. 10a. Unlike the two-dimensional overexpanded flow, the incident flow angle θ_i (see Fig. 3) is not zero at the triple point in these underexpanded gas jets, and the interpretation of the angular relationship associated with the triple point solution must take this inclination, θ_i, into proper account.

7. CONCLUDING REMARKS

Based on the numerical results obtained through extensive calculations on problems with Mach reflection or Mach disc; it may be concluded that:

1. The one-strip method of integral relations and the method of characteristics, together with the one-dimensional isentropic nozzle analysis for the downstream part of the central core, are useful to give a more detailed description of the Mach reflection pattern from the two-dimensional overexpanded nozzle flows with weak reflected shock at the triple point. Their application to strong reflected shock is not successful.
2. The approximate method to estimate the Mach stem height for the two-dimensional overexpanded flow problems, which was originally developed for flow cases with strong reflected shocks, would give meaningful results even if the reflected shock at the triple point were weak.
3. For axially symmetric gas flow with Mach disc, the vorticity must be taken into account. The wave interactions, including their coalescence into shock waves within the jet flow field, are extremely complicated; accurate calculations seem to be difficult, if not impossible, to achieve.
4. Although the viscous effects tend to modify and influence the ultimate flow patterns, it is believed that the inviscid investigation of these problems is already yielding fruitful results.

FIGURES AND TABLES

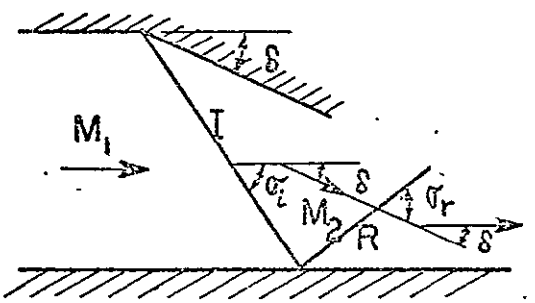

Figure 1a Pattern of Regular Reflection

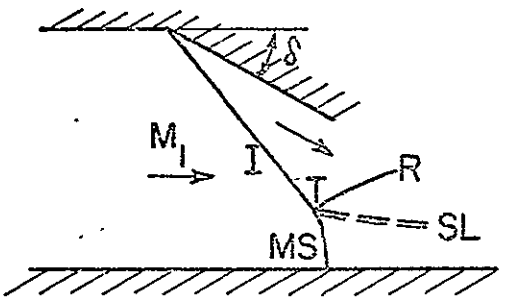

Figure 1b Pattern of Mach Reflection

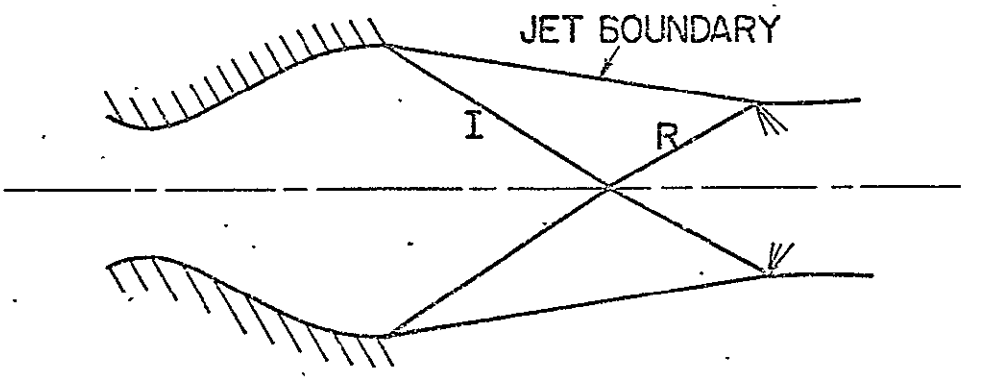

Figure 2a Regular Reflection produced from Two-Dimensional Overexpanded Nozzle Flow

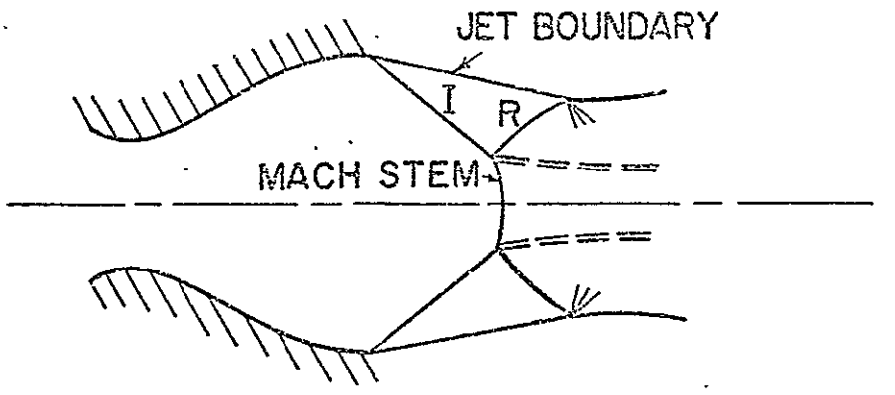

Figure 2b Mach Reflection produced from Two-Dimensional Overexpanded Nozzle Flow

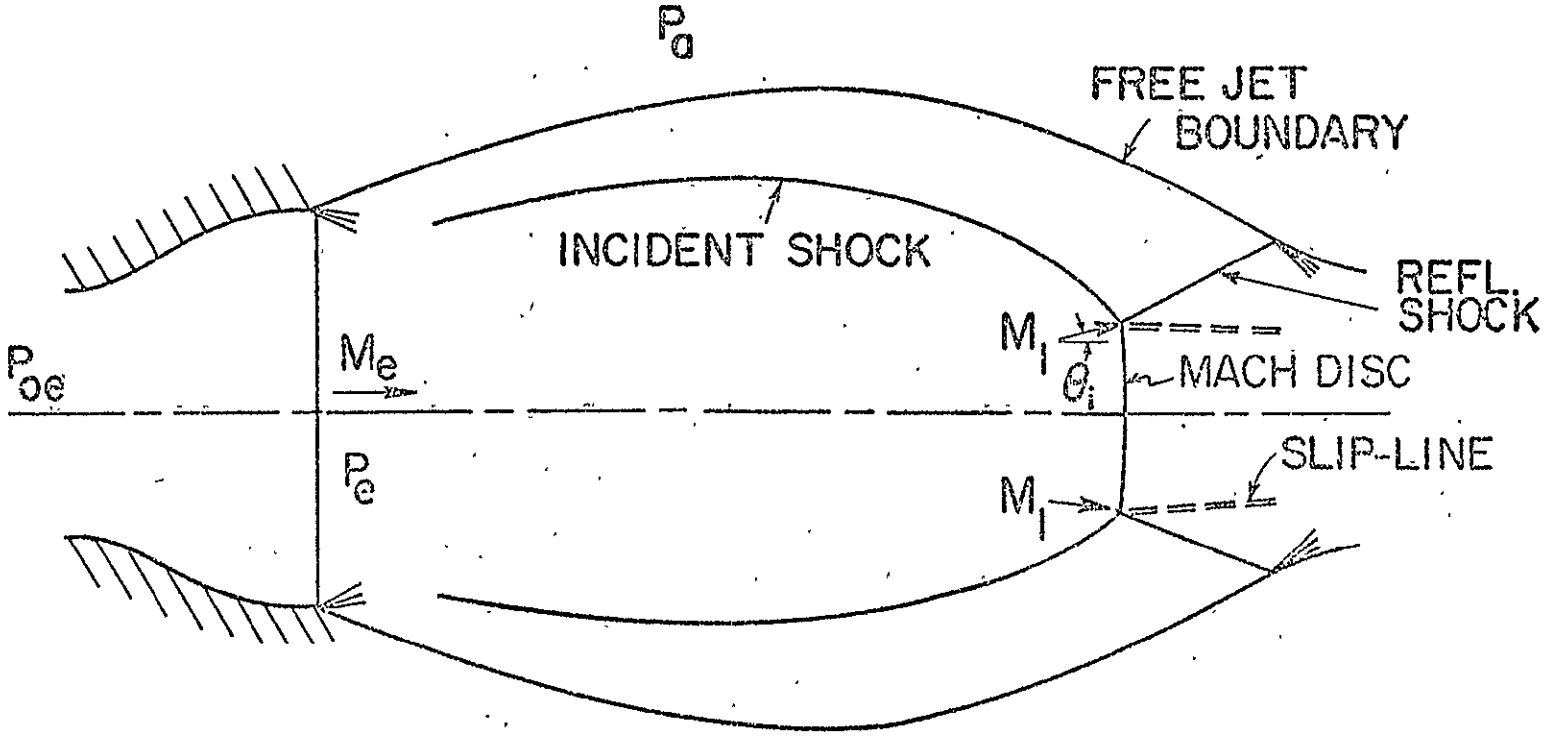

Figure 3 Mach Disc produced from Axisymmetric Underexpanded Nozzle Flow

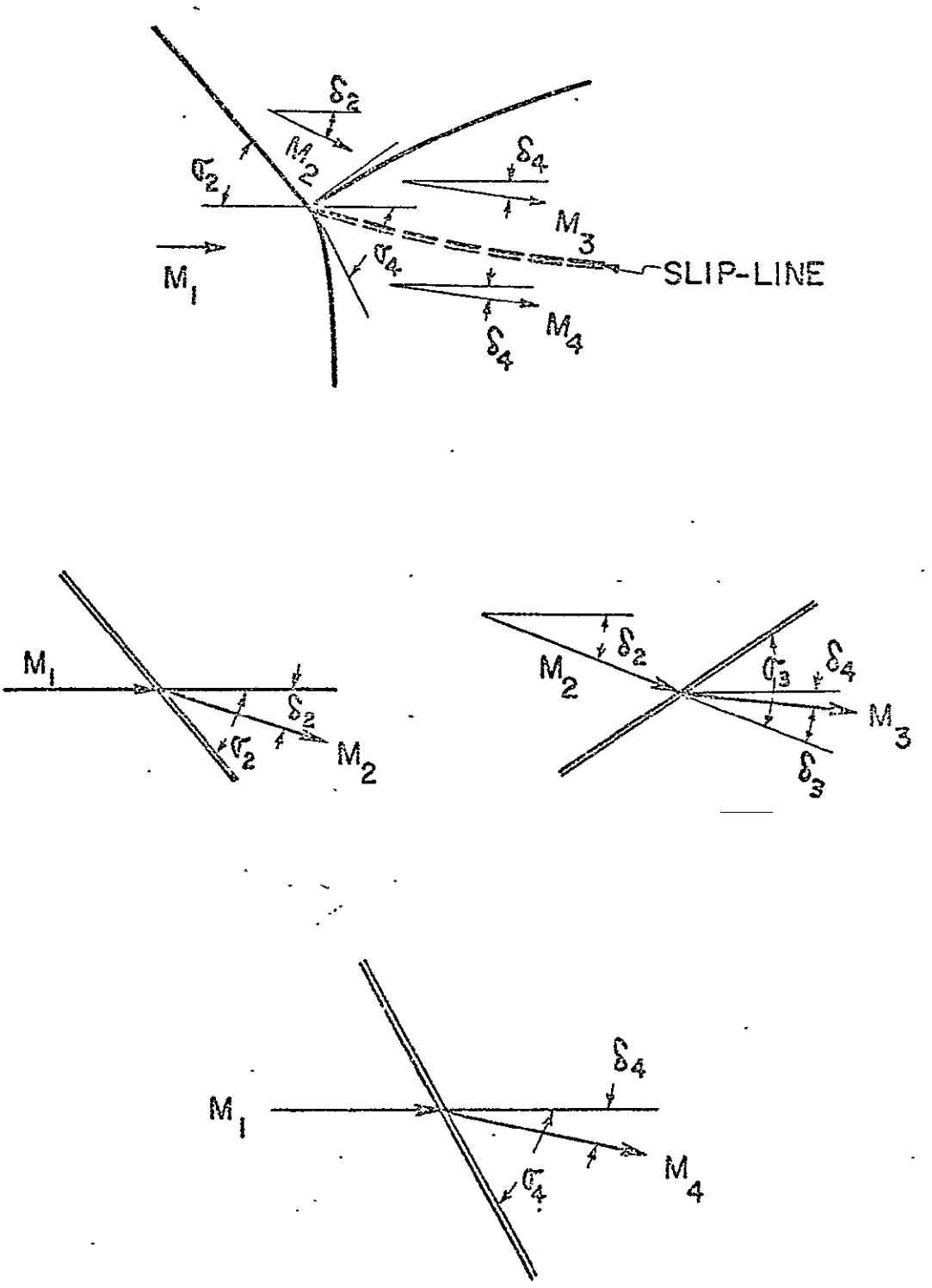

Figure 4 Triple Shocks Intersection of Mach Reflection from Nozzle Flows

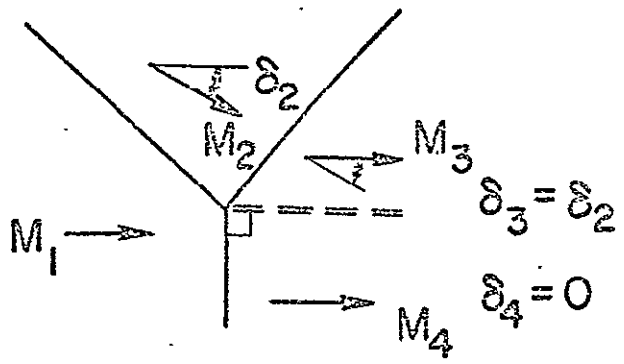

Figure 4a Limiting Case of Triple Shocks Intersection ($\sigma_4 = 90°$)

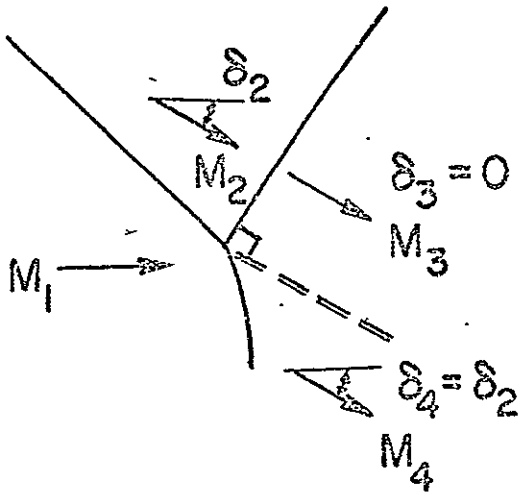

Figure 4b Limiting Case of Triple Shocks Intersection ($\sigma_3 = 90°$)

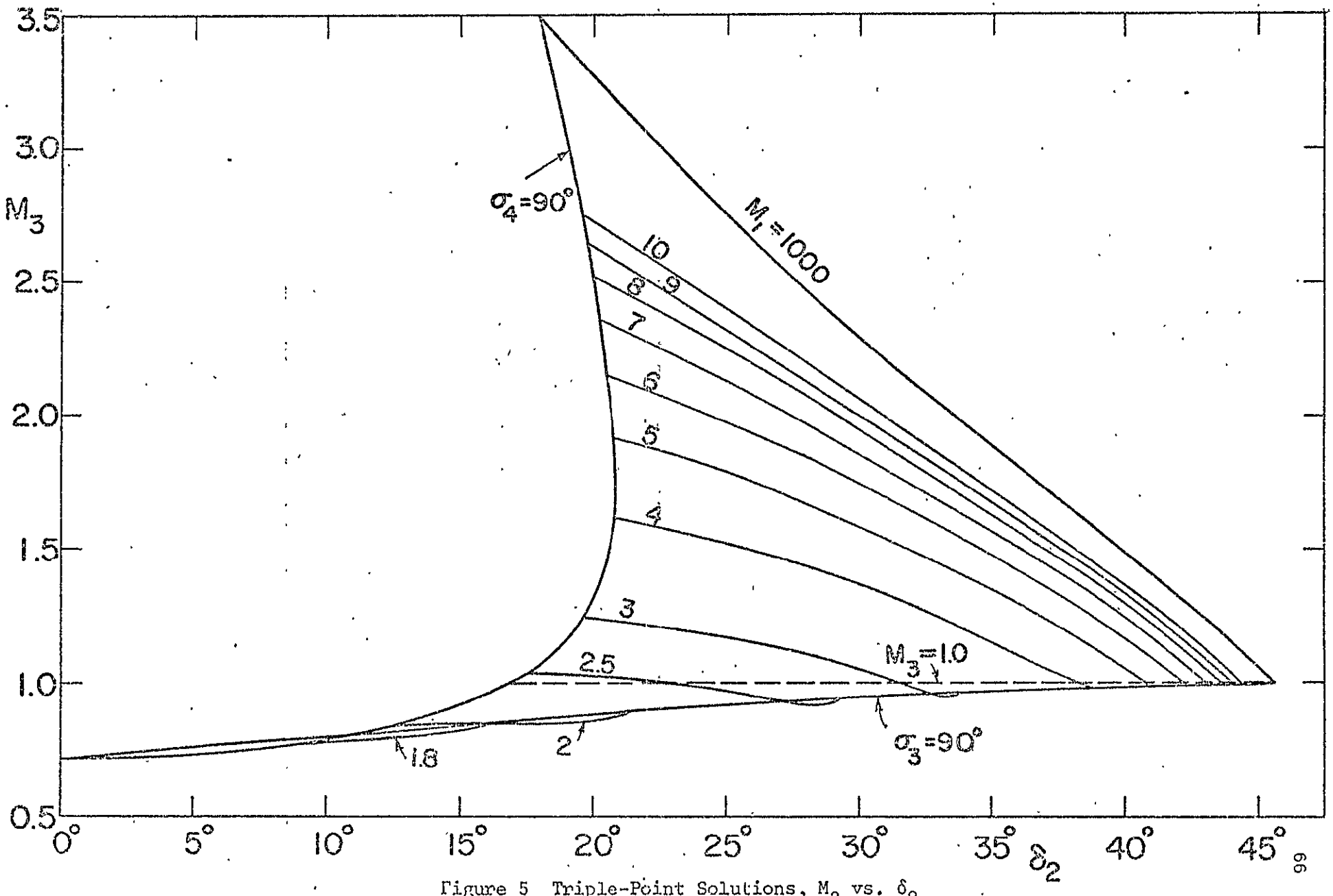

Figure 5 Triple-Point Solutions, M_3 vs. δ_2

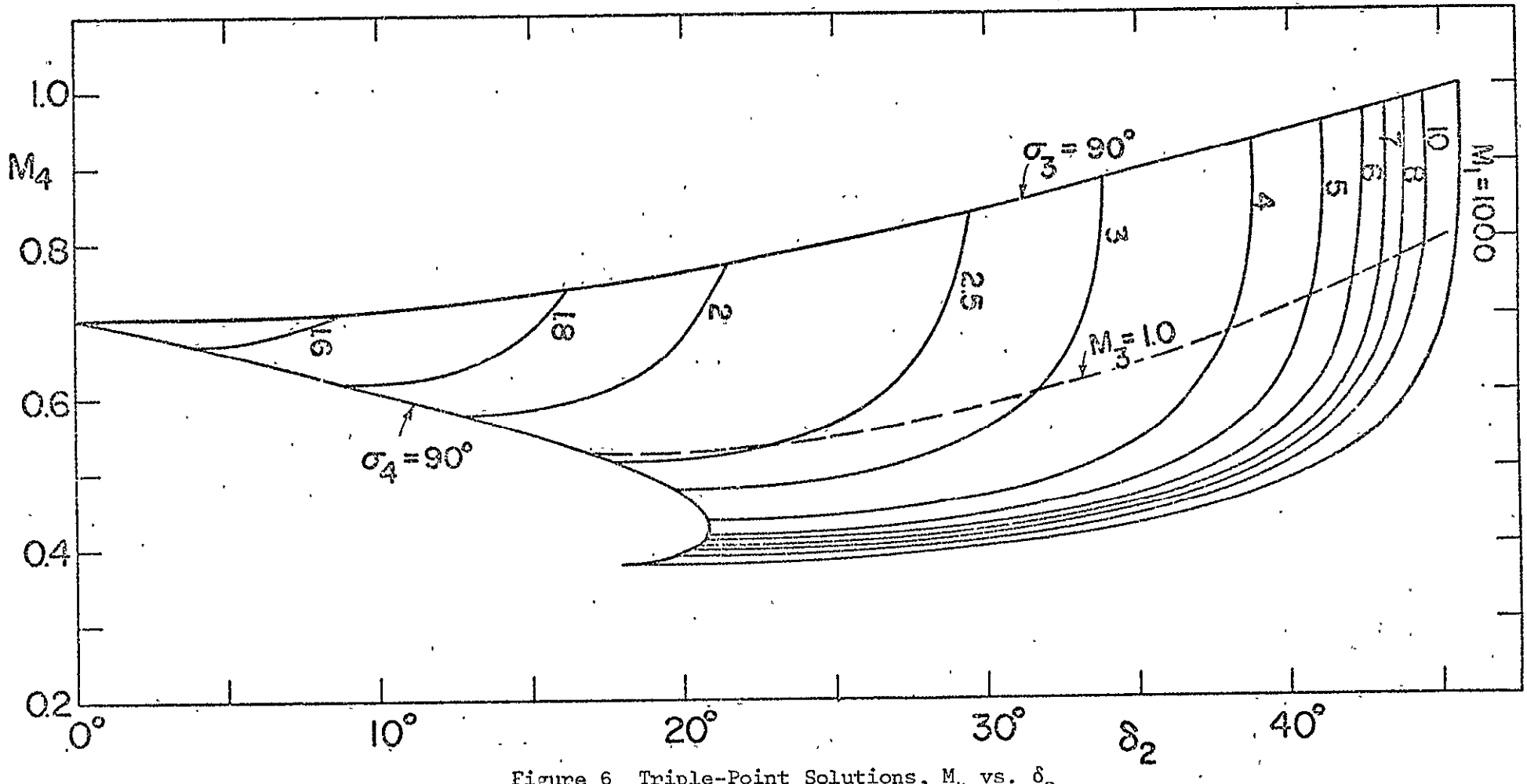

Figure 6 Triple-Point Solutions, M_4 vs. δ_2

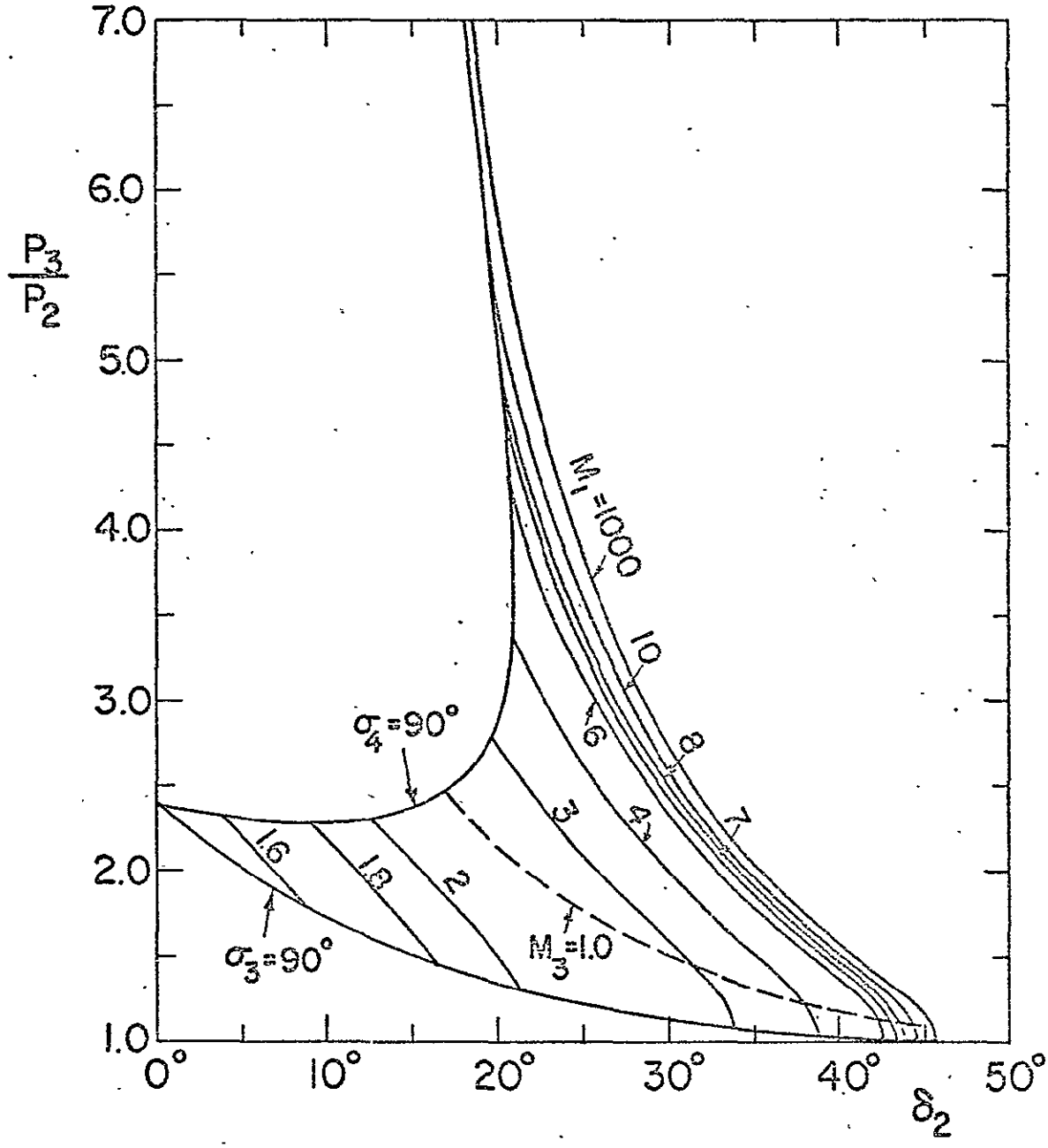

Figure 7 Triple-Point Solutions, P_3/P_2 vs. δ_2

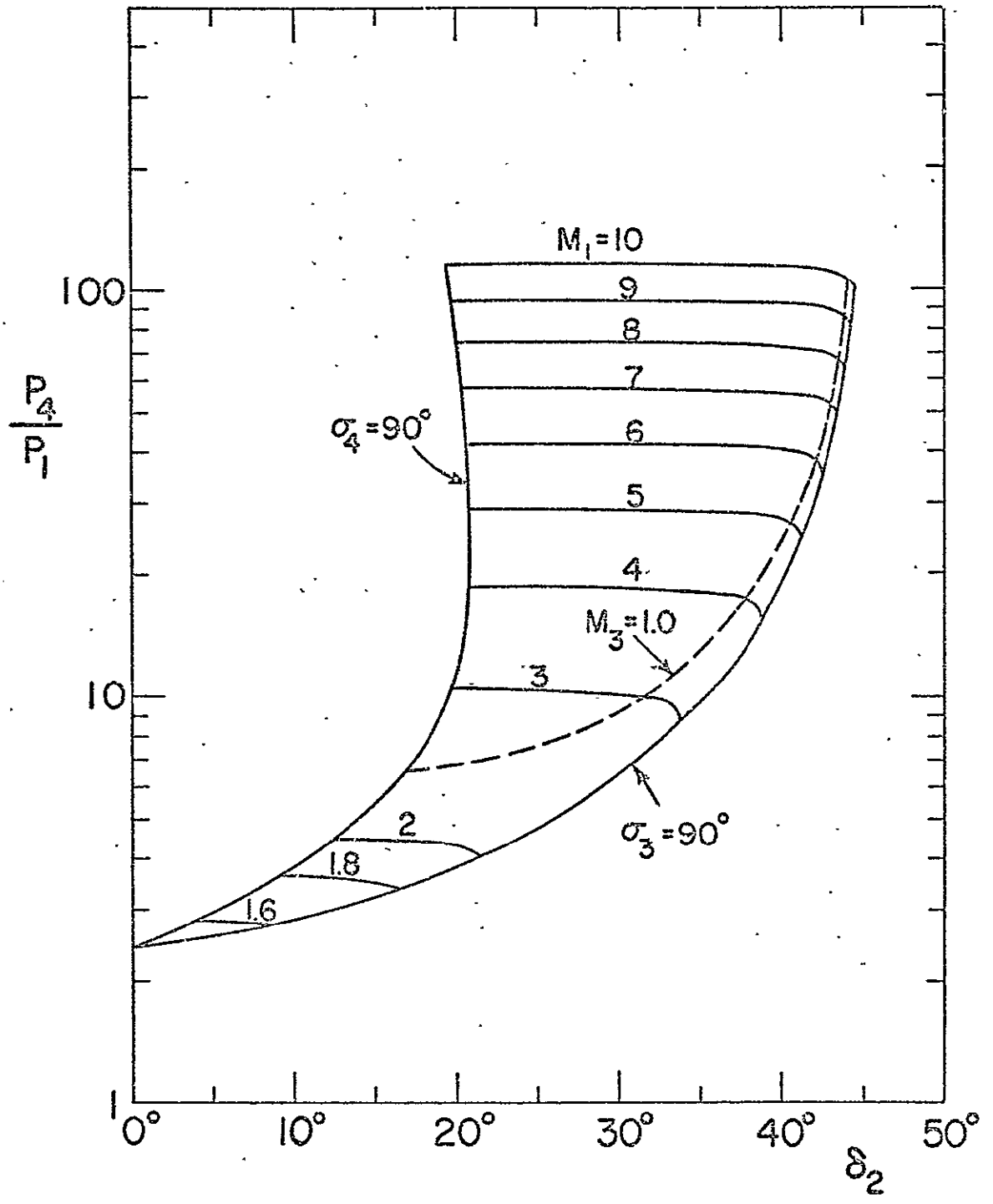

Figure 8 Triple-Point Solutions, P_4/P_1 vs. δ_2

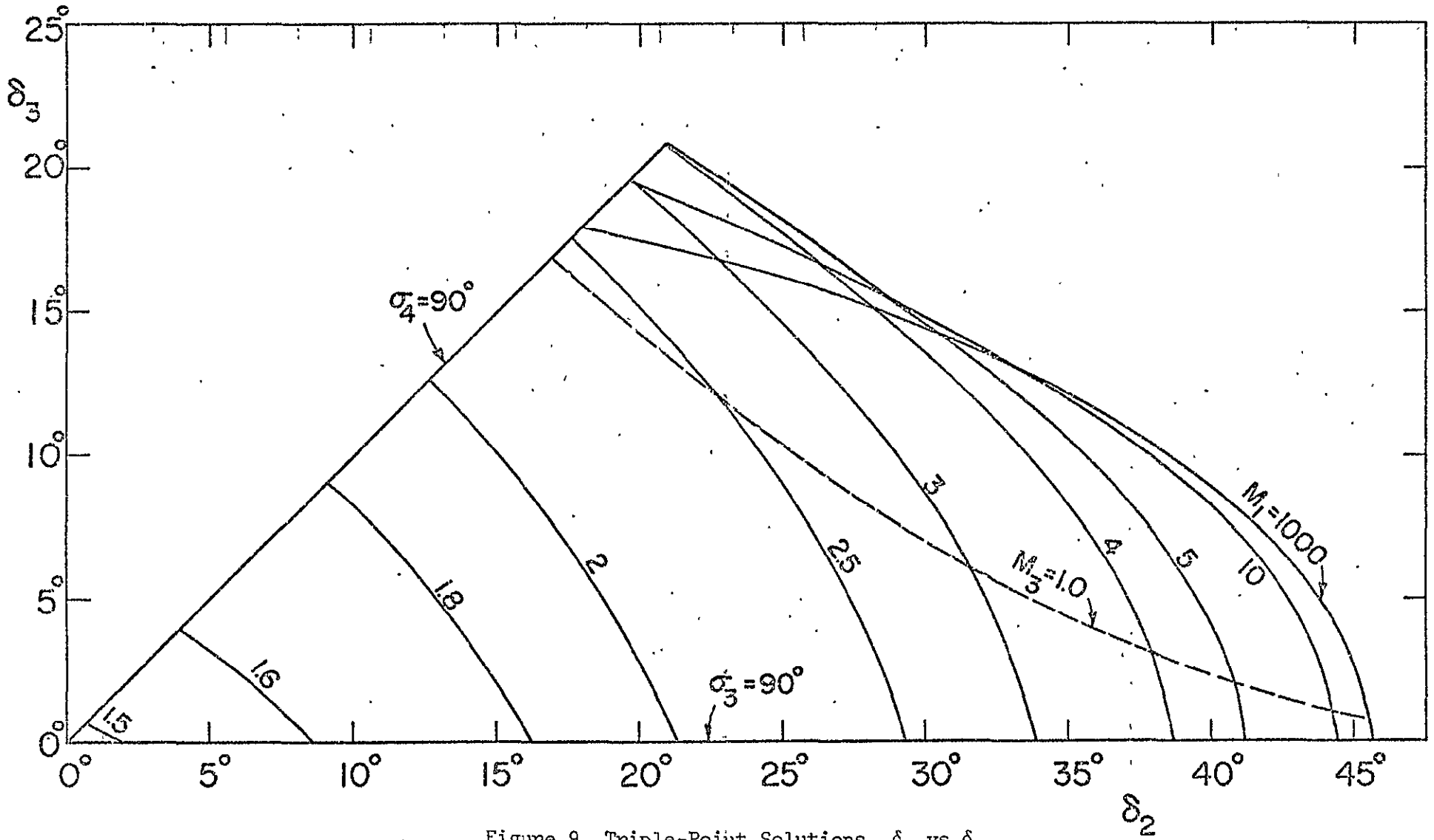

Figure 9 Triple-Point Solutions, δ_3 vs. δ_2

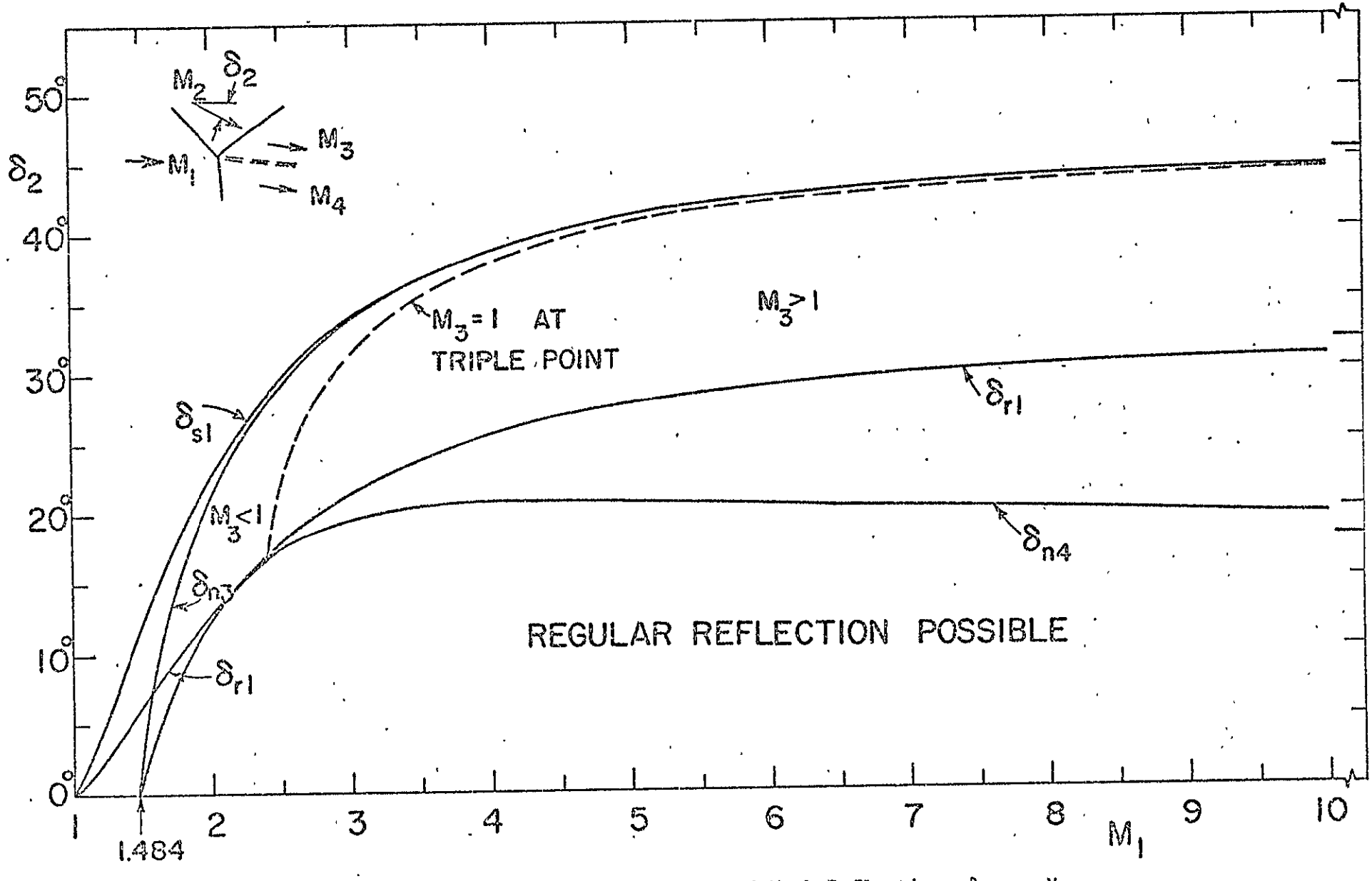

Figure 10a Regions of Regular and Mach Reflection, δ_2 vs. M_1

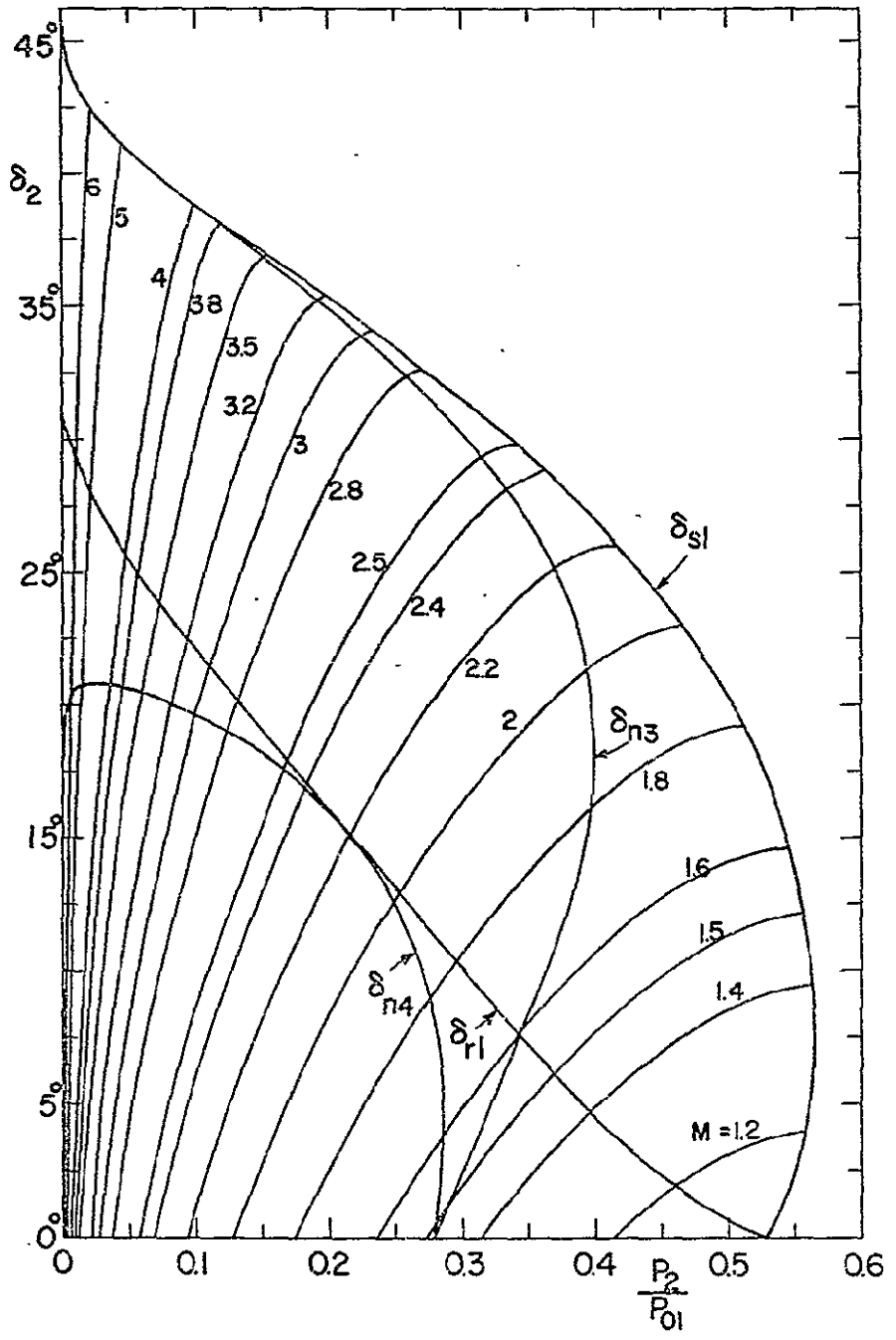

Figure 10b Jet Deflection Angle δ_2 vs. Pressure Ratio P_2/P_{01}

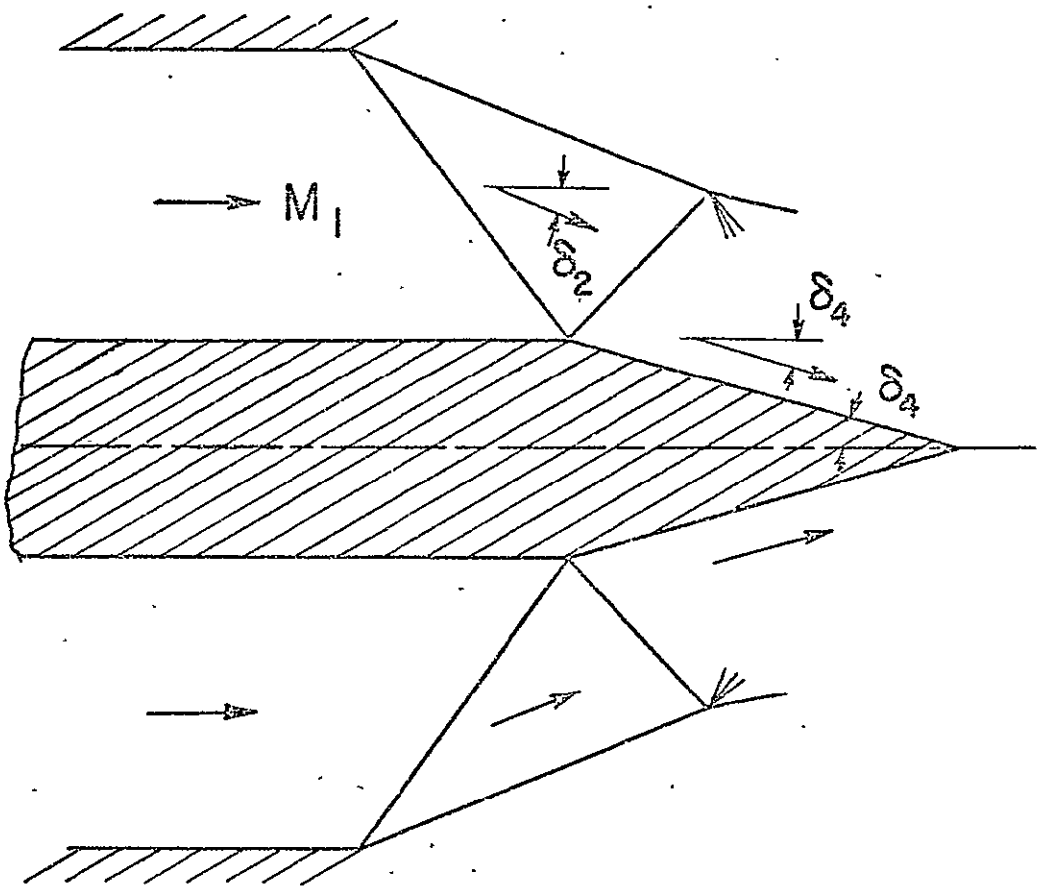

Figure 11 Oblique Reflection of Shock Wave from the Central Plug at a Nozzle Exit

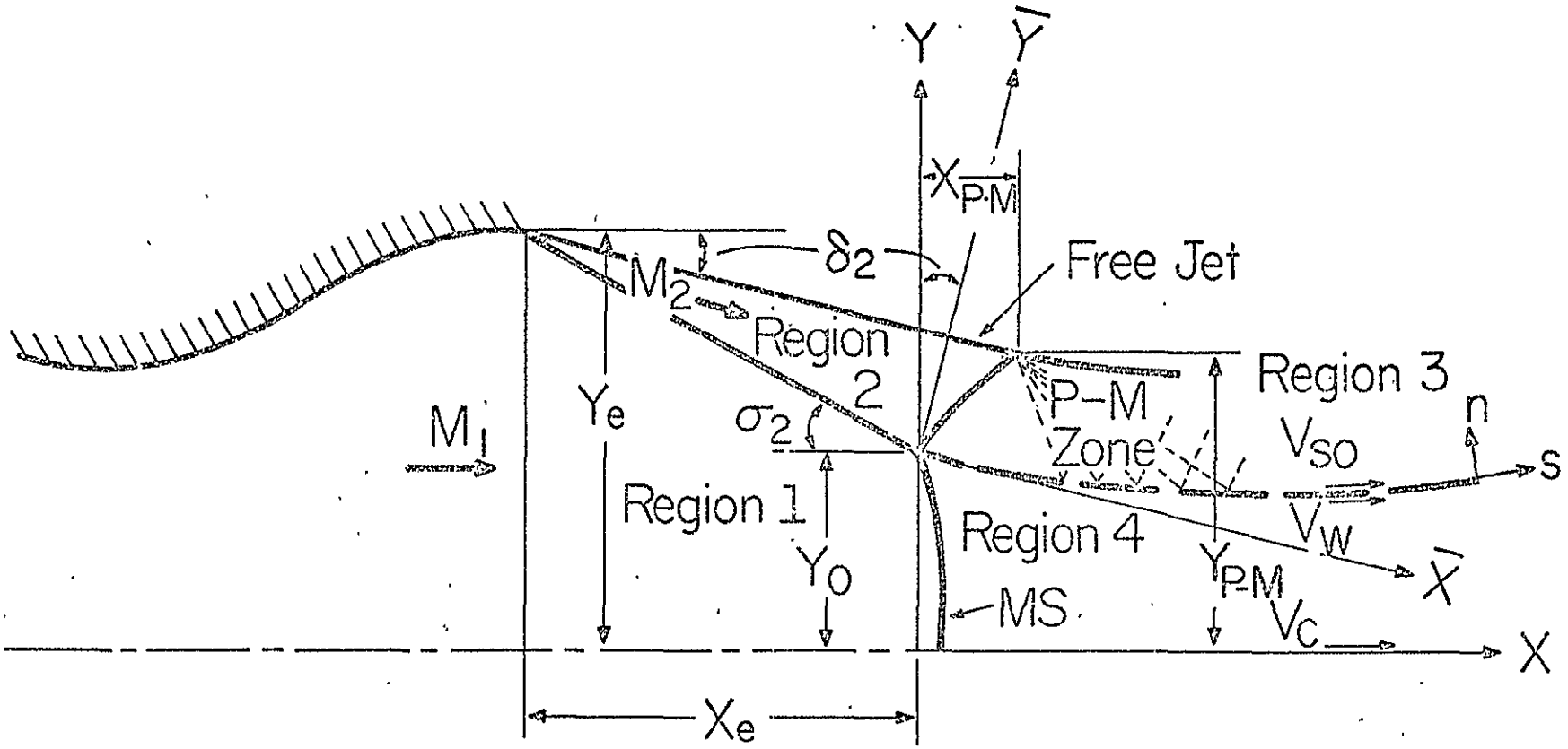

Figure 12 Detailed Figure for Mach Reflection from Two-Dimensional Overexpanded Nozzle Flow

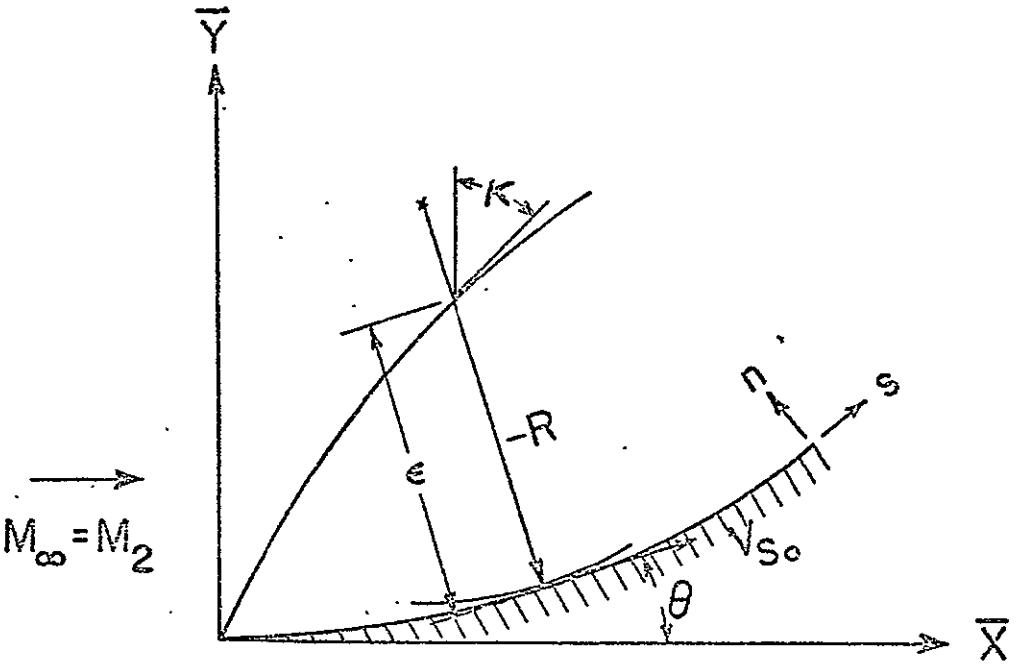

Figure 13a Isolated Region for Upper Part of Slipline (External Flow)

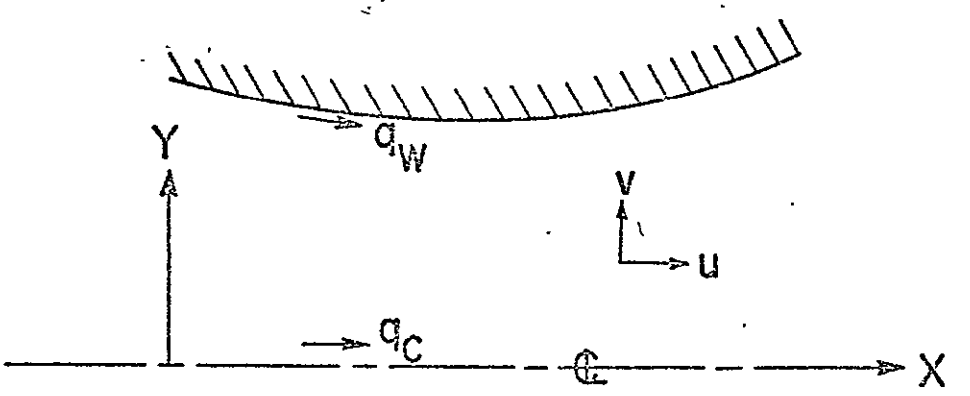

Figure 13b Isolated Region for Lower Part of Slipline (Internal Flow)

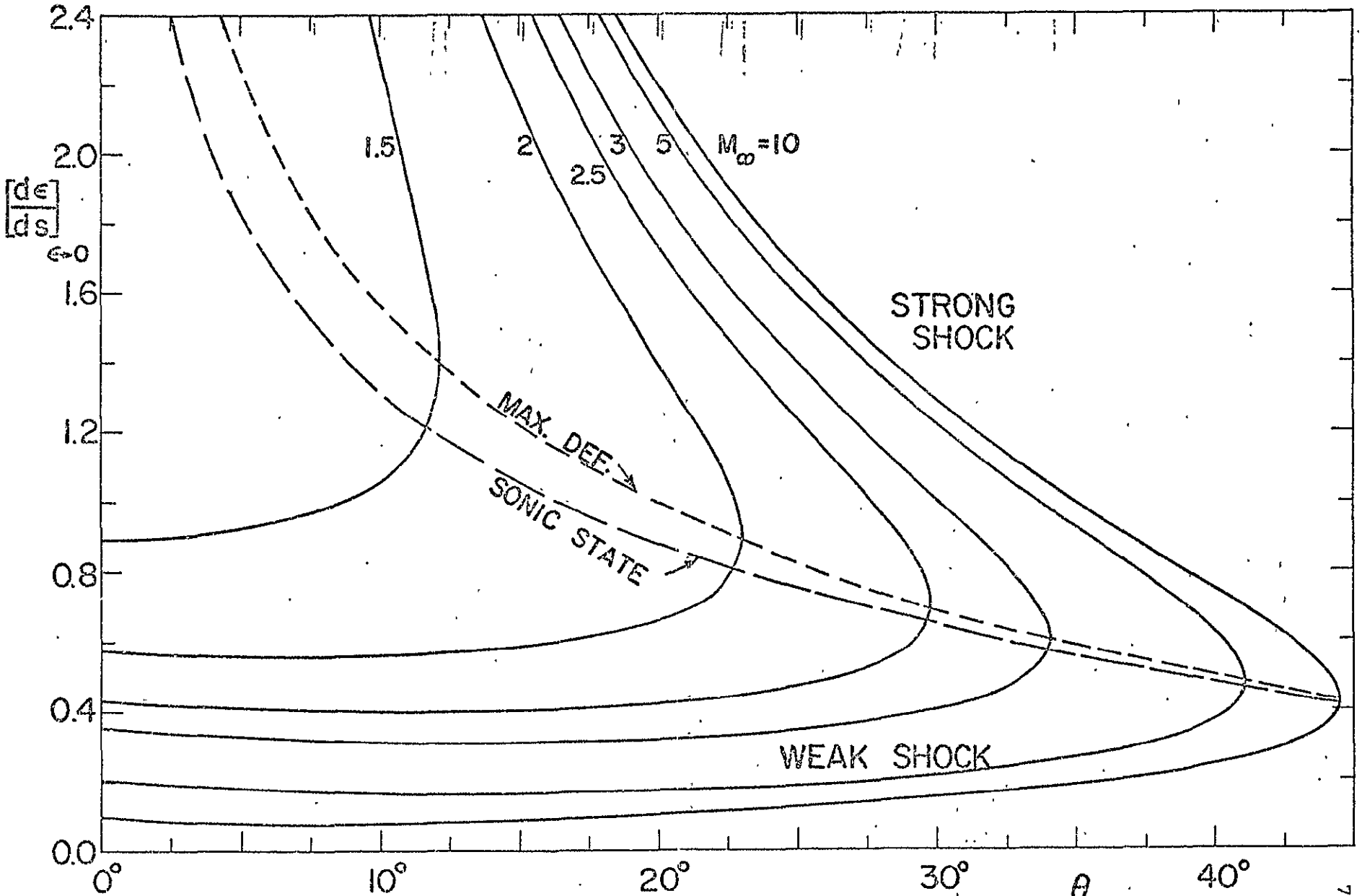

Figure 14 Plot of Eq. (28) for Attached Shock Wave, $\left.\frac{d\epsilon}{ds}\right|_{\epsilon \to 0}$ vs. θ

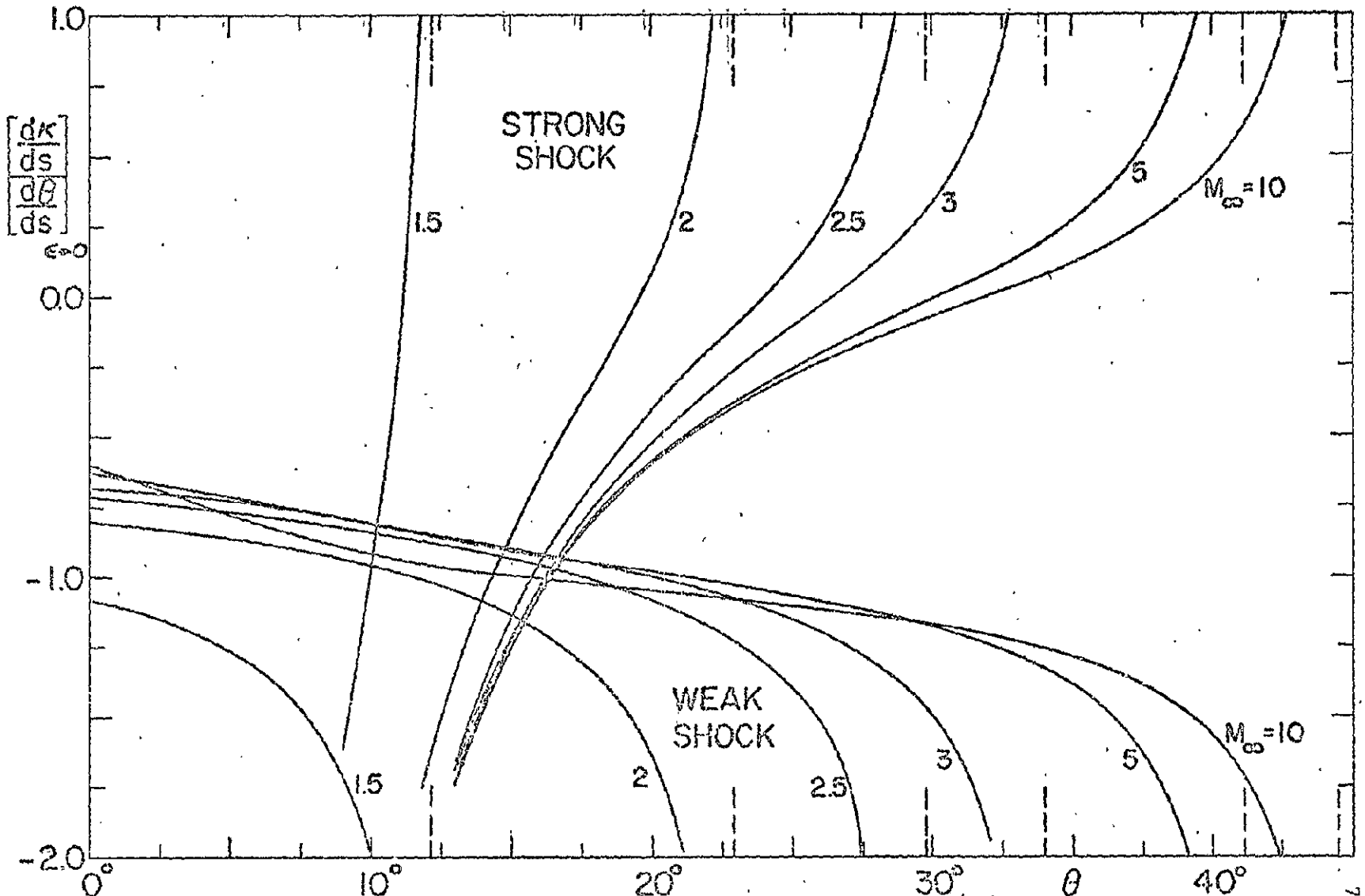

Figure 15 Plot of Eq. (29) for Attached Shock Wave, $\frac{dK}{ds}\Big/\frac{d\theta}{ds}\Big|_{\varepsilon \to 0}$ vs. θ

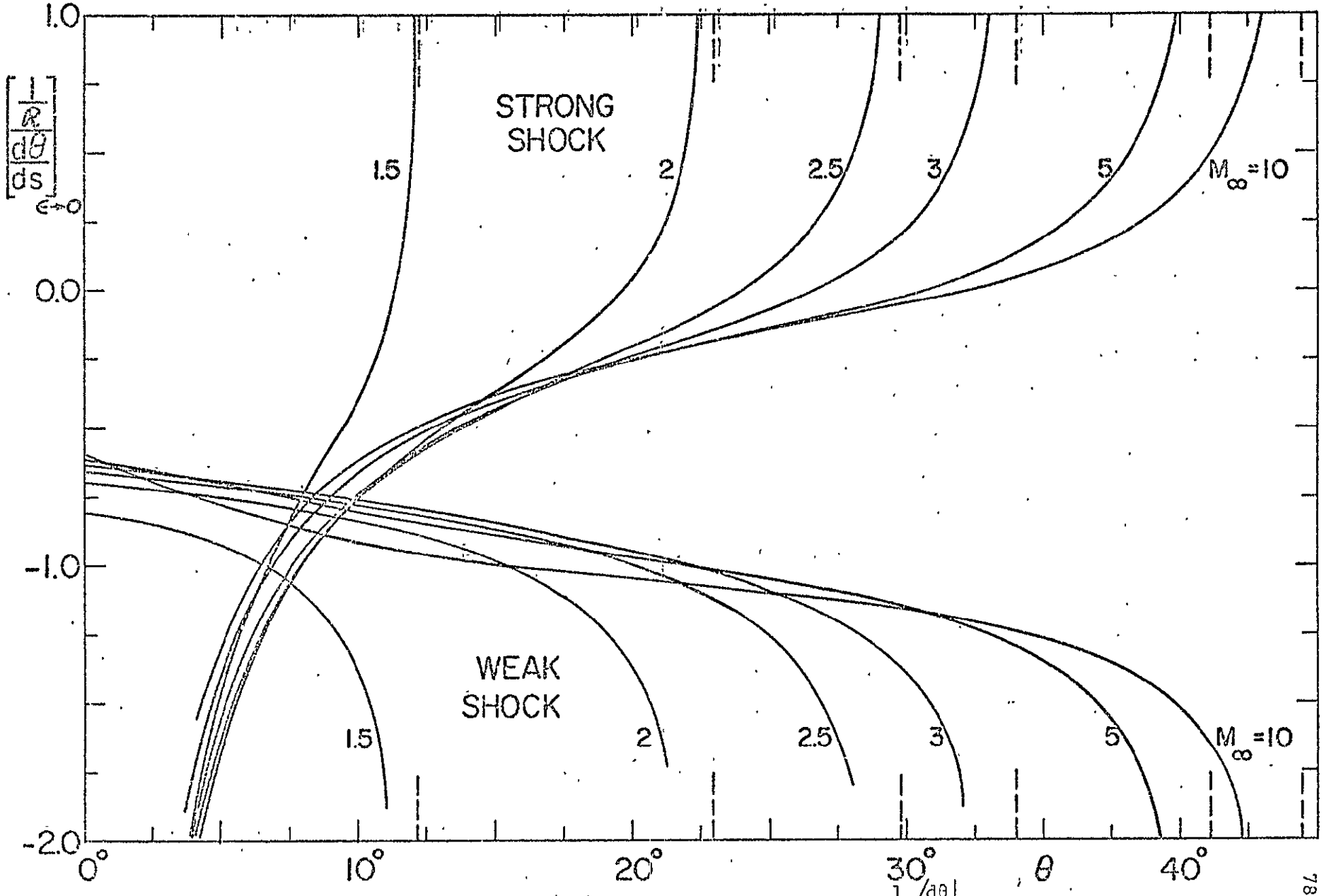

Figure 16 Plot of Eq. (30) for Attached Shock Wave, $\frac{1}{R}\left/\frac{d\theta}{ds}\right|_{\epsilon \to 0}$ vs. θ

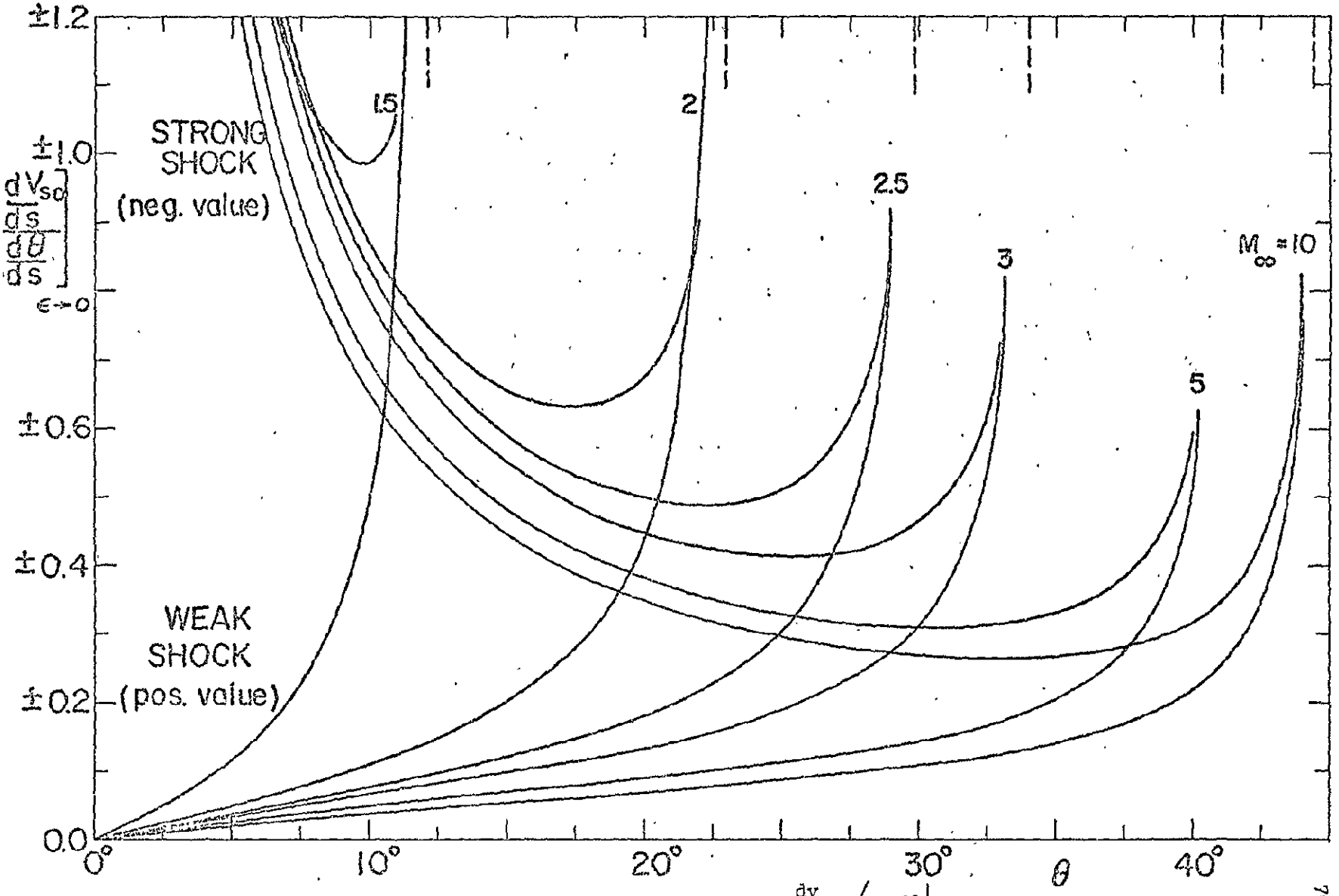

Figure 17 Plot of Eq. (31) for Attached Shock Wave, $\frac{dv_{so}}{ds}\Big/\omega_\infty \frac{d\theta}{ds}\Big|_{\varepsilon \to 0}$ vs. θ

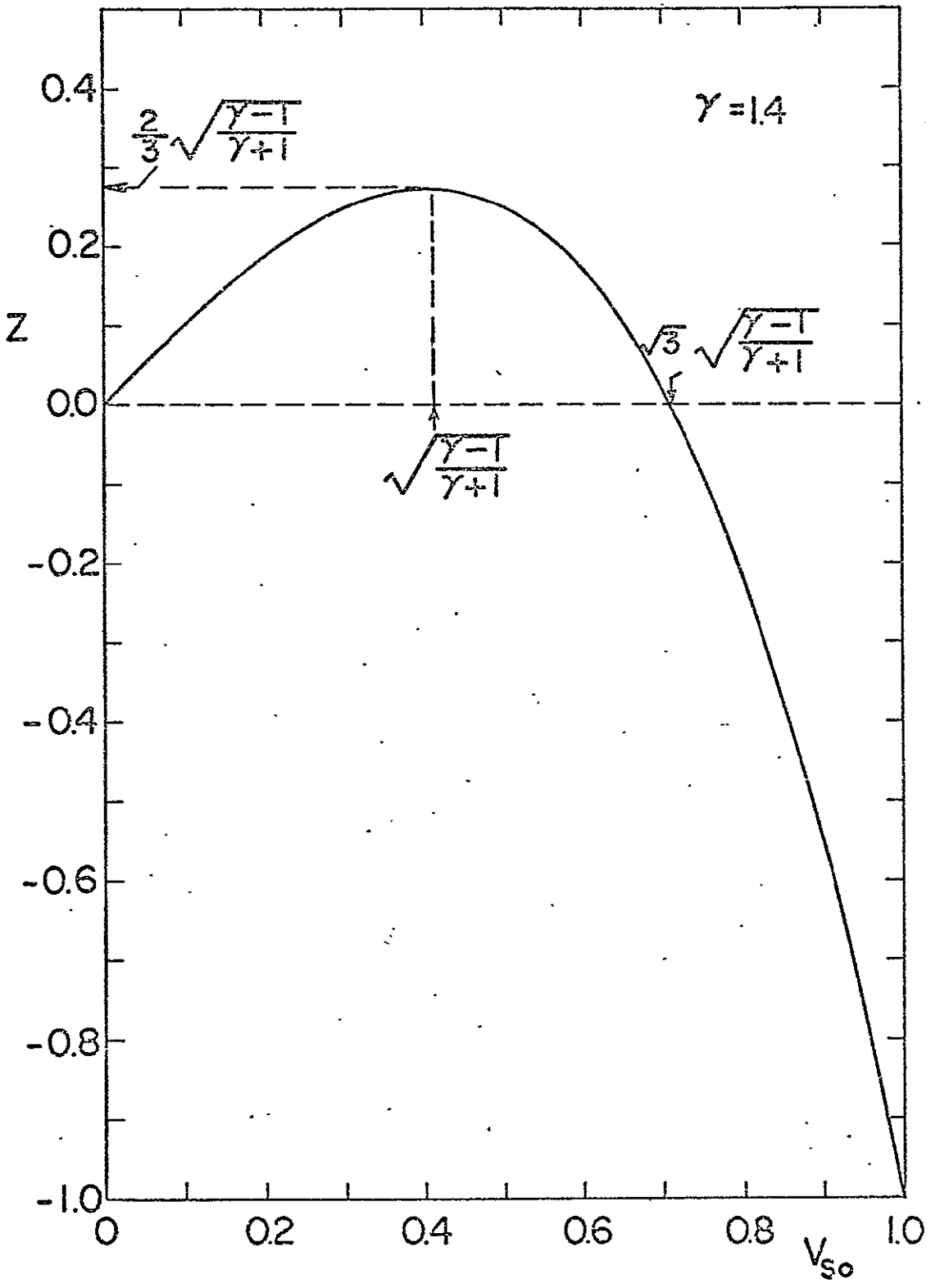

Figure 18 Z vs. V_{so} from Eq. (32)

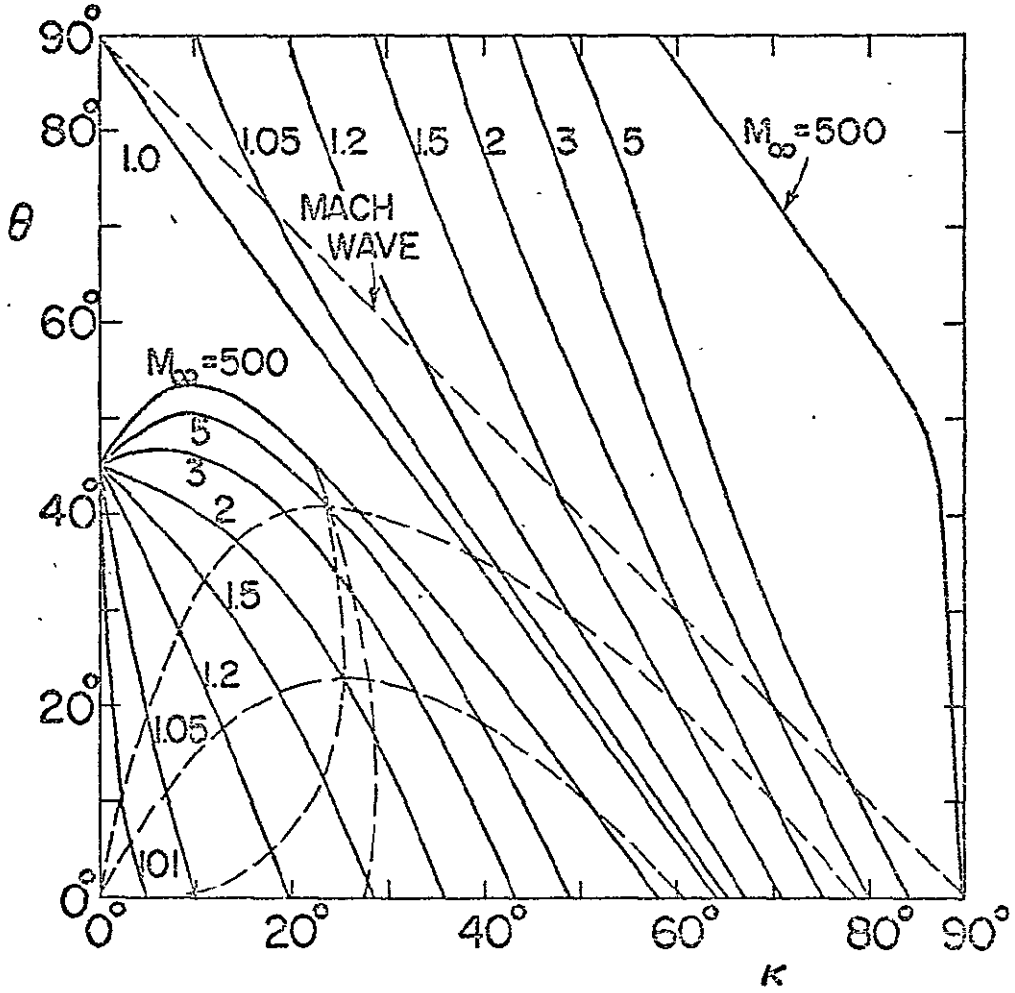

Figure 19 Roots of F/ε from Eq. (24) and the Equations given in APPENDIX A

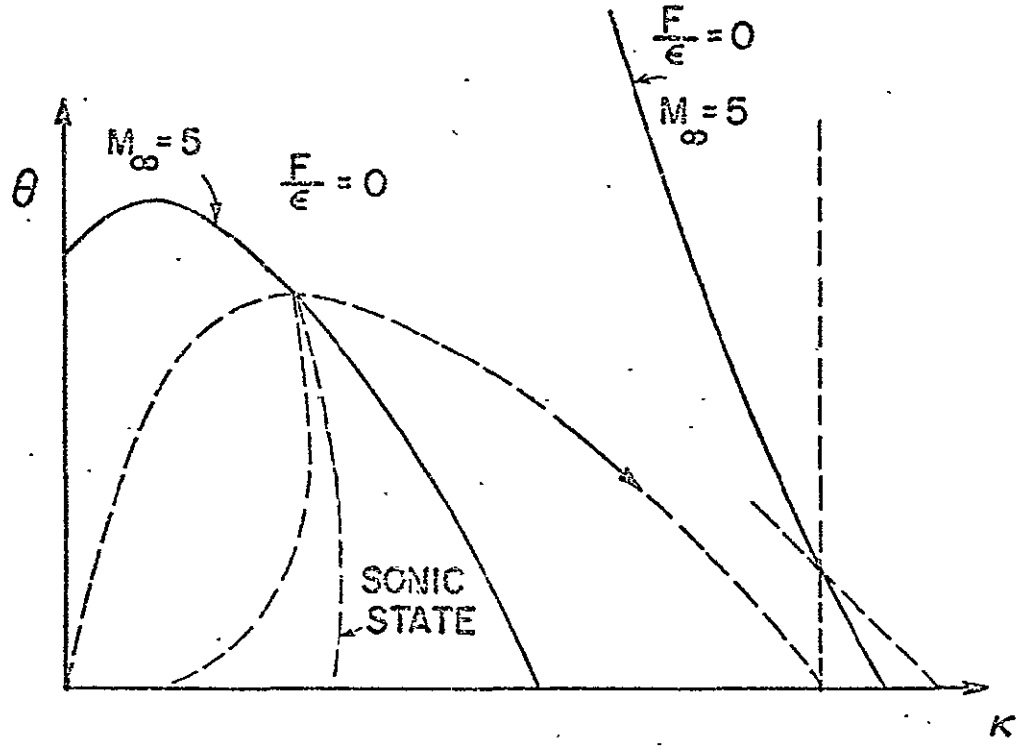

Figure 19a Illustration of Applicability of the One-Strip Method of Integral Relations for Weak Attached Shock Wave

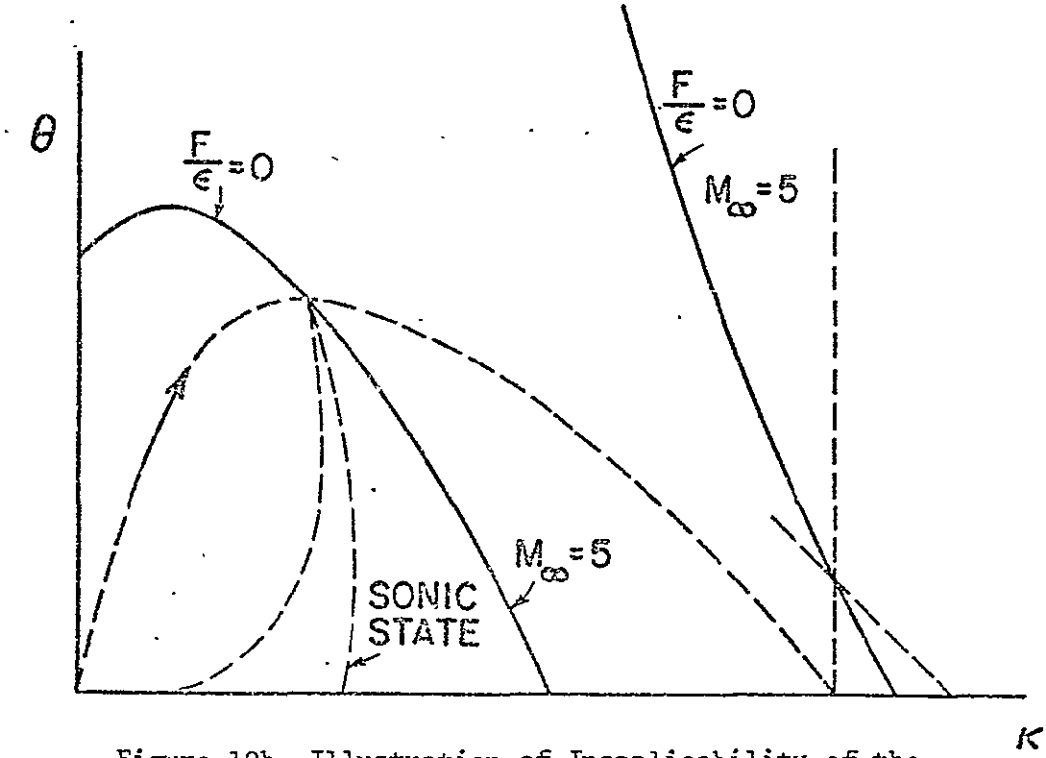

Figure 19b Illustration of Inapplicability of the One-Strip Method of Integral Relations for Strong Attached Shock Wave

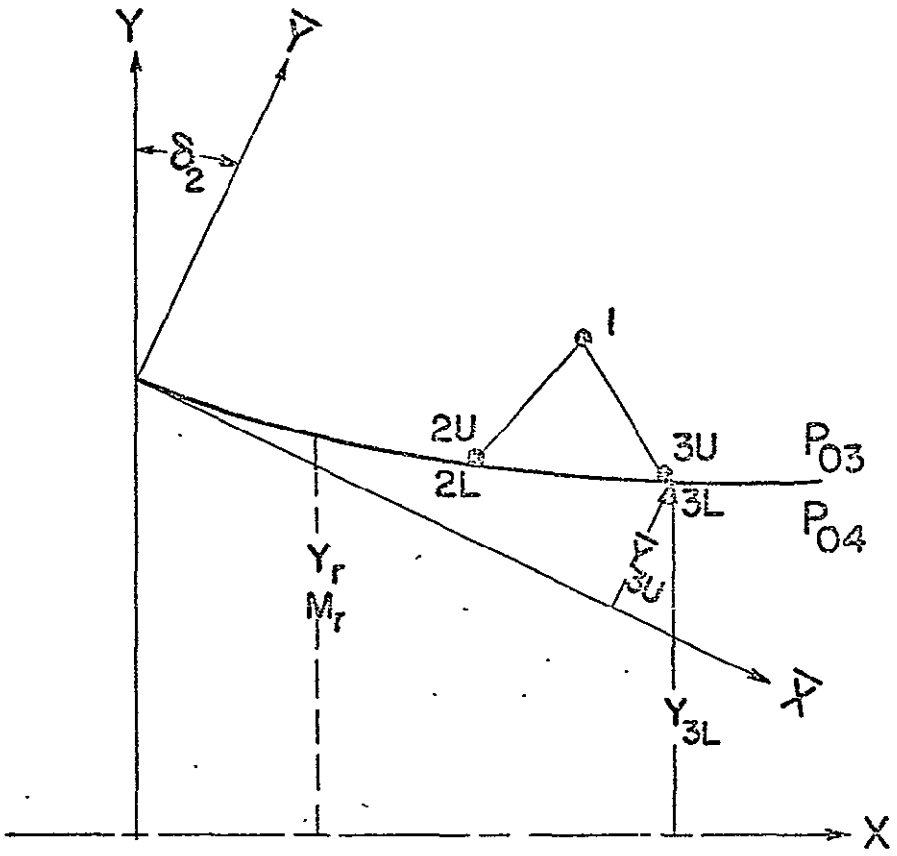

Figure 20 Detailed Figure for the Solution of Slipline Point for Eqs. (43) through (48)

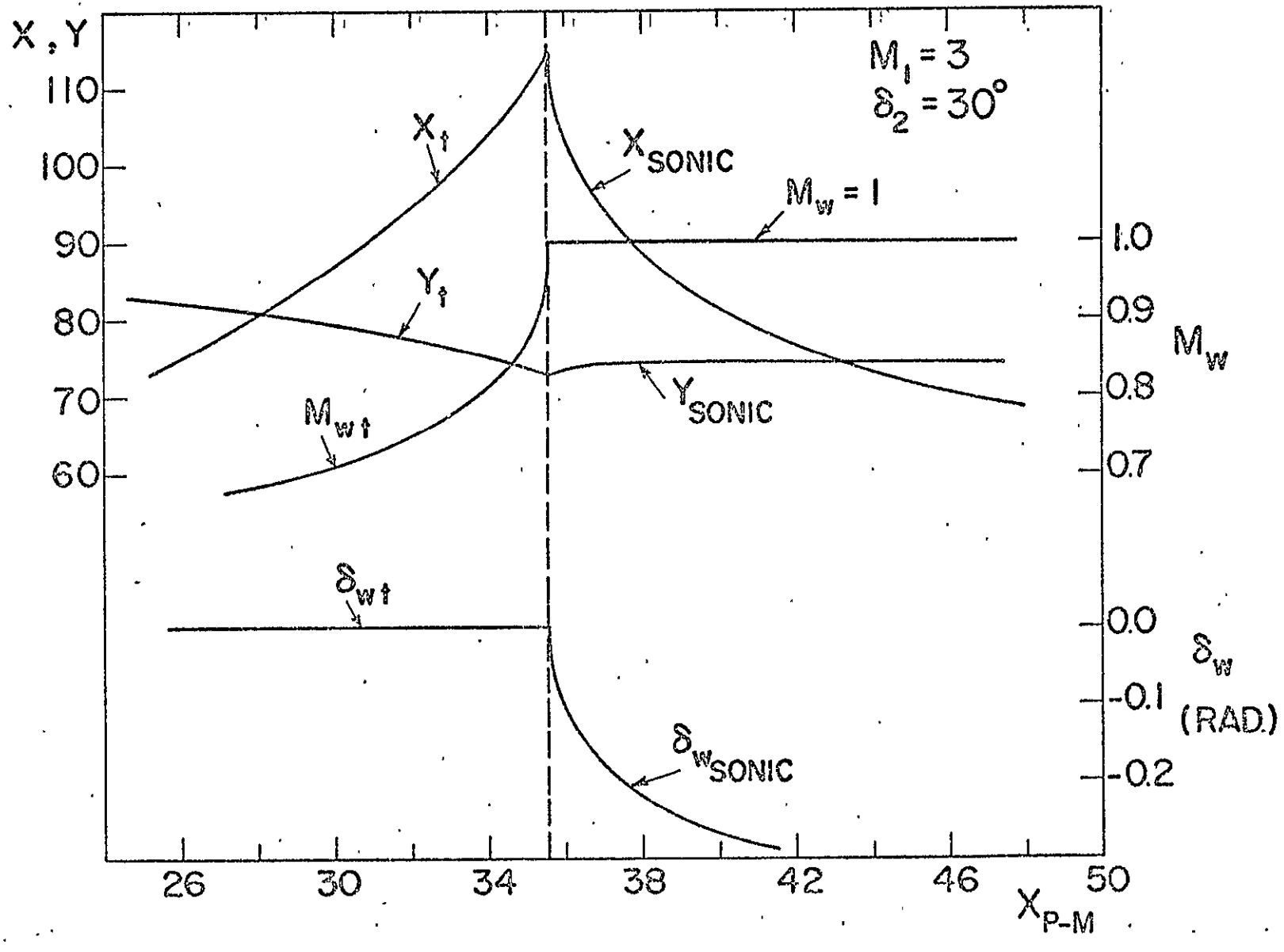

Figure 21 Illustration of the Dependence of Sonic Condition in Region 4 on the P-M Fan Location

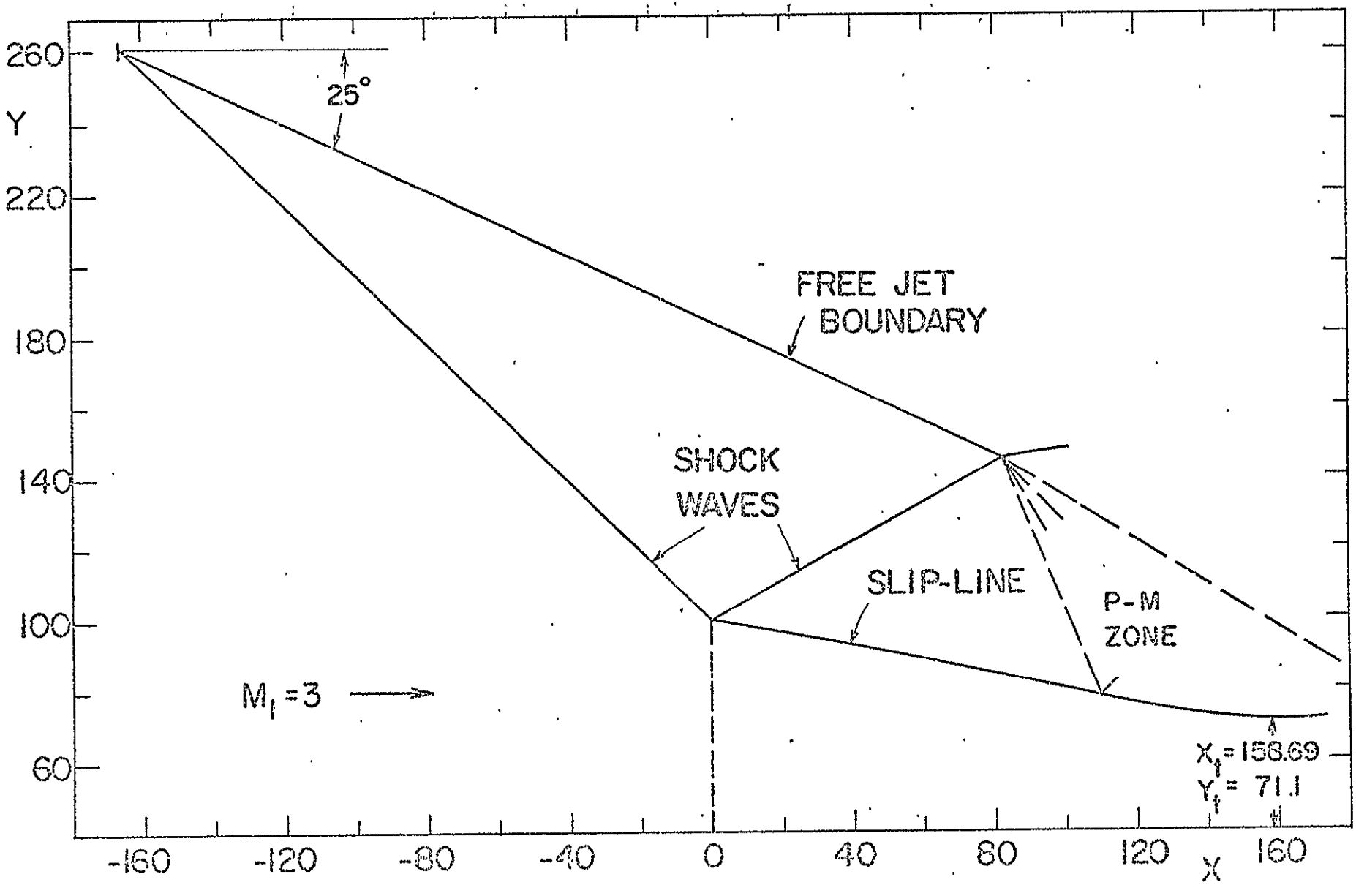

Figure 22 In-Scale Plot of Two-Dimensional Mach Reflection Pattern (M_1 = 3.0, δ_2 = 25°)

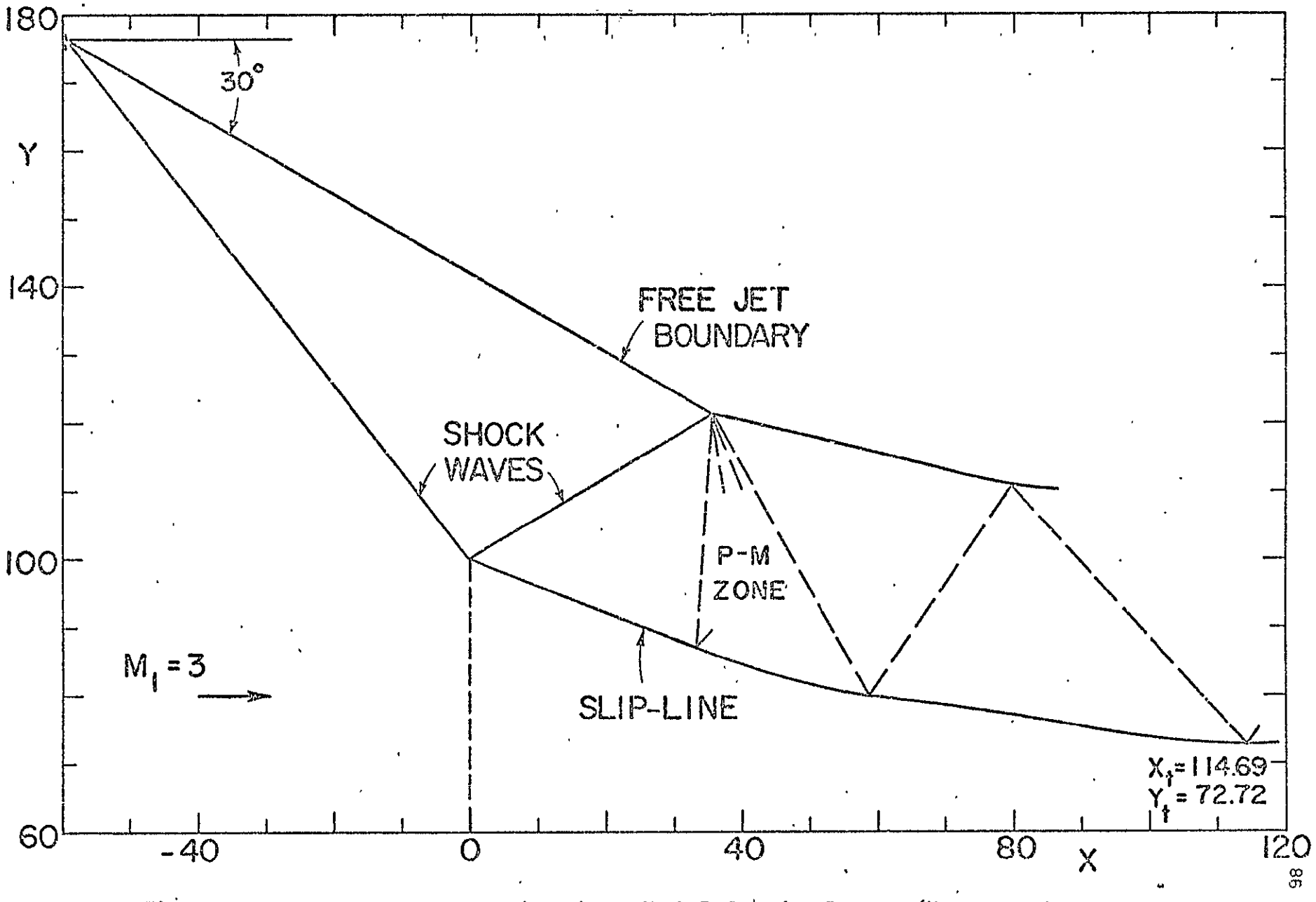

Figure 23 In-Scale Plot of Two-Dimensional Mach Reflection Pattern ($M_1 = 3.0$, $\delta_2 = 30°$)

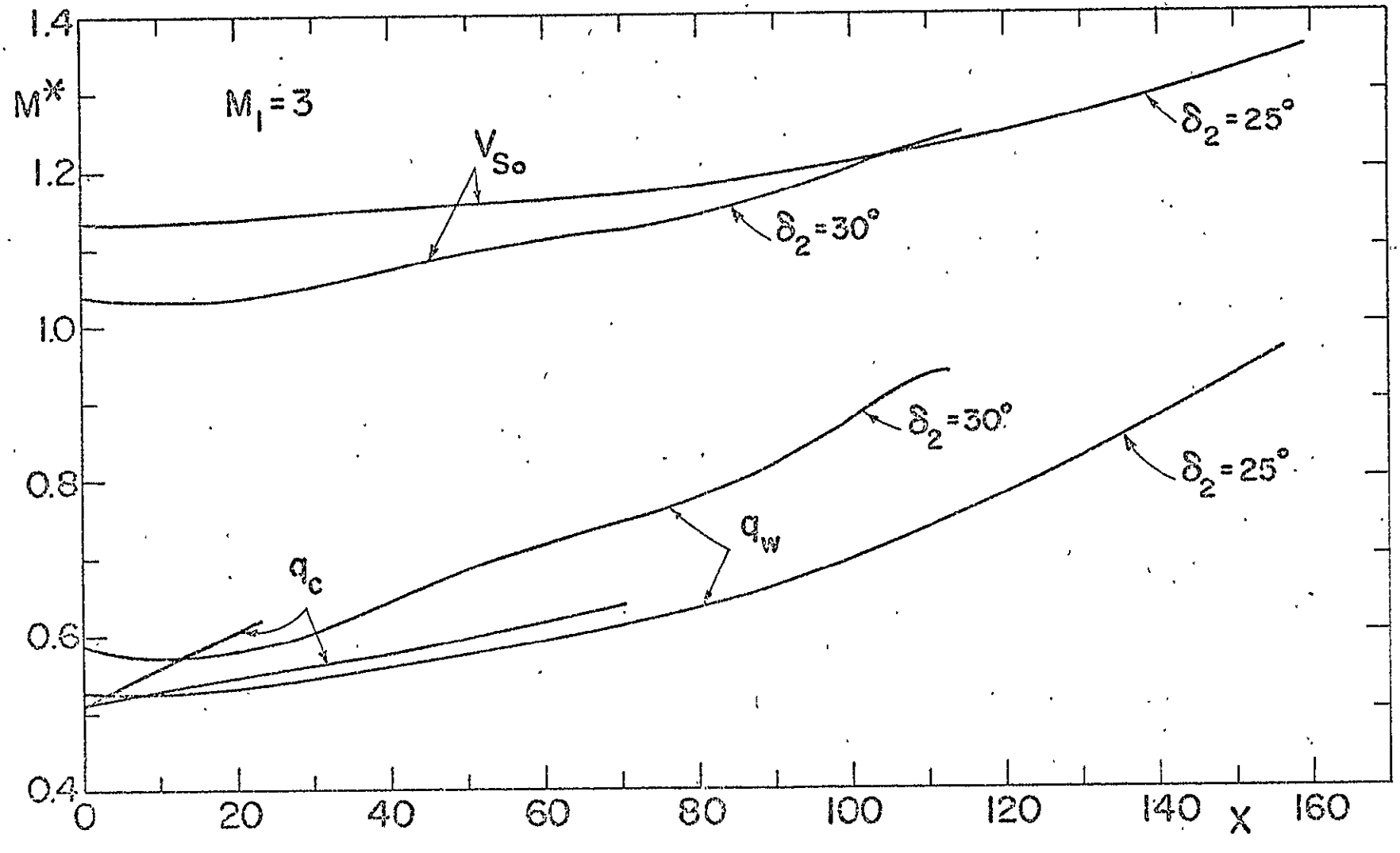

Figure 24 Velocity Distribution along Slipline for $\delta_2 = 25°$, and $\delta_2 = 30°$ at $M_1 = 3.0$

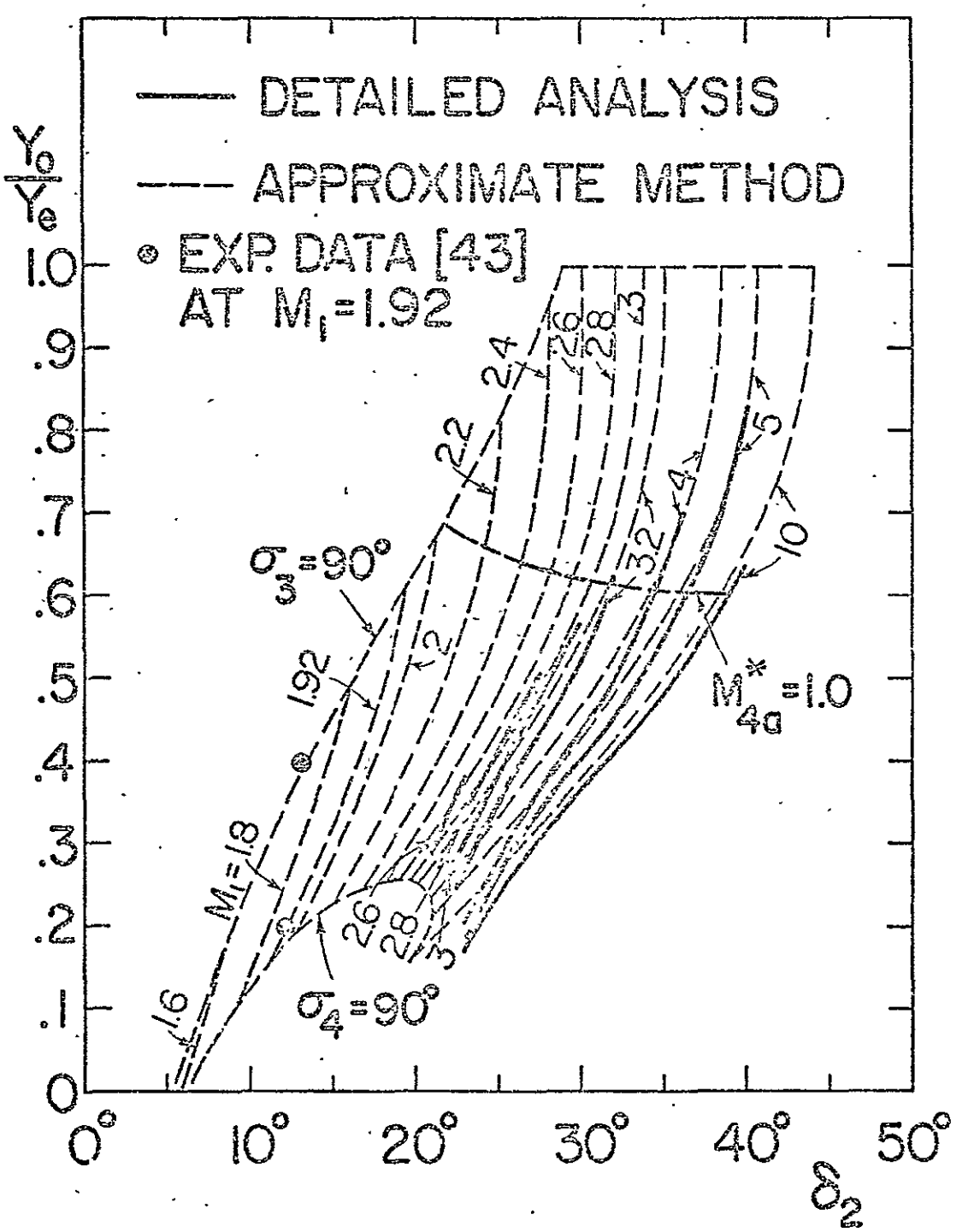

Figure 25 Mach Stem Height Y_o/Y_e vs. δ_2 for Two-Dimensional Overexpanded Nozzle Flow

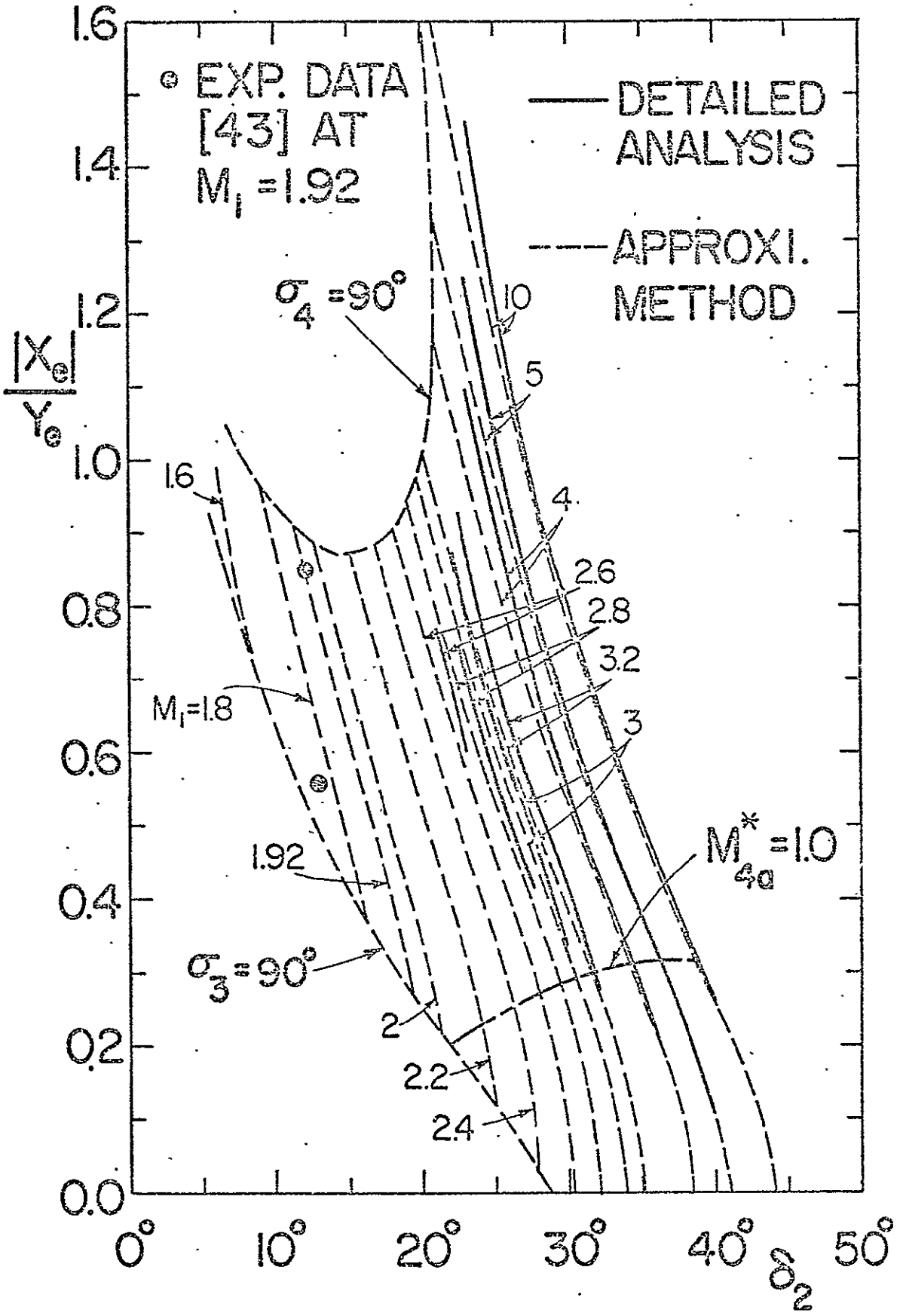

Figure 26 Mach Stem Location $|x_e|/Y_e$ vs. δ_2 for Two-Dimensional Overexpanded Nozzle Flow

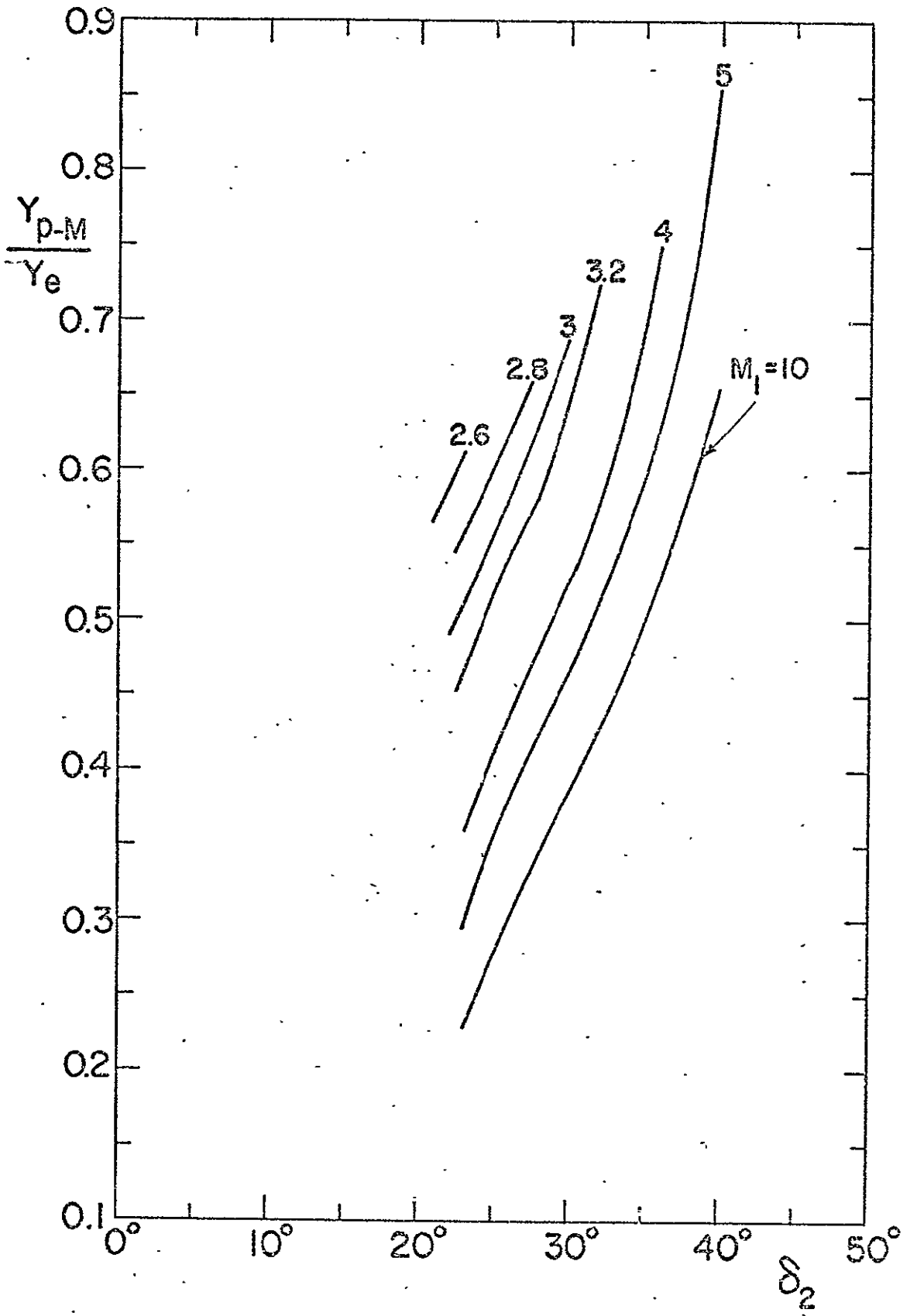

Figure 27 P-M Fan Position Y_{P-M}/Y_e vs. δ_2 for Two-Dimensional Overexpanded Nozzle Flow

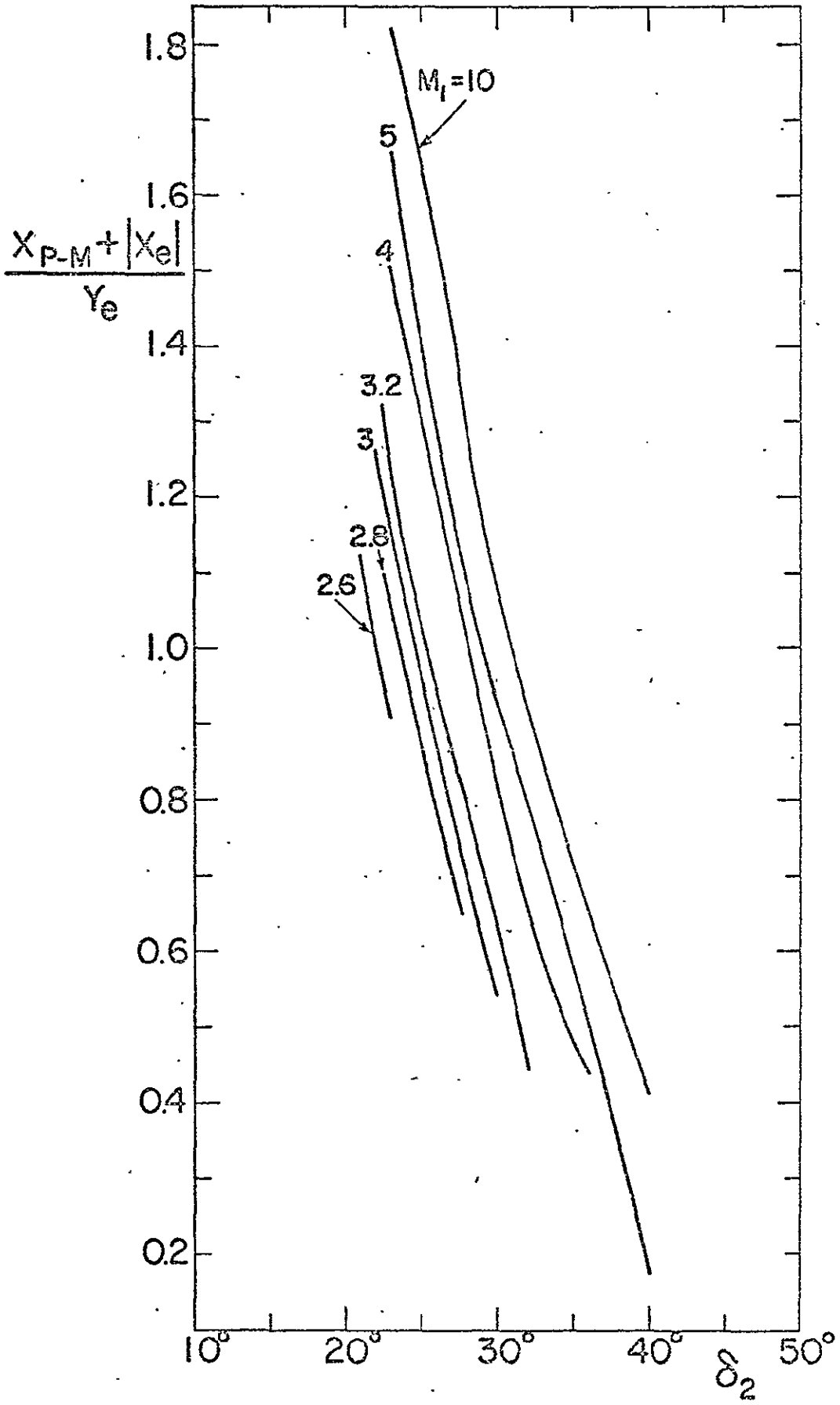

Figure 28 P-M Fan Location $(x_{P-M} + |x_e|)/Y_e$ vs. δ_2 for Two-Dimensional Overexpanded Nozzle Flow

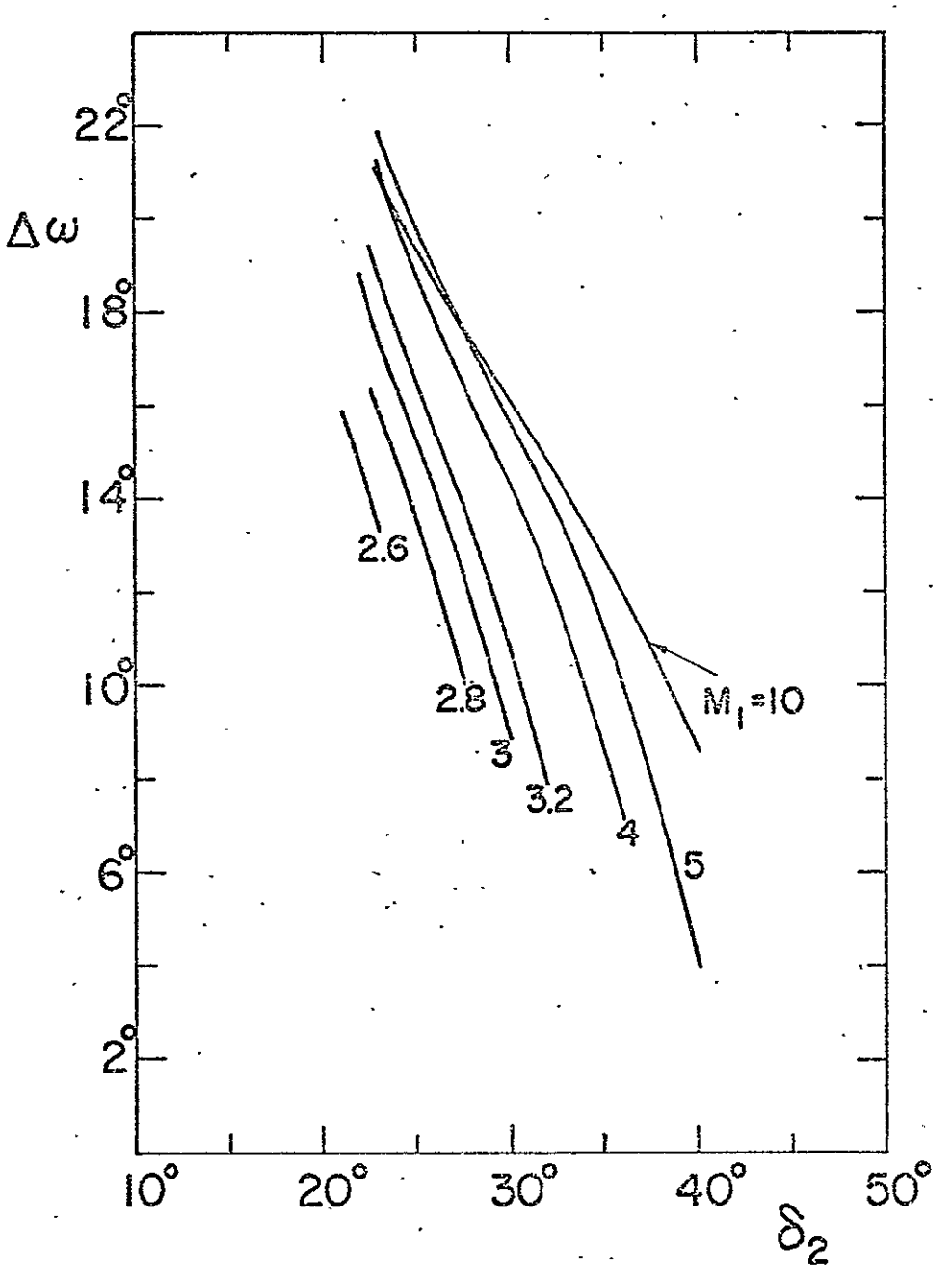

Figure 29 P-M Fan Range $\Delta\omega$ vs. δ_2 for Two-Dimensional Overexpanded Nozzle Flow

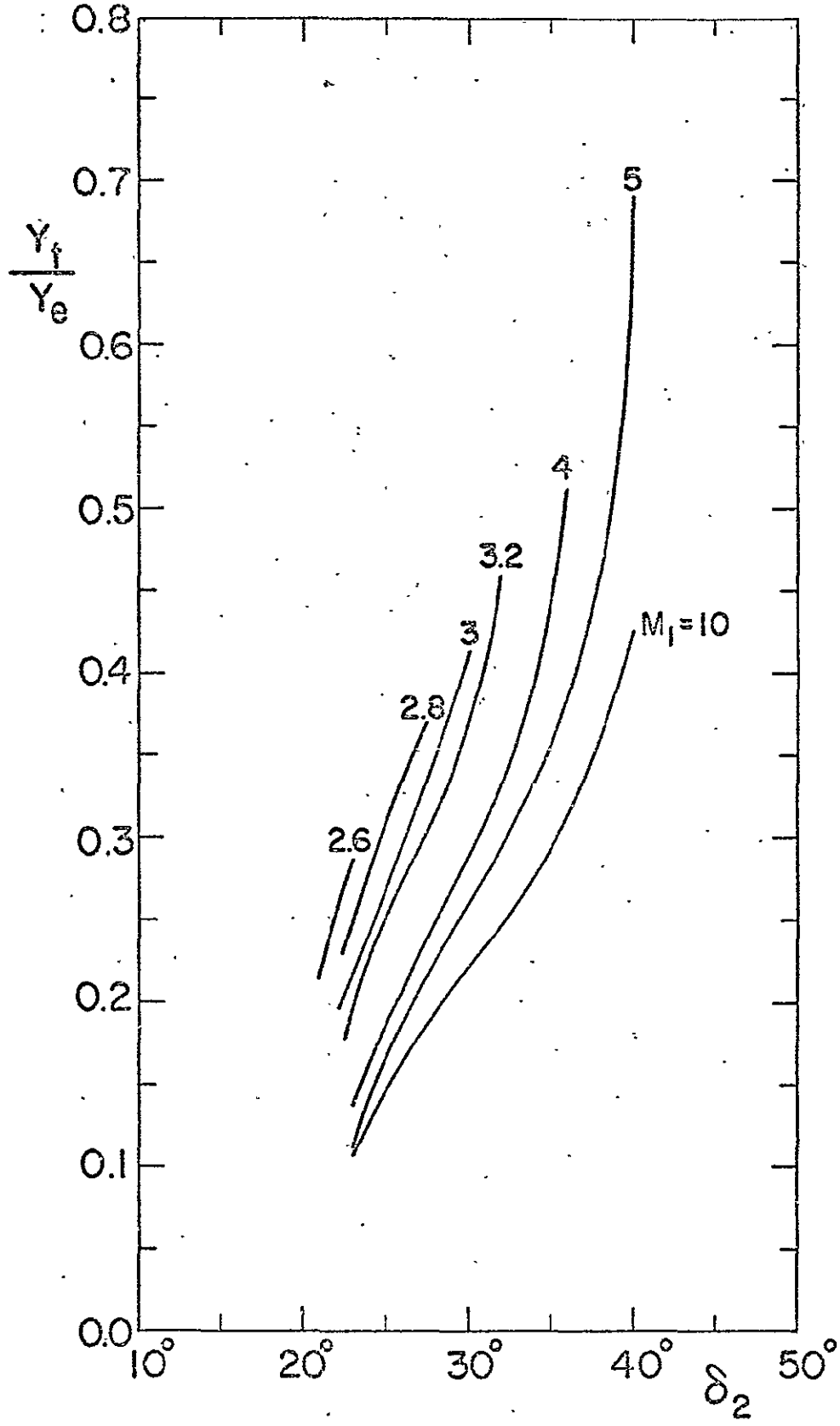

Figure 30 Central Core Throat Height Y_t/Y_e vs. δ_2 for Two-Dimensional Overexpanded Nozzle Flow

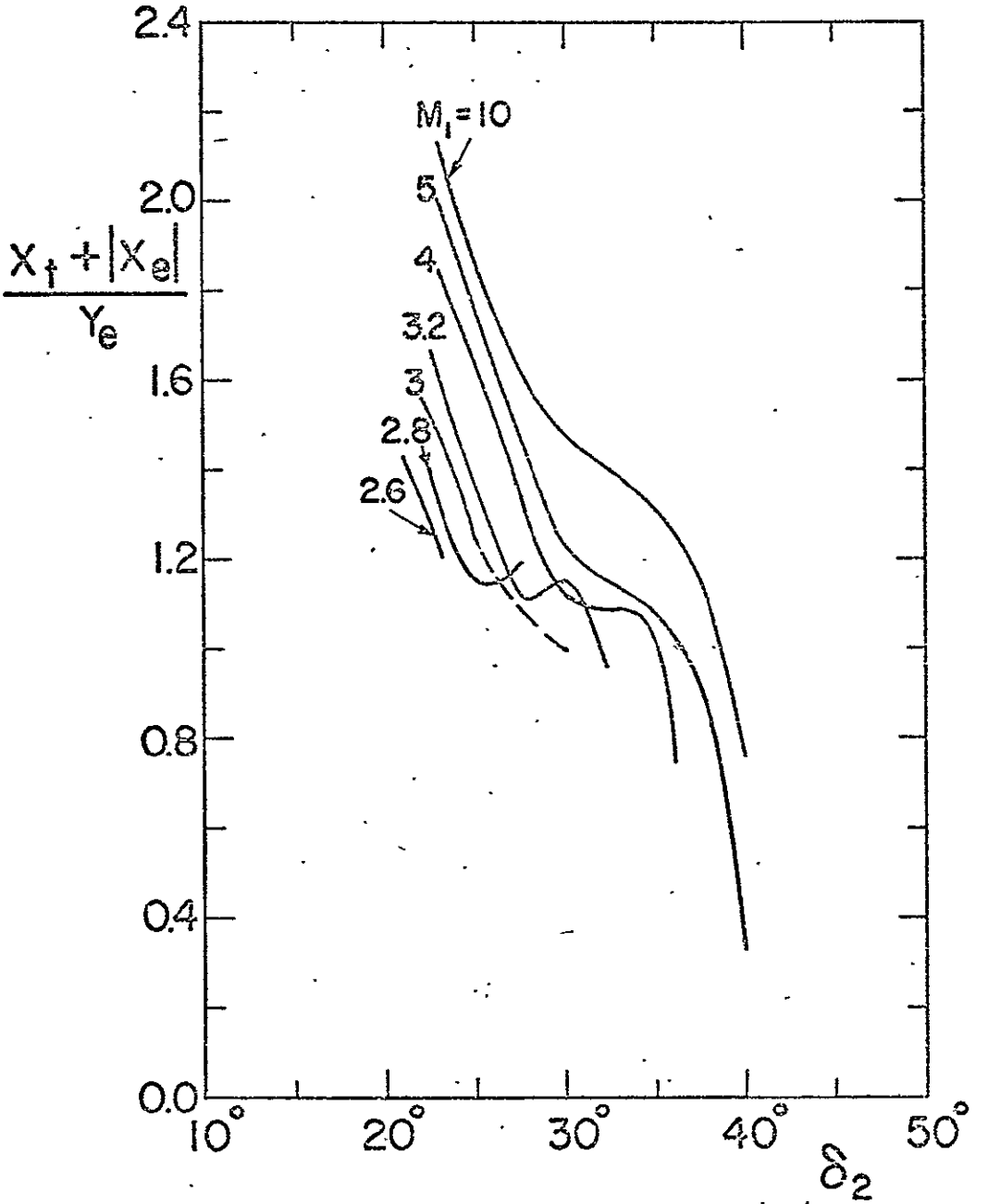

Figure 31 Central Core Throat Location $(x_t + |x_e|)/Y_e$ vs. δ_2 for Two-Dimensional Overexpanded Nozzle Flow

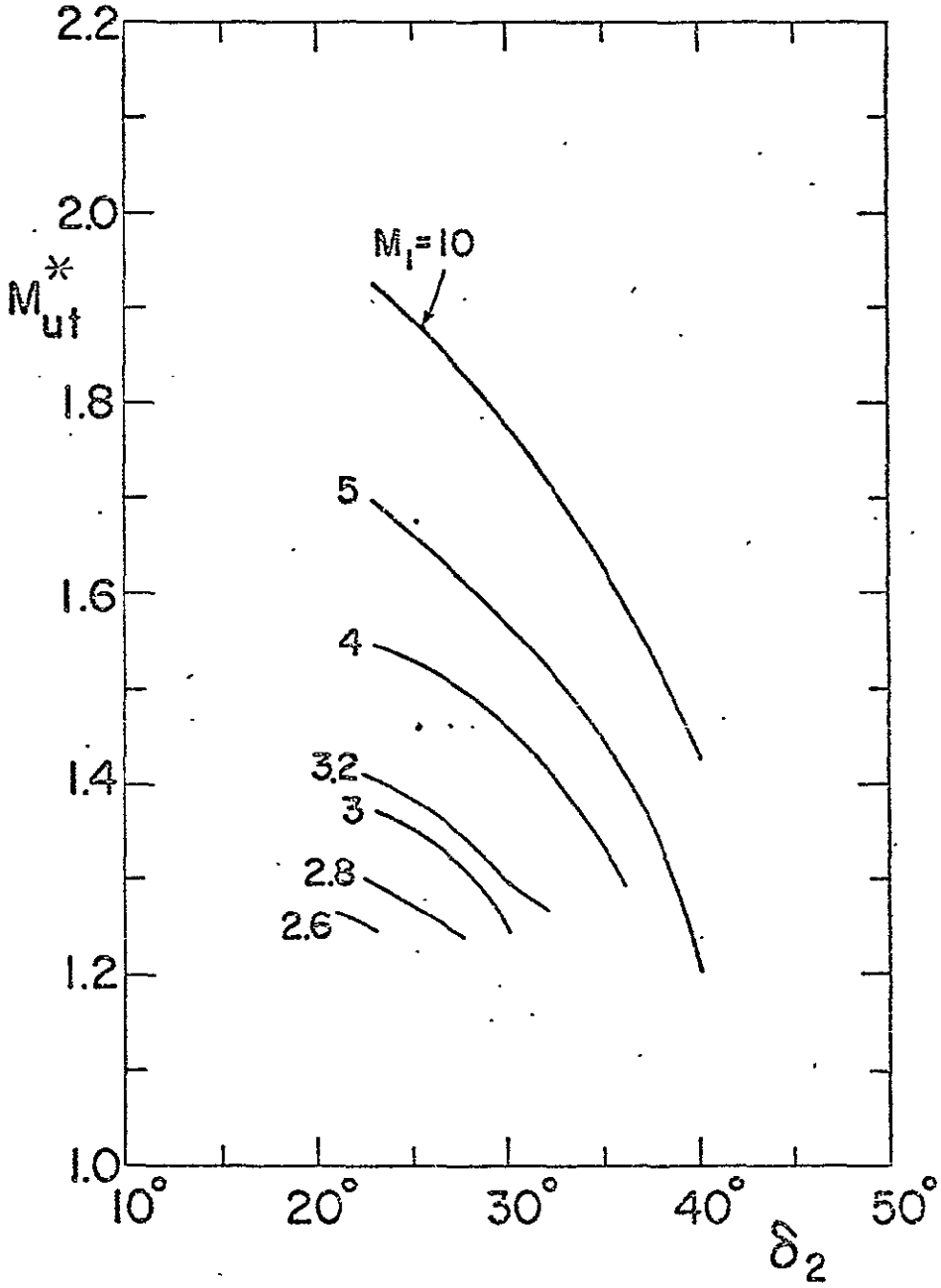

Figure 32 Speed on the Upper Side of Slipline at Throat. M^*_{ut} vs. δ_2 for Two-Dimensional Overexpanded Nozzle Flow

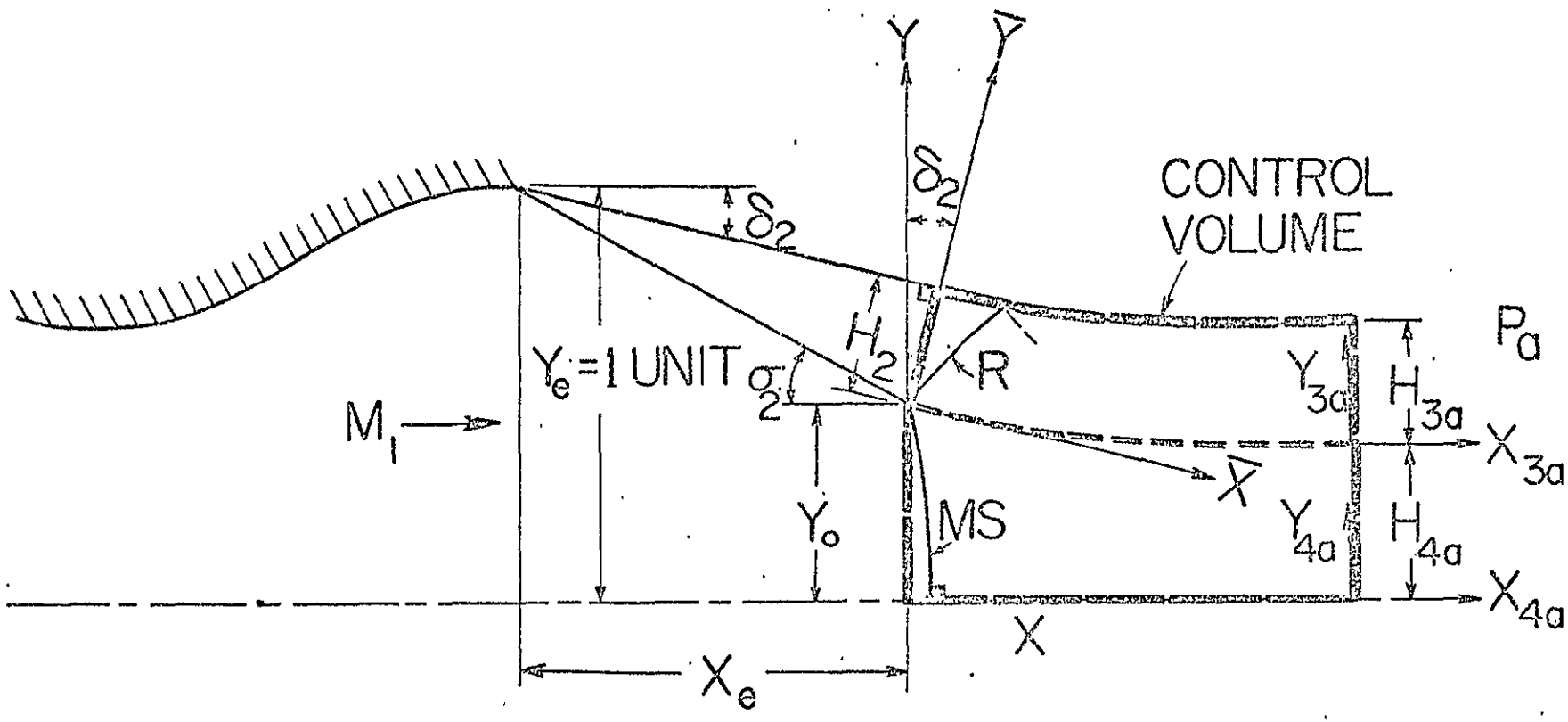

Figure 33 Control Volume and Coordinates used in the Approximate Method for Estimating Mach Stem Height and Location

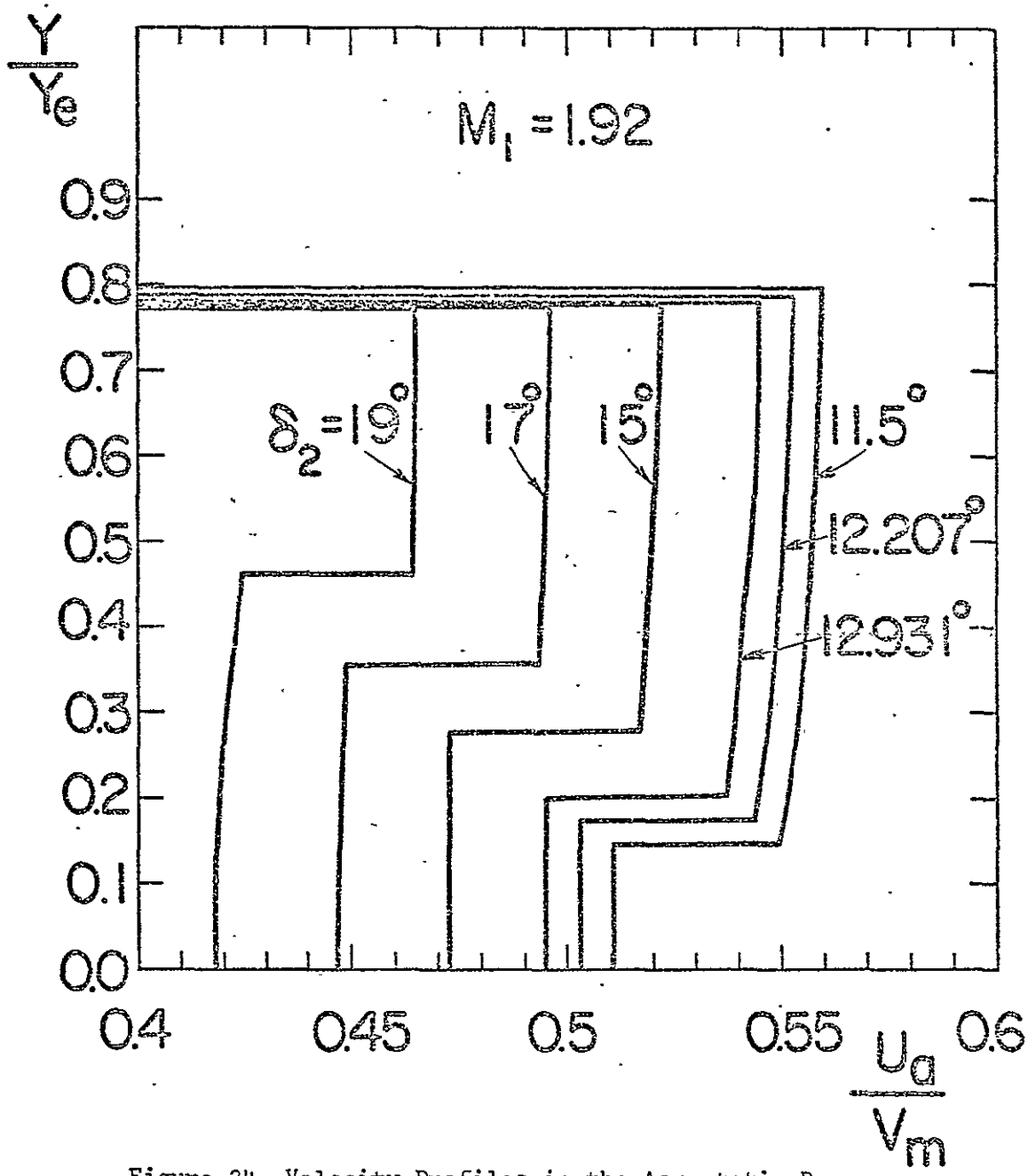

Figure 34 Velocity Profiles in the Asymptotic Downstream Flow from the Approximate Method for Different Pressure Ratios at $M_1 = 1.92$

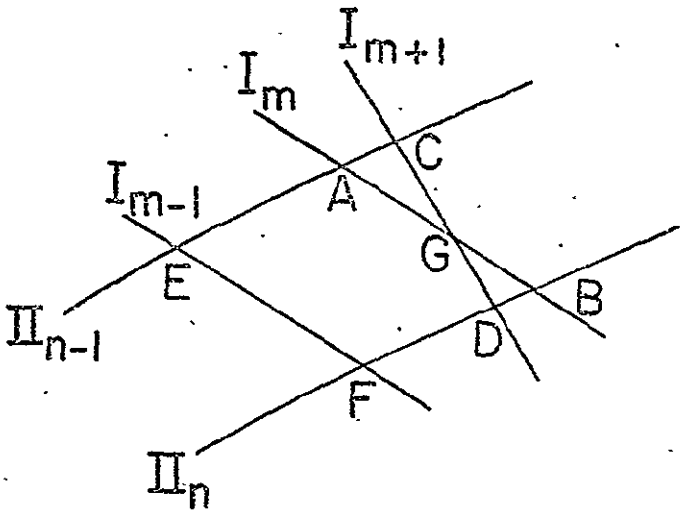

Figure 35a Intersection of Two Compression Waves of the Same Family

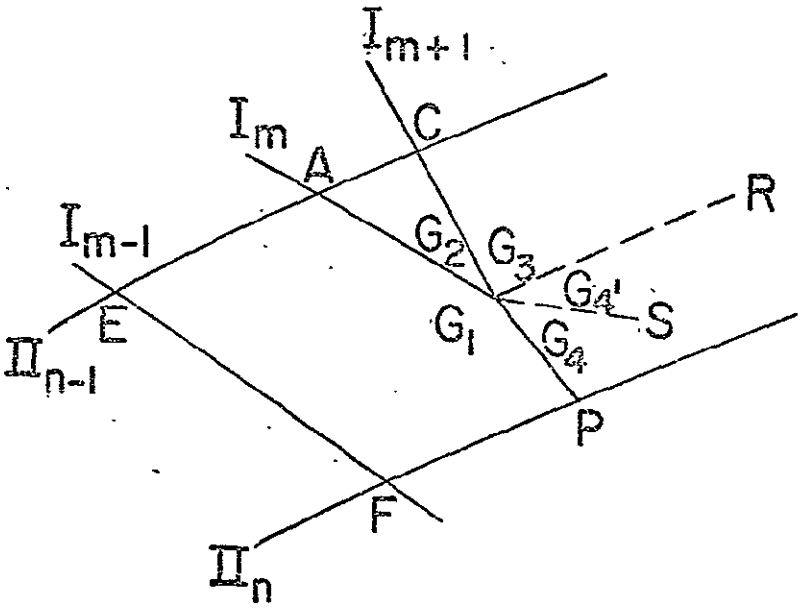

Figure 35b Coalescence of the Compression Waves of the Same Family into Stronger Shock Waves

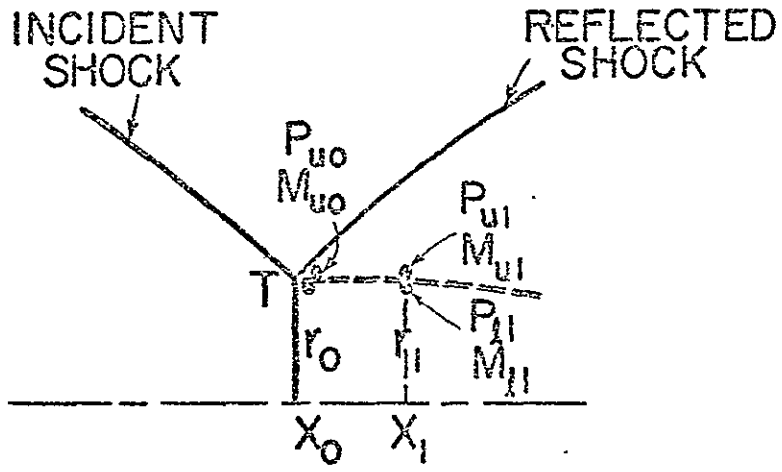

Figure 36 First Step along the Slipline for Axisymmetric Underexpanded Flow

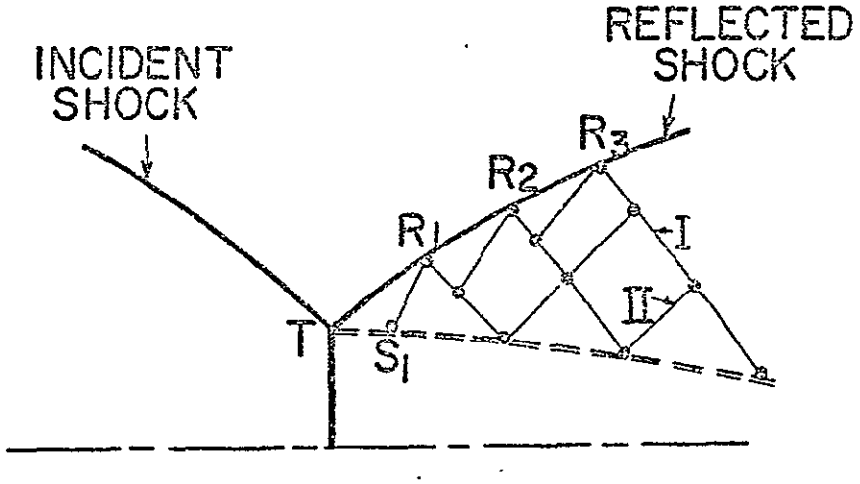

Figure 37 Characteristic Net Layout behind the Reflected Shock Wave

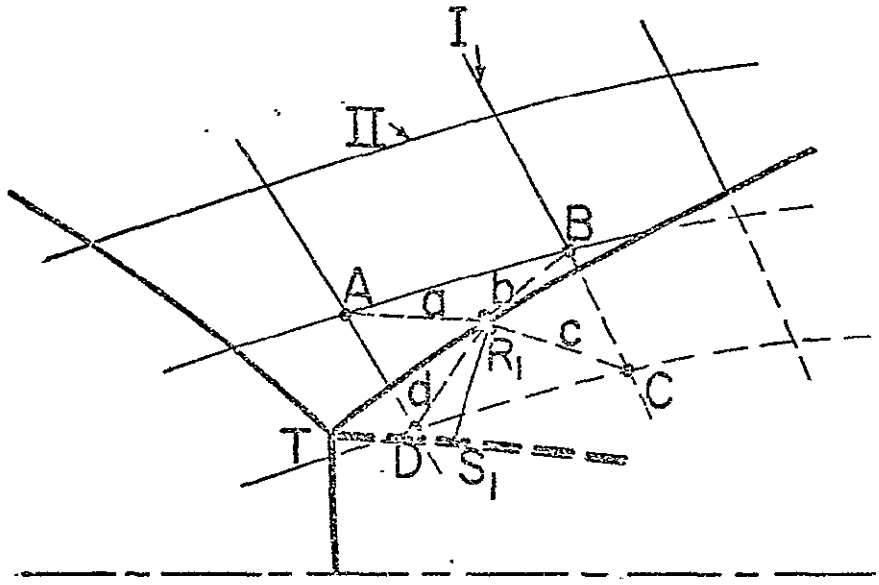

Figure 38 Determination of the Flow Properties in Front of the Reflected Shock

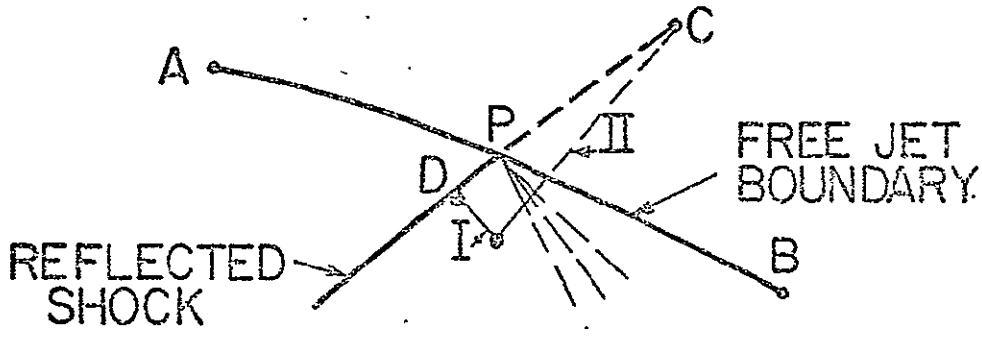

Figure 39 Determination of Flow Properties and Coordinates at the Intersection Point of Reflected Shock and Free Jet Boundary

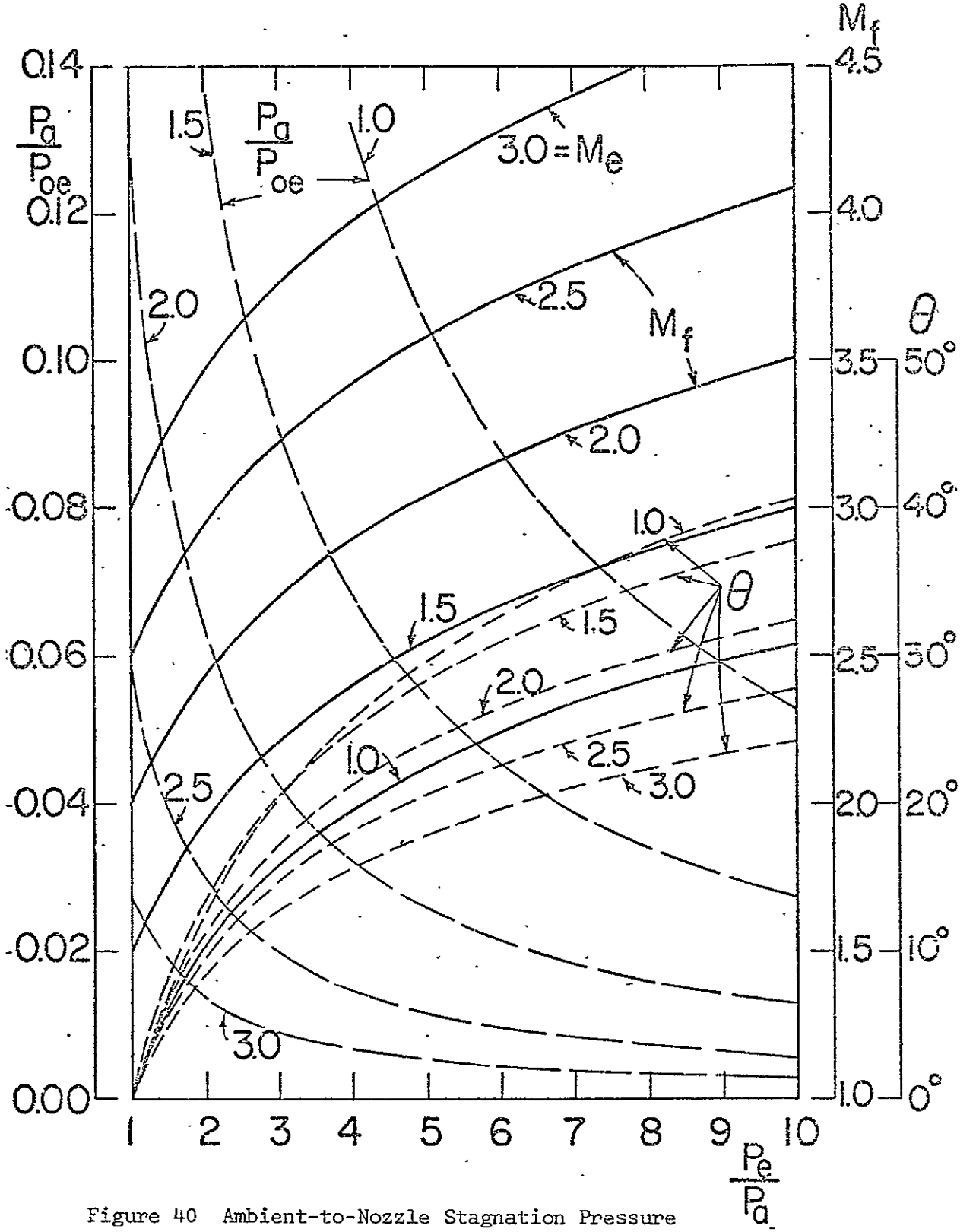

Figure 40 Ambient-to-Nozzle Stagnation Pressure Ratio, P_a/P_{oe}, Free Jet Mach Number, M_f, and Initial Free Jet Inclination Angle at Nozzle Lip, θ_f, vs. Nozzle Exit-to-Ambient Pressure Ratio, P_e/P_a

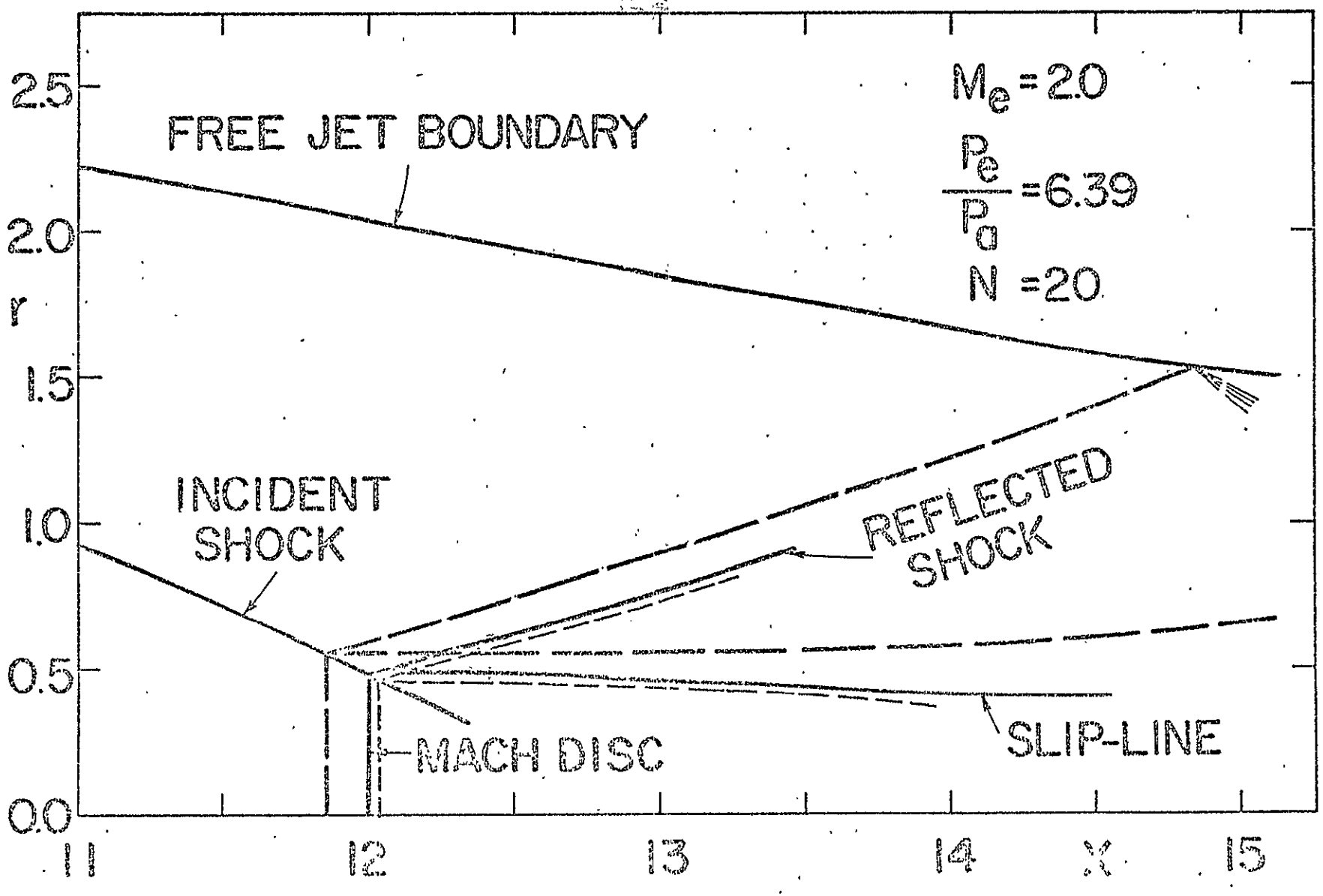

Figure 11a Dependence of the Sonic State on the Location of Mach Disc without Entropy Gradient at $M_e = 2.0$, $P_e/P_a = 6.39$, N = 20

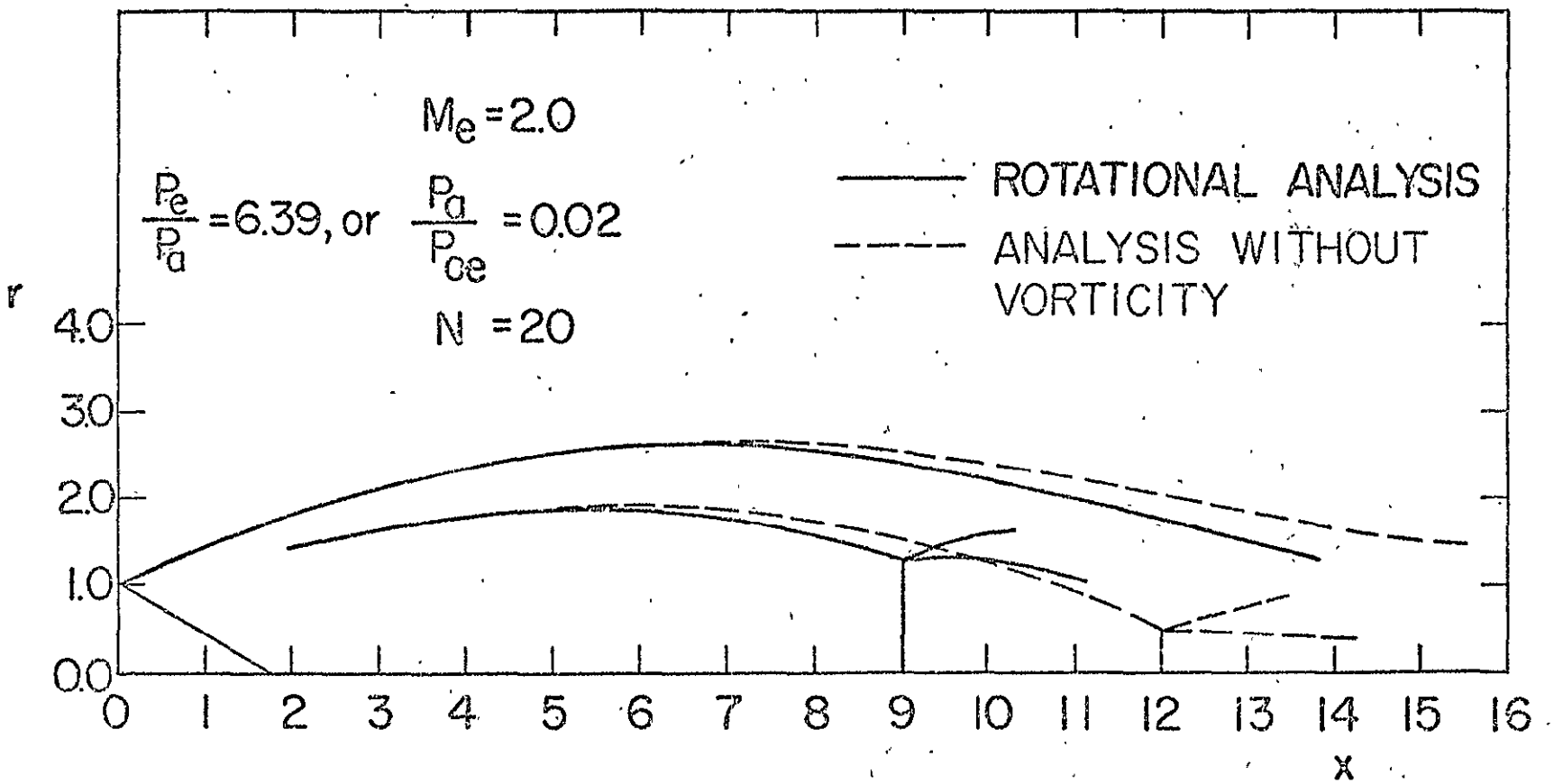

Figure 41b Comparison of Analysis with and without Vorticity at $M_e = 2.0$, $P_e/P_a = 6.39$, $N = 20$

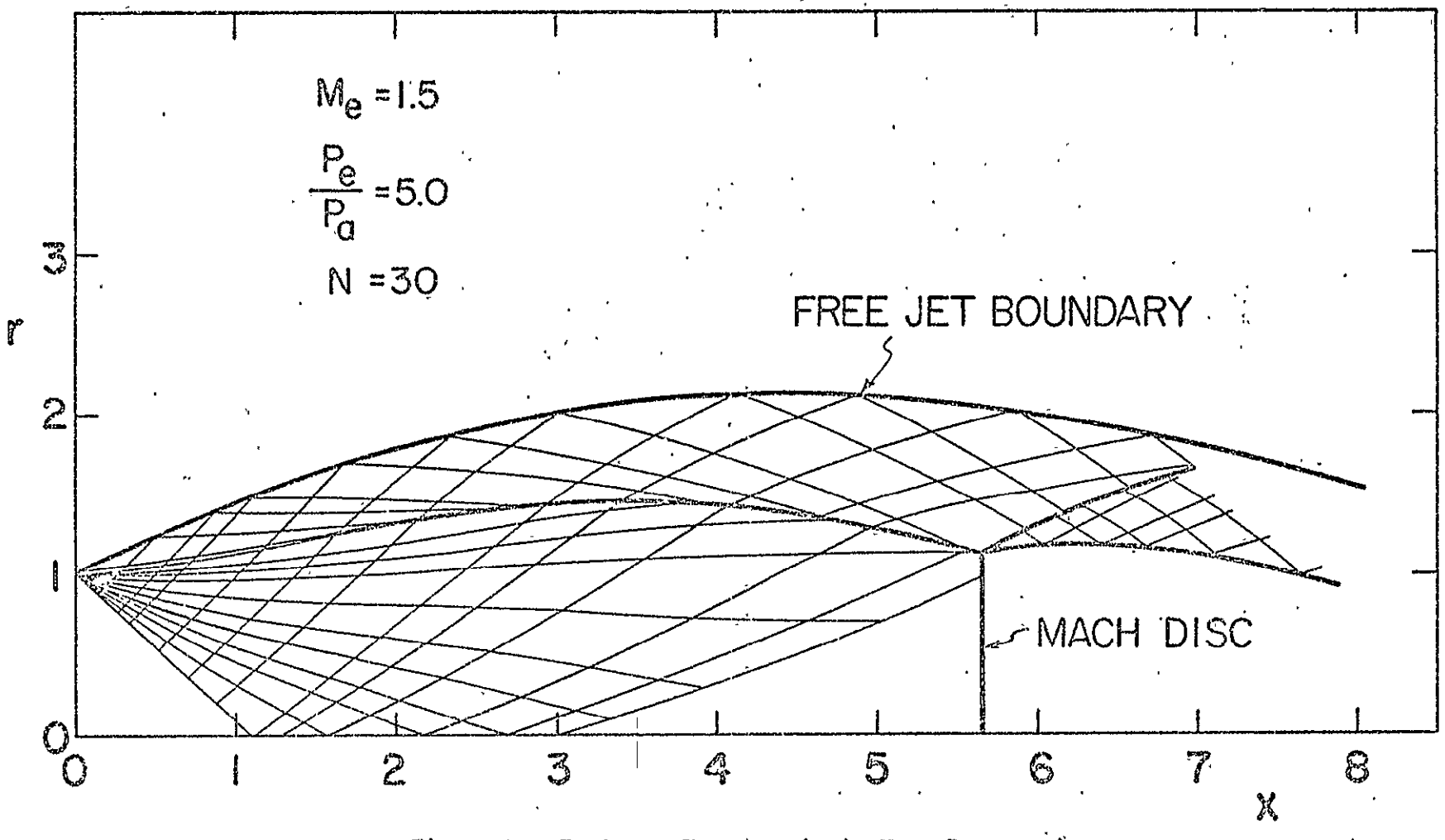

Figure 42 In-Scale Characteristic Wave Pattern in Physical Scale at $M_e = 1.5$, $P_e/P_a = 5.0$, N = 30

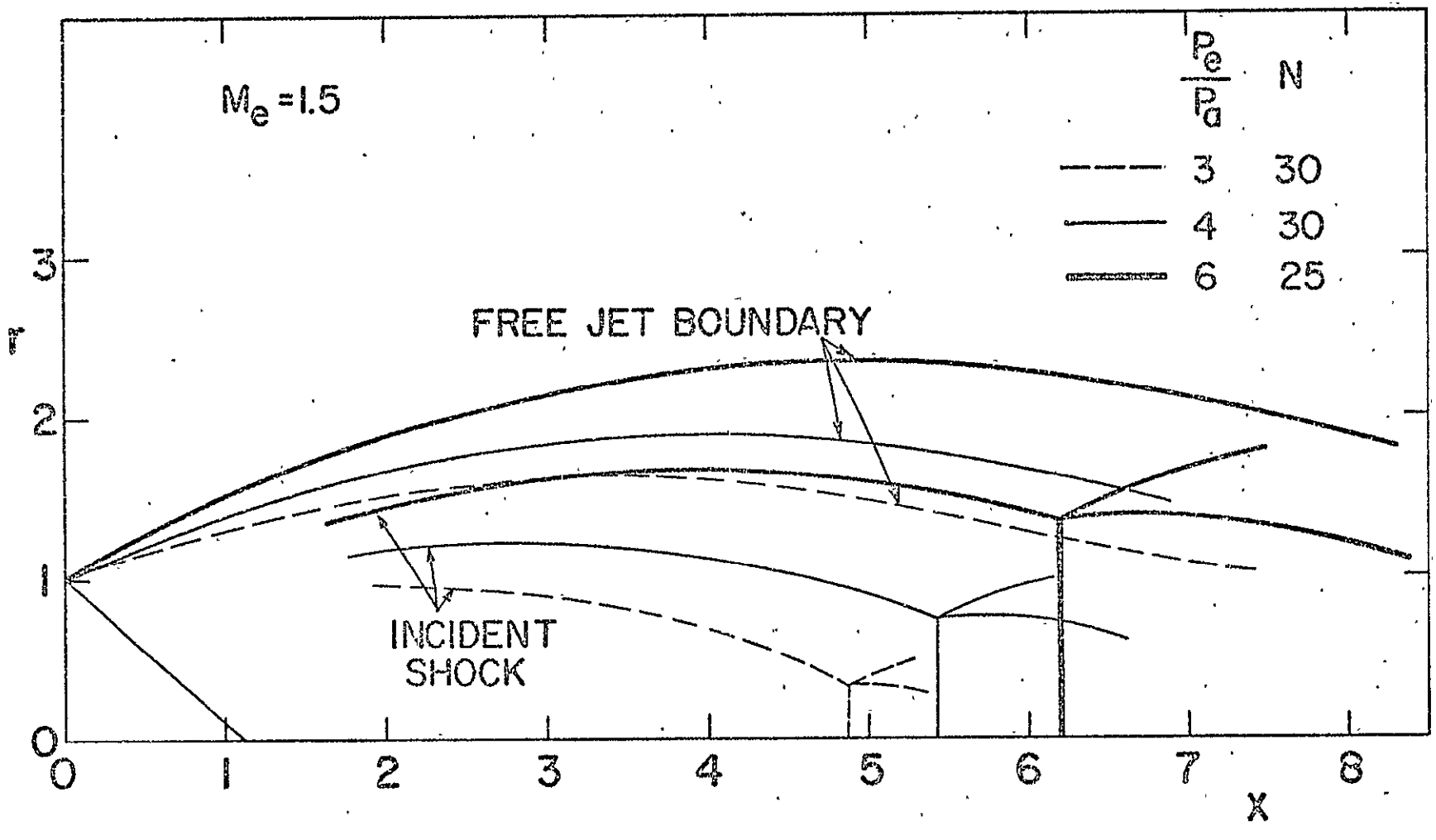

Figure 43 Free Jet Boundaries and Shock Wave Patterns at Different Pressure Ratios for M_e = 1.5

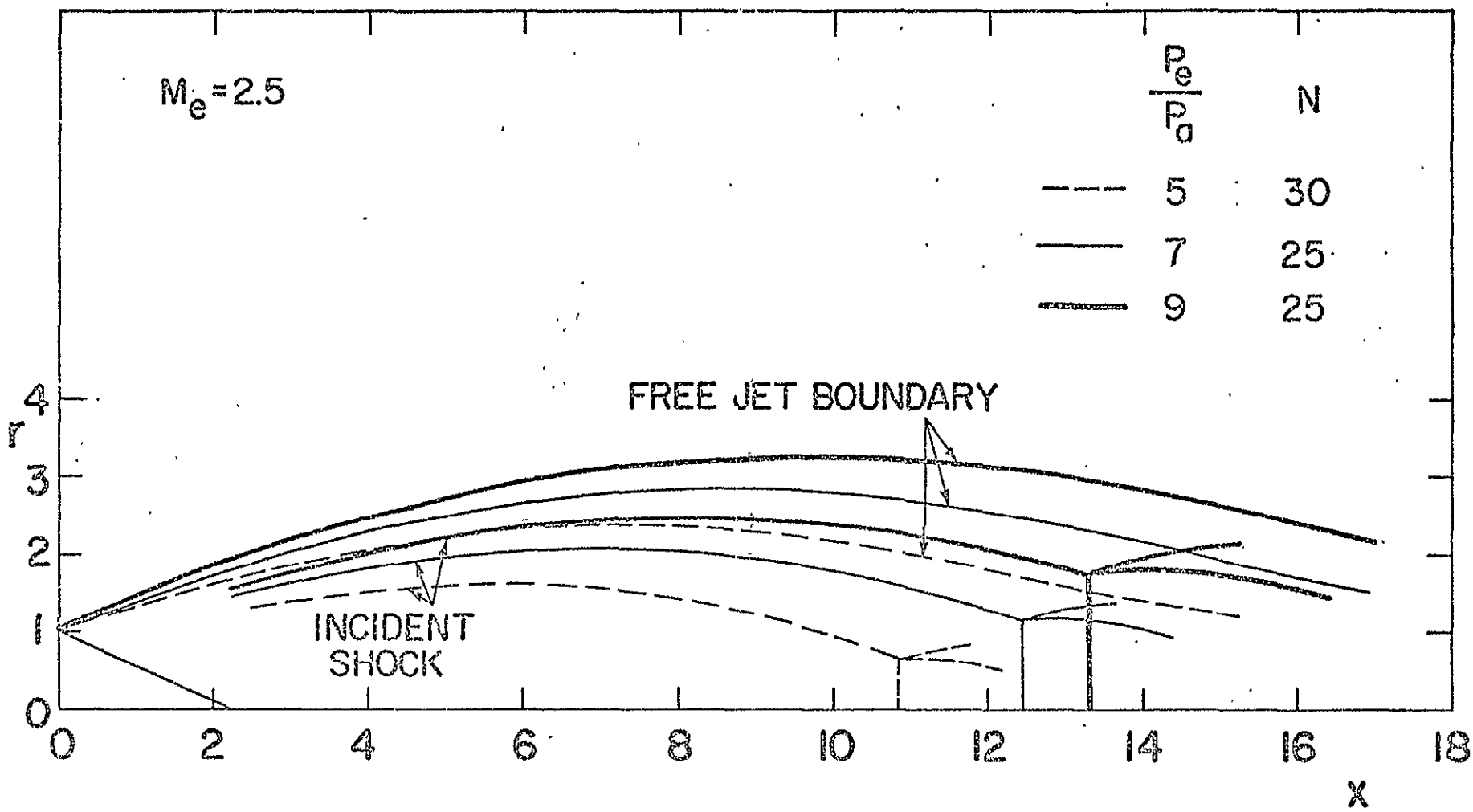

Figure 44 Free Jet Boundaries and Shock Wave Patterns at Different Pressure Ratios for $M_e = 2.5$

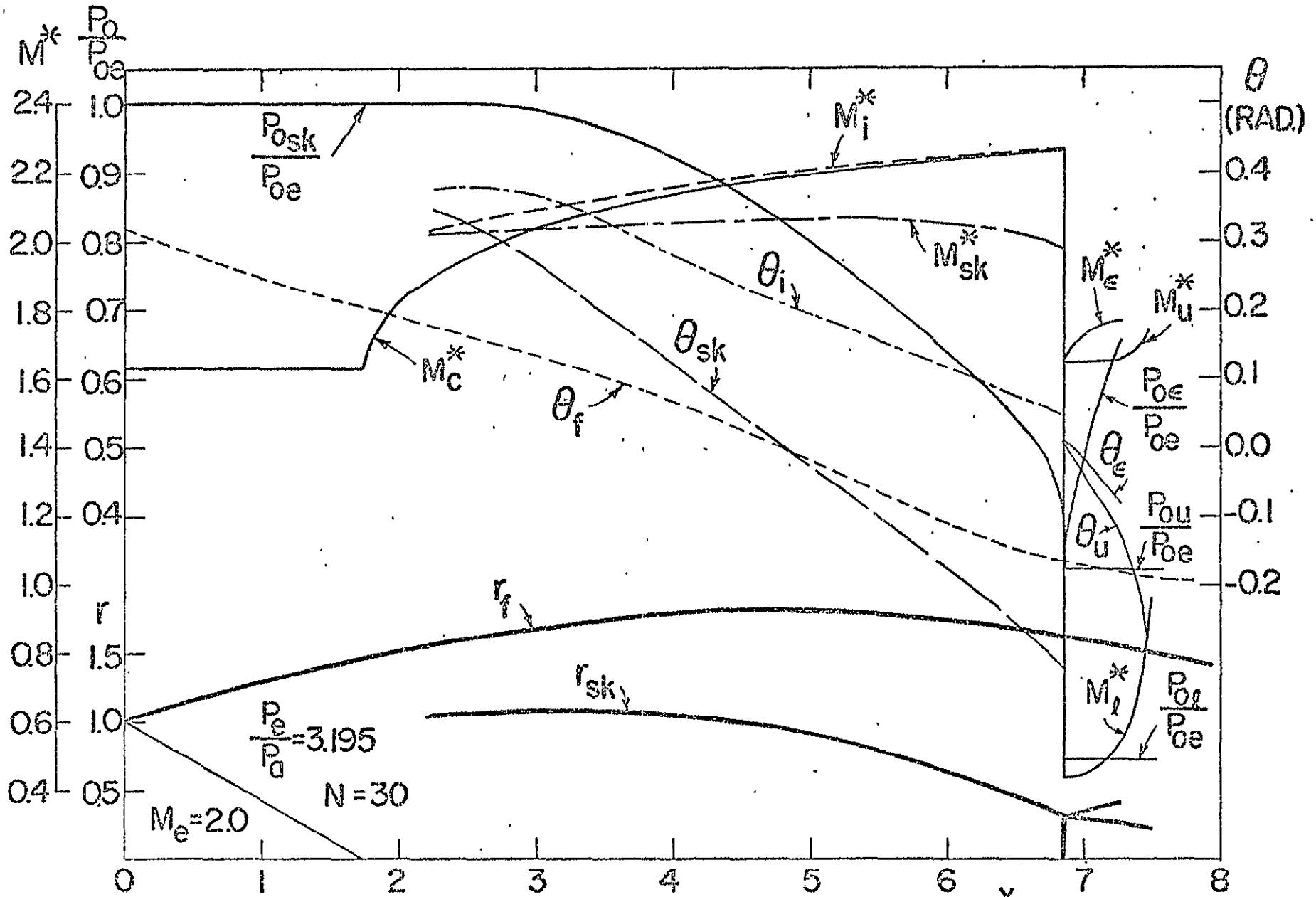

Figure 45 Distributions of Various Flow Properties at $M_e = 2.0$, $P_e/P_a = 3.195$

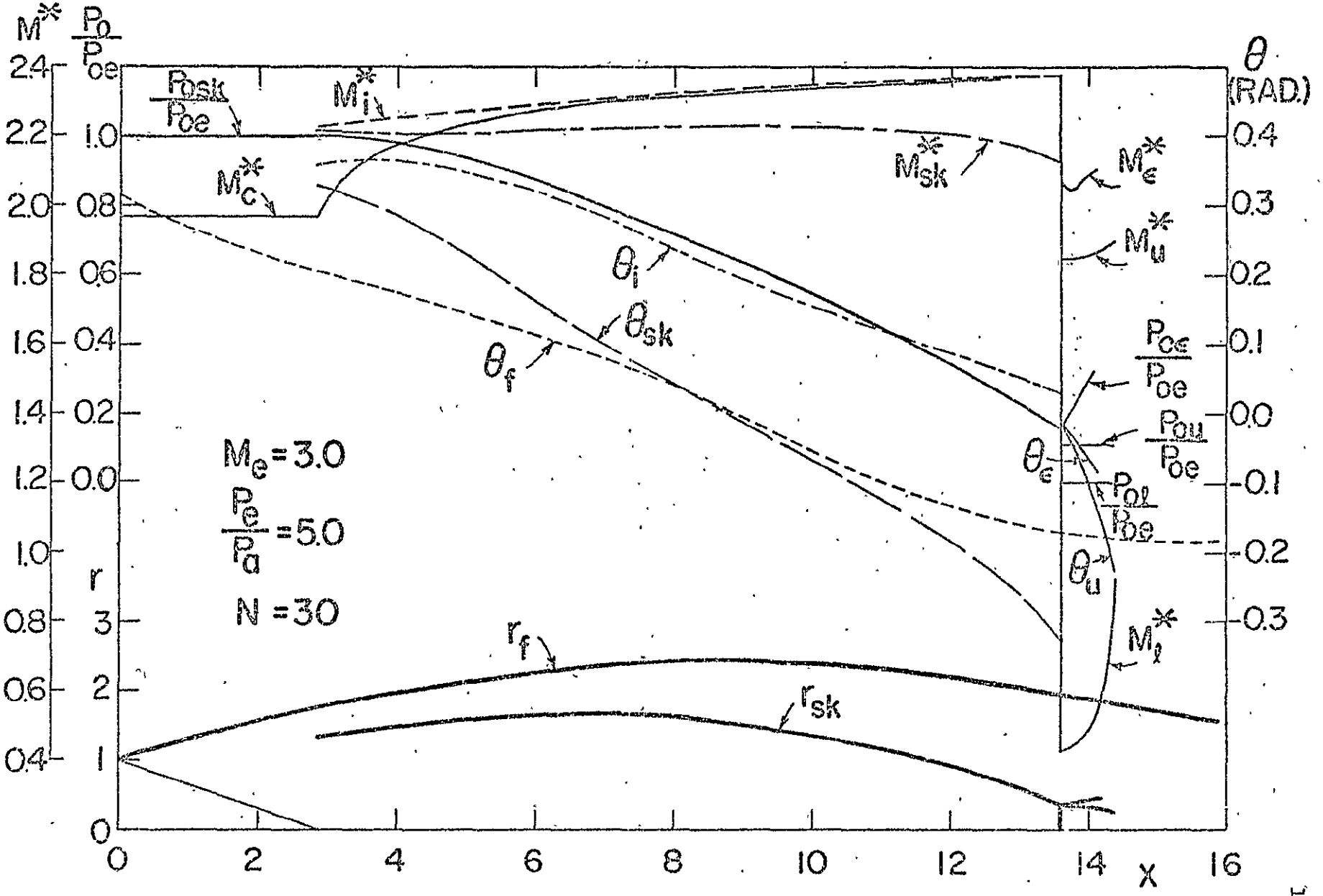

Figure 46 Distributions of Various Flow Properties at $M_e = 3.0$, $P_e/P_a = 5.0$

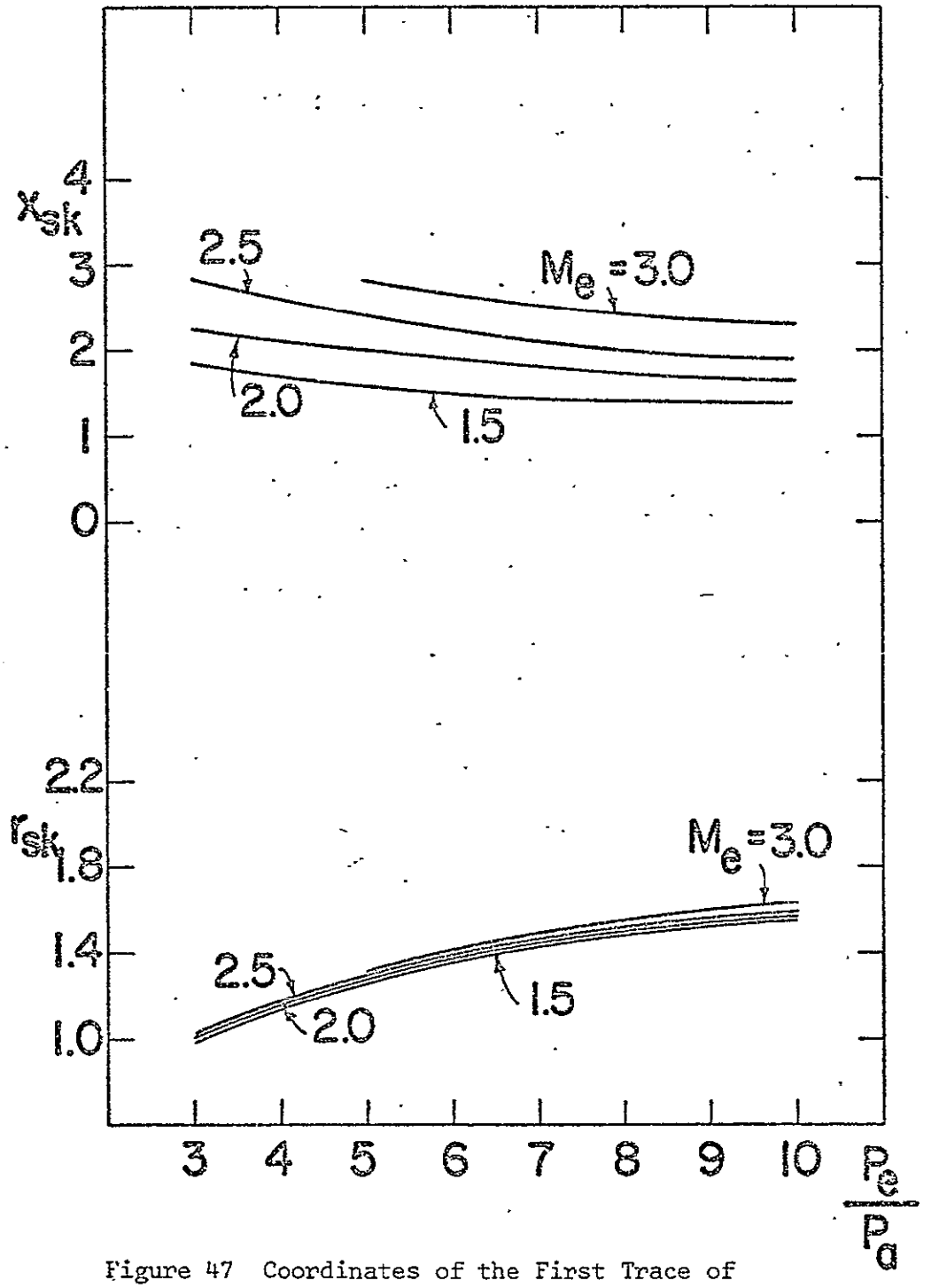

Figure 47 Coordinates of the First Trace of Imbedded Shock Waves, X_{sk} and r_{sk}, vs. P_e/P_a

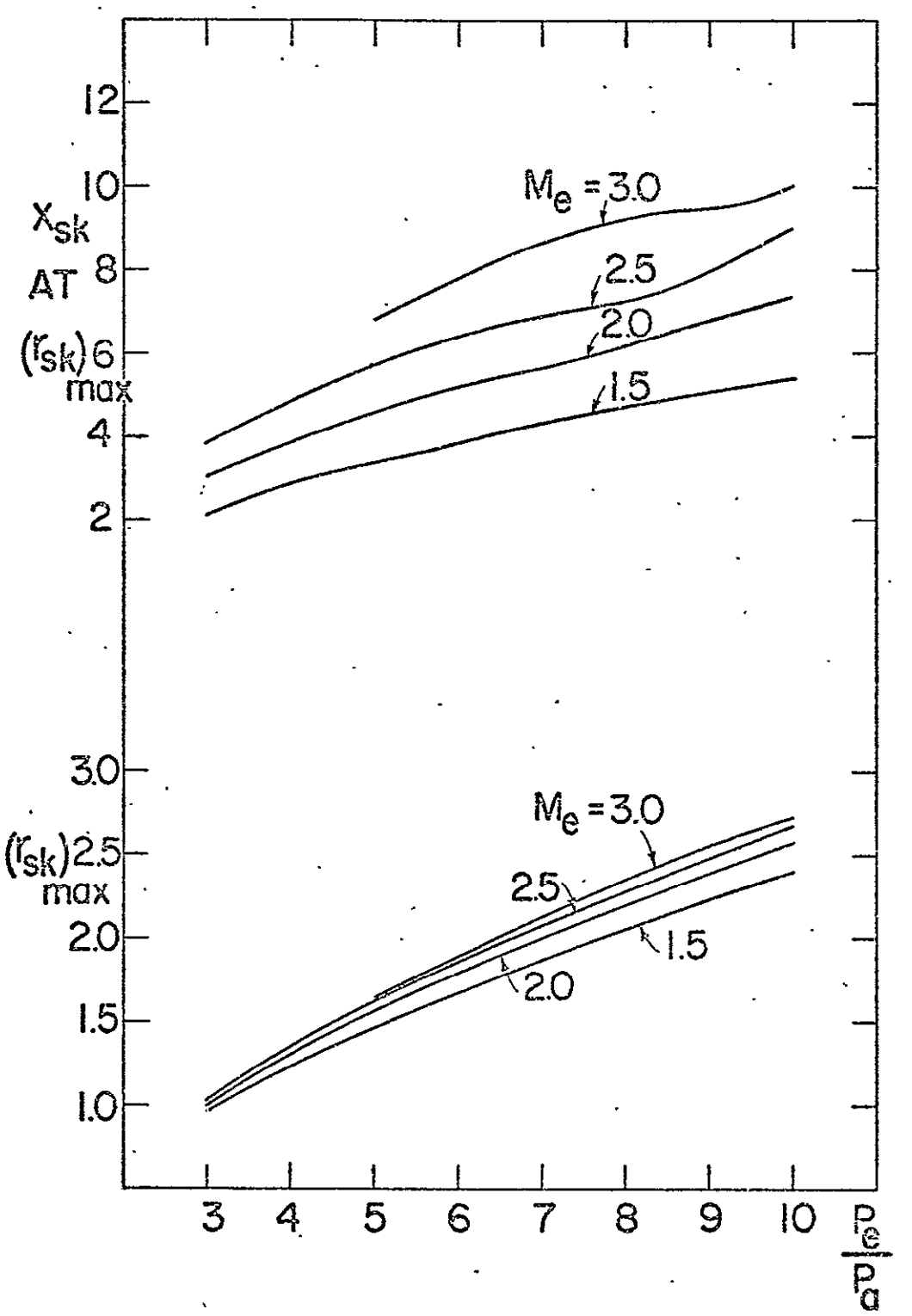

Figure 48 Coordinates of the Maximum Radius of the Imbedded Shock Wave, X_{sk} (at $r_{sk_{max}}$) and $r_{sk_{max}}$, vs. P_e/P_a

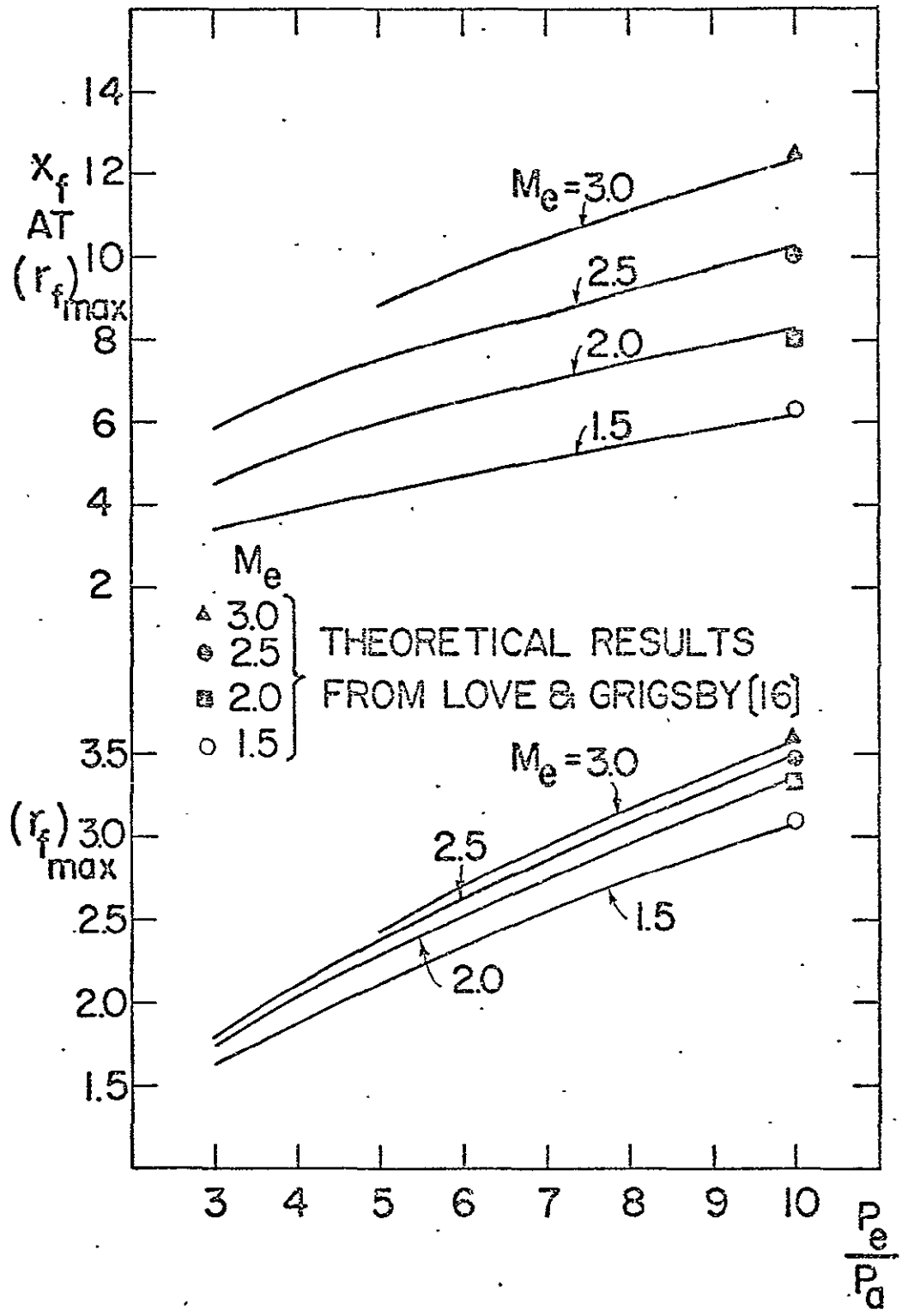

Figure 49 Coordinates of the Maximum Height of the Free Jet Boundary, x_f (at $r_{f_{max}}$) and $r_{f_{max}}$, vs. P_e/P_a

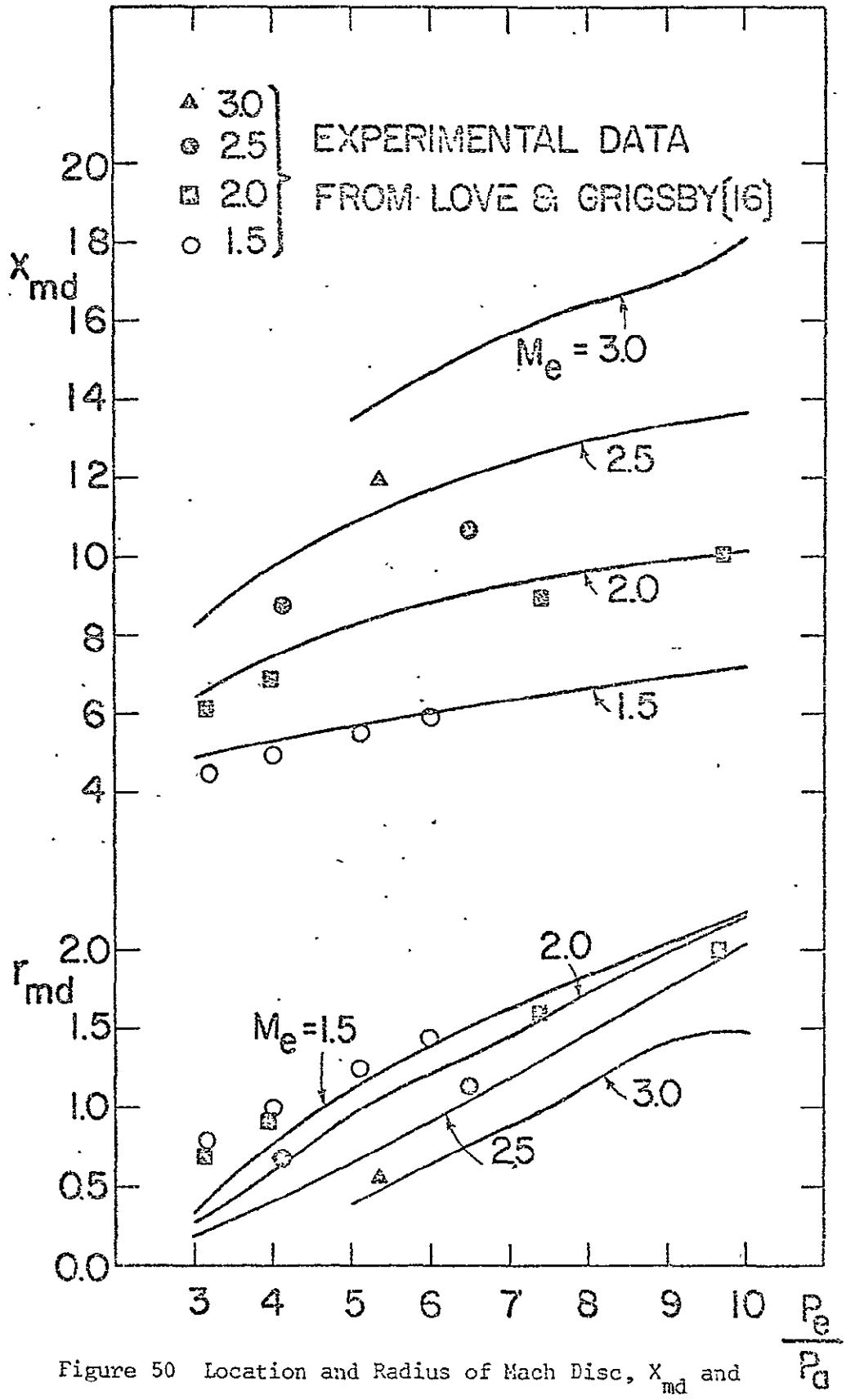

Figure 50 Location and Radius of Mach Disc, X_{md} and r_{md}, vs. P_e/P_a

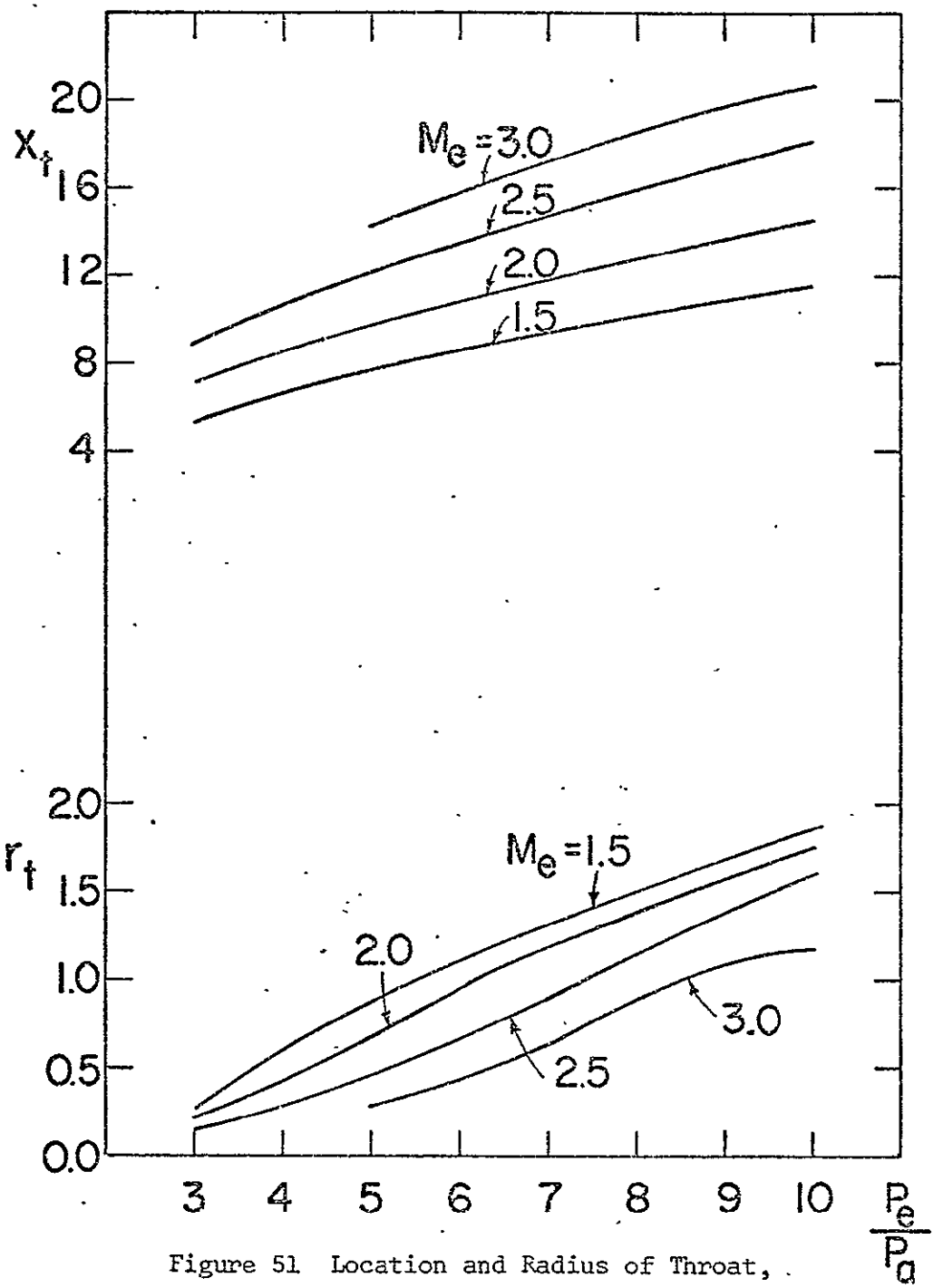

Figure 51 Location and Radius of Throat, X_t and r_t, vs. P_e/P_a

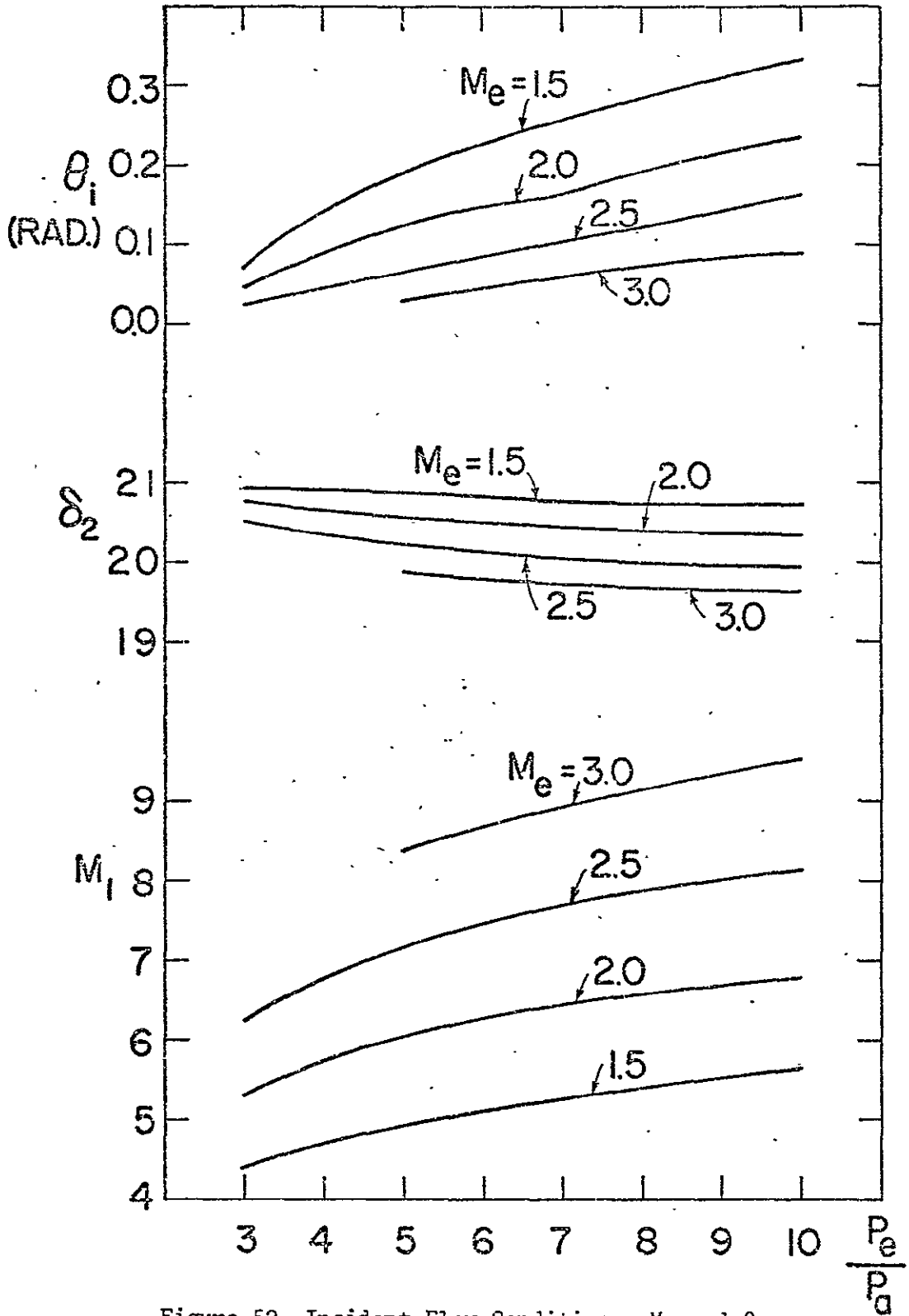

Figure 52 Incident Flow Conditions, M_1 and θ_i, and Deflection Angle δ_2 at Triple Point vs. P_e/P_a

Table 1 Triple-Point Solutions, $M_1 = 1.6$

TRIPLE POINT SOLUTION M1 = 1.600 GAMMA = 1.400

DELTA2	P2/P01	M2	M3	M4	DELTA3	DELTA4	SIGMA2	SIGMA3	SIGMA4	P2/P1	P3/P2	P4/P1	(P4/P1)*
3.975	0.296	1.465	0.725	0.668	3.975	0.0	42.902	84.912	90.000	1.217	2.316	2.820	2.010
4.120	0.298	1.460	0.727	0.668	3.830	0.240	43.069	84.983	89.767	1.226	2.300	2.820	2.010
4.260	0.300	1.455	0.728	0.669	3.800	0.440	43.208	85.044	89.573	1.233	2.286	2.820	2.010
4.360	0.302	1.451	0.729	0.669	3.718	0.642	43.348	85.109	89.378	1.241	2.273	2.820	2.010
4.480	0.304	1.447	0.731	0.669	3.635	0.845	43.489	85.176	89.181	1.248	2.259	2.819	2.010
4.600	0.305	1.443	0.732	0.669	3.551	1.049	43.631	85.247	88.982	1.255	2.246	2.819	2.010
4.720	0.307	1.439	0.733	0.669	3.466	1.255	43.773	85.321	88.782	1.263	2.232	2.819	2.010
4.840	0.309	1.435	0.735	0.669	3.378	1.462	43.916	85.398	88.580	1.270	2.219	2.818	2.011
4.960	0.311	1.430	0.736	0.670	3.289	1.671	44.060	85.478	88.376	1.278	2.205	2.818	2.011
5.080	0.312	1.426	0.737	0.670	3.199	1.881	44.205	85.562	88.170	1.285	2.192	2.817	2.011
5.200	0.314	1.422	0.739	0.670	3.107	2.093	44.350	85.649	87.963	1.293	2.178	2.816	2.011
5.320	0.316	1.418	0.740	0.671	3.014	2.306	44.497	85.739	87.753	1.300	2.165	2.815	2.011
5.440	0.318	1.413	0.741	0.671	2.919	2.521	44.644	85.834	87.541	1.308	2.152	2.815	2.011
5.560	0.320	1.409	0.743	0.672	2.823	2.737	44.792	85.932	87.328	1.316	2.138	2.814	2.012
5.680	0.321	1.405	0.744	0.673	2.725	2.955	44.942	86.034	87.112	1.324	2.125	2.812	2.012
5.800	0.323	1.401	0.746	0.673	2.626	3.174	45.092	86.140	86.893	1.331	2.111	2.811	2.012
5.920	0.325	1.396	0.747	0.674	2.526	3.394	45.243	86.251	86.673	1.339	2.098	2.810	2.012
6.040	0.327	1.392	0.749	0.675	2.424	3.616	45.395	86.365	86.450	1.347	2.085	2.809	2.013
6.160	0.329	1.388	0.750	0.675	2.320	3.840	45.547	86.485	86.224	1.355	2.071	2.807	2.013
6.280	0.331	1.383	0.752	0.676	2.215	4.065	45.701	86.608	85.995	1.363	2.058	2.805	2.013
6.400	0.333	1.379	0.753	0.677	2.109	4.291	45.856	86.737	85.764	1.371	2.045	2.804	2.014
6.520	0.335	1.375	0.755	0.678	2.001	4.519	46.012	86.870	85.530	1.379	2.031	2.802	2.014
6.640	0.336	1.370	0.756	0.679	1.891	4.749	46.169	87.009	85.293	1.388	2.018	2.800	2.015
6.760	0.338	1.366	0.758	0.680	1.780	4.980	46.327	87.152	85.052	1.396	2.004	2.798	2.015
6.880	0.340	1.361	0.759	0.682	1.668	5.212	46.487	87.302	84.809	1.404	1.991	2.796	2.016
7.000	0.342	1.357	0.761	0.683	1.554	5.446	46.647	87.457	84.561	1.412	1.978	2.793	2.016
7.120	0.344	1.353	0.762	0.684	1.439	5.681	46.808	87.617	84.310	1.421	1.964	2.791	2.017
7.240	0.346	1.348	0.765	0.686	1.322	5.918	46.971	87.784	84.055	1.429	1.951	2.788	2.017
7.360	0.348	1.344	0.766	0.687	1.203	6.157	47.135	87.958	83.796	1.438	1.937	2.785	2.018
7.480	0.350	1.339	0.768	0.688	1.084	6.396	47.300	88.138	83.533	1.446	1.923	2.782	2.019
7.600	0.352	1.335	0.770	0.691	0.963	6.637	47.466	83.324	83.266	1.455	1.910	2.779	2.019
7.720	0.354	1.330	0.772	0.692	0.840	6.880	47.634	88.519	82.994	1.464	1.896	2.776	2.020
7.840	0.356	1.326	0.774	0.694	0.716	7.124	47.802	88.720	82.717	1.473	1.882	2.772	2.021
7.960	0.358	1.321	0.776	0.696	0.591	7.369	47.973	89.930	82.435	1.481	1.869	2.768	2.022
8.080	0.360	1.316	0.780	0.707	0.000	8.509	48.771	90.000	81.069	1.523	1.805	2.748	2.026

Table 2 Triple-Point Solutions, $M_1 = 1.8$

TRIPLE POINT SOLUTION M1 = 1.800 GAMMA = 1.400

DELTA2	P2/P01	M2	M3	M4	DELTA3	DELTA4	SIGMA2	SIGMA3	SIGMA4	P2/P1	P3/P2	P4/P1	(P4/P1)*
9.069	0.276	1.484	0.776	0.617	9.059	0.0	42.920	77.293	90.000	1.584	2.278	3.613	2.467
9.200	0.278	1.479	0.777	0.617	8.952	0.248	43.078	77.352	89.817	1.597	2.263	3.613	2.467
9.400	0.281	1.472	0.778	0.617	8.771	0.629	43.319	77.440	89.537	1.612	2.241	3.613	2.467
9.600	0.283	1.464	0.780	0.617	8.587	1.013	43.563	77.530	89.254	1.629	2.218	3.613	2.467
9.800	0.286	1.457	0.781	0.617	8.399	1.401	43.808	77.620	88.968	1.645	2.195	3.612	2.467
10.000	0.289	1.449	0.782	0.618	8.207	1.793	44.057	77.712	88.673	1.661	2.174	3.611	2.467
10.200	0.292	1.442	0.784	0.618	8.011	2.189	44.307	77.873	88.383	1.678	2.152	3.610	2.468
10.400	0.295	1.434	0.785	0.619	7.812	2.588	44.561	78.003	88.088	1.694	2.130	3.609	2.468
10.600	0.298	1.427	0.786	0.619	7.608	2.992	44.816	78.143	87.787	1.711	2.108	3.608	2.469
10.800	0.301	1.419	0.787	0.620	7.401	3.399	45.075	78.292	87.481	1.728	2.087	3.606	2.469
11.000	0.304	1.412	0.789	0.621	7.189	3.811	45.336	78.452	87.171	1.745	2.065	3.604	2.470
11.200	0.307	1.404	0.790	0.622	6.974	4.226	45.600	78.623	86.856	1.763	2.043	3.602	2.470
11.400	0.310	1.396	0.791	0.623	6.754	4.646	45.867	78.805	86.536	1.781	2.022	3.600	2.471
11.600	0.313	1.388	0.793	0.625	6.530	5.070	46.137	79.000	86.210	1.798	2.000	3.597	2.472
11.800	0.316	1.380	0.794	0.626	6.302	5.498	46.410	79.207	85.878	1.816	1.979	3.594	2.473
12.000	0.319	1.373	0.795	0.628	6.070	5.930	46.686	79.427	85.539	1.834	1.957	3.590	2.474
12.200	0.322	1.365	0.797	0.630	5.832	6.368	46.966	79.662	85.195	1.853	1.936	3.587	2.475
12.400	0.326	1.357	0.798	0.632	5.591	6.809	47.249	79.911	84.840	1.872	1.914	3.583	2.477
12.600	0.329	1.348	0.800	0.634	5.344	7.256	47.536	80.177	84.478	1.890	1.893	3.578	2.478
12.800	0.332	1.340	0.801	0.636	5.093	7.707	47.826	80.459	84.108	1.910	1.871	3.573	2.480
13.000	0.336	1.332	0.803	0.639	4.837	8.163	48.121	80.760	83.728	1.929	1.850	3.568	2.481
13.200	0.339	1.324	0.804	0.642	4.576	8.624	48.420	81.080	83.337	1.948	1.828	3.562	2.483
13.400	0.343	1.315	0.806	0.645	4.309	9.091	48.723	81.420	82.935	1.968	1.807	3.556	2.485
13.600	0.346	1.307	0.808	0.648	4.038	9.562	49.031	81.783	82.521	1.988	1.785	3.549	2.487
13.800	0.350	1.298	0.810	0.652	3.761	10.039	49.343	82.171	82.093	2.009	1.763	3.542	2.490
14.000	0.353	1.290	0.812	0.656	3.478	10.522	49.661	82.584	81.649	2.029	1.741	3.534	2.492
14.200	0.357	1.281	0.814	0.660	3.190	11.010	49.984	83.025	81.189	2.050	1.719	3.525	2.495
14.400	0.361	1.272	0.816	0.665	2.897	11.503	50.313	83.500	80.711	2.072	1.696	3.515	2.498
14.600	0.364	1.263	0.818	0.670	2.597	12.003	50.647	84.003	80.212	2.094	1.674	3.504	2.502
14.800	0.368	1.254	0.821	0.676	2.292	12.508	50.989	84.554	79.690	2.116	1.651	3.492	2.506
15.000	0.372	1.245	0.824	0.682	1.982	13.018	51.336	85.142	79.142	2.138	1.627	3.479	2.510
15.200	0.376	1.235	0.827	0.689	1.665	13.535	51.692	85.778	78.564	2.161	1.603	3.465	2.514
15.400	0.380	1.226	0.831	0.697	1.344	14.056	52.055	86.467	77.953	2.184	1.579	3.449	2.520
15.600	0.384	1.216	0.835	0.705	1.016	14.582	52.426	87.217	77.302	2.208	1.554	3.431	2.525
16.213	0.397	1.185	0.852	0.738	0.000	16.213	53.625	90.000	74.989	2.284	1.471	3.360	2.548

Table 3 Triple-Point Solutions, $M_1 = 1.92$

TRIPLE POINT SOLUTION M1 = 1.920 GAMMA = 1.400

DELTA2	P2/P01	M2	M3	M4	DELTA3	DELTA4	SIGMA2	SIGMA3	SIGMA4	P2/P1	P3/P2	P4/P1	(P4/P1)*
11.353	0.261	1.515	0.814	0.592	11.353	0.0	42.611	73.359	90.000	1.805	2.291	4.134	2.768
11.500	0.263	1.509	0.815	0.592	11.212	0.288	42.769	73.411	89.814	1.818	2.274	4.134	2.768
11.750	0.266	1.500	0.815	0.592	10.969	0.781	43.093	73.509	89.495	1.841	2.246	4.134	2.768
12.000	0.270	1.490	0.817	0.592	10.720	1.280	43.401	73.618	89.172	1.864	2.218	4.133	2.768
12.250	0.273	1.480	0.818	0.593	10.466	1.784	43.713	73.730	88.845	1.887	2.190	4.132	2.769
12.500	0.276	1.471	0.819	0.593	10.207	2.293	44.028	73.843	88.513	1.911	2.162	4.131	2.769
12.750	0.280	1.461	0.820	0.594	9.943	2.807	44.347	74.021	88.177	1.936	2.135	4.130	2.770
13.000	0.283	1.451	0.821	0.595	9.673	3.327	44.671	74.181	87.836	1.959	2.107	4.128	2.770
13.250	0.287	1.441	0.822	0.596	9.397	3.853	44.998	74.357	87.489	1.984	2.080	4.126	2.771
13.500	0.291	1.431	0.823	0.597	9.115	4.385	45.329	74.548	87.137	2.008	2.053	4.123	2.772
13.750	0.294	1.421	0.824	0.598	8.828	4.922	45.665	74.755	86.777	2.034	2.026	4.121	2.773
14.000	0.298	1.411	0.825	0.600	8.534	5.466	46.006	74.980	86.411	2.059	1.999	4.117	2.774
14.250	0.302	1.401	0.826	0.602	8.235	6.015	46.352	75.223	86.036	2.085	1.973	4.114	2.776
14.500	0.306	1.390	0.826	0.604	7.928	6.572	46.702	75.485	85.653	2.111	1.946	4.109	2.777
14.750	0.309	1.380	0.827	0.606	7.615	7.135	47.058	75.768	85.261	2.138	1.920	4.105	2.779
15.000	0.313	1.369	0.828	0.608	7.294	7.706	47.420	76.074	84.858	2.165	1.893	4.100	2.781
15.250	0.317	1.358	0.829	0.611	6.967	8.283	47.787	76.405	84.444	2.193	1.867	4.094	2.783
15.500	0.321	1.348	0.829	0.614	6.631	8.869	48.161	76.760	84.018	2.221	1.841	4.087	2.785
15.750	0.325	1.337	0.830	0.616	6.288	9.462	48.542	77.144	83.577	2.249	1.814	4.080	2.788
16.000	0.330	1.325	0.831	0.621	5.937	10.063	48.929	77.558	83.121	2.278	1.788	4.072	2.791
16.250	0.334	1.314	0.832	0.625	5.576	10.674	49.324	78.007	82.648	2.307	1.761	4.064	2.795
16.500	0.338	1.303	0.833	0.630	5.207	11.293	49.727	78.492	82.156	2.337	1.735	4.054	2.798
16.750	0.343	1.291	0.835	0.635	4.828	11.922	50.138	79.018	81.642	2.367	1.708	4.043	2.802
17.000	0.347	1.279	0.836	0.641	4.439	12.561	50.559	79.590	81.103	2.398	1.681	4.031	2.807
17.250	0.352	1.267	0.837	0.647	4.040	13.210	50.990	80.214	80.536	2.430	1.653	4.018	2.812
17.500	0.356	1.255	0.839	0.654	3.630	13.870	51.431	80.895	79.937	2.462	1.626	4.003	2.818
17.750	0.361	1.243	0.841	0.661	3.208	14.542	51.884	81.642	79.300	2.496	1.597	3.986	2.824
18.000	0.366	1.230	0.844	0.670	2.775	15.225	52.351	82.467	78.618	2.529	1.568	3.967	2.831
18.250	0.371	1.217	0.847	0.680	2.330	15.920	52.831	83.380	77.884	2.564	1.538	3.945	2.840
18.500	0.376	1.204	0.851	0.691	1.874	16.626	53.328	84.400	77.085	2.600	1.507	3.919	2.850
18.750	0.382	1.190	0.855	0.704	1.405	17.344	53.842	85.549	76.208	2.637	1.475	3.890	2.861
19.482	0.398	1.147	0.877	0.758	0.000	19.482	55.479	90.000	72.949	2.753	1.367	3.764	2.909

Table 4 Triple-Point Solutions, $M_1 = 2.0$

TRIPLE POINT SOLUTION M1 = 2.000 GAMMA = 1.400

DELTA2	P2/P01	M2	M3	M4	DELTA3	DELTA4	SIGMA2	SIGMA3	SIGMA4	P2/P1	P3/P2	P4/P1	(P4/P1)*
12.627	0.249	1.541	0.842	0.577	12.627	0.0	42.322	70.973	90.000	1.949	2.309	4.500	2.980
13.250	0.257	1.517	0.844	0.573	12.004	1.246	43.083	71.197	89.232	2.011	2.238	4.499	2.980
13.500	0.260	1.507	0.845	0.575	11.745	1.755	43.395	71.305	88.945	2.038	2.209	4.498	2.980
13.750	0.263	1.497	0.846	0.579	11.482	2.268	43.710	71.427	88.636	2.062	2.181	4.497	2.981
14.000	0.267	1.487	0.846	0.579	11.214	2.786	44.029	71.561	88.322	2.088	2.154	4.496	2.981
14.250	0.270	1.476	0.847	0.580	10.940	3.310	44.351	71.707	88.004	2.114	2.129	4.494	2.982
14.500	0.274	1.466	0.847	0.581	10.662	3.838	44.678	71.868	87.682	2.140	2.099	4.492	2.983
14.750	0.277	1.456	0.848	0.582	10.378	4.372	45.009	72.042	87.354	2.167	2.072	4.490	2.984
15.000	0.280	1.446	0.848	0.583	10.089	4.911	45.344	72.232	87.021	2.195	2.045	4.487	2.985
15.250	0.284	1.435	0.848	0.585	9.795	5.455	45.683	72.437	86.681	2.222	2.018	4.484	2.986
15.500	0.288	1.425	0.849	0.586	9.495	6.006	46.027	72.660	86.335	2.250	1.991	4.481	2.988
15.750	0.291	1.414	0.849	0.588	9.187	6.563	46.376	72.900	85.982	2.279	1.965	4.477	2.989
16.000	0.295	1.403	0.849	0.590	8.874	7.126	46.731	73.159	85.621	2.308	1.938	4.473	2.991
16.250	0.299	1.393	0.849	0.592	8.555	7.695	47.090	73.439	85.252	2.337	1.912	4.468	2.993
16.500	0.302	1.382	0.849	0.595	8.228	8.272	47.455	73.740	84.872	2.366	1.886	4.463	2.995
16.750	0.306	1.371	0.849	0.598	7.895	8.855	47.827	74.065	84.483	2.397	1.860	4.457	2.998
17.000	0.310	1.359	0.850	0.601	7.554	9.446	48.204	74.415	84.082	2.427	1.834	4.450	3.000
17.250	0.314	1.348	0.850	0.604	7.205	10.045	48.588	74.792	83.669	2.458	1.808	4.443	3.003
17.500	0.318	1.337	0.850	0.608	6.848	10.652	48.980	75.199	83.241	2.490	1.781	4.435	3.007
17.750	0.322	1.325	0.850	0.612	6.482	11.268	49.378	75.638	82.798	2.522	1.755	4.427	3.010
18.000	0.326	1.313	0.850	0.616	6.106	11.894	49.785	76.112	82.337	2.555	1.729	4.417	3.014
18.250	0.331	1.301	0.851	0.621	5.722	12.528	50.201	76.626	81.856	2.588	1.703	4.406	3.019
18.500	0.335	1.289	0.851	0.626	5.327	13.173	50.625	77.184	81.353	2.622	1.676	4.395	3.024
18.750	0.340	1.276	0.852	0.632	4.920	13.830	51.060	77.790	80.825	2.657	1.649	4.381	3.029
19.000	0.344	1.264	0.853	0.639	4.503	14.497	51.506	78.451	80.267	2.692	1.622	4.367	3.035
19.250	0.349	1.251	0.854	0.646	4.073	15.177	51.964	79.175	79.675	2.728	1.596	4.350	3.042
19.500	0.353	1.238	0.855	0.654	3.630	15.870	52.435	79.972	79.044	2.765	1.566	4.331	3.050
19.750	0.358	1.224	0.857	0.663	3.174	16.576	52.921	80.852	78.365	2.804	1.537	4.310	3.059
20.000	0.363	1.210	0.859	0.674	2.703	17.297	53.423	81.832	77.630	2.843	1.508	4.286	3.069
20.250	0.369	1.195	0.862	0.686	2.218	18.032	53.943	82.932	76.825	2.883	1.477	4.259	3.081
20.500	0.374	1.181	0.866	0.700	1.719	18.781	54.485	84.177	75.934	2.925	1.444	4.229	3.095
20.750	0.379	1.166	0.871	0.716	1.207	19.543	55.050	85.610	74.941	2.969	1.410	4.185	3.112
21.329	0.393	1.128	0.891	0.770	0.000	21.329	56.479	90.000	71.935	3.077	1.317	4.051	3.169

Table 5 Triple-Point Solutions, $M_1 = 2.2$

TRIPLE POINT SOLUTION M1 = 2.200 GAMMA = 1.400

DELTA2	P2/P01	M2	M3	M4	DELTA3	DELTA4	SIGMA2	SIGMA3	SIGMA4	P2/P1	P3/P2	P4/P1	(P4/P1)*
15.128	0.216	1.620	0.918	0.547	15.128	0.0	41.422	65.754	90.000	2.305	2.377	5.480	3.548
15.300	0.217	1.612	0.918	0.547	14.955	0.345	41.530	65.794	89.823	2.325	2.357	5.480	3.548
15.600	0.221	1.600	0.918	0.547	14.650	0.950	41.995	65.875	89.513	2.361	2.321	5.480	3.548
15.900	0.224	1.587	0.918	0.548	14.339	1.561	42.365	65.970	89.199	2.397	2.285	5.479	3.549
16.200	0.228	1.575	0.918	0.548	14.024	2.176	42.739	66.079	88.883	2.434	2.250	5.478	3.549
16.500	0.231	1.562	0.917	0.549	13.703	2.797	43.118	66.204	88.562	2.471	2.215	5.476	3.550
16.800	0.235	1.549	0.917	0.549	13.376	3.424	43.502	66.345	88.238	2.509	2.182	5.475	3.551
17.100	0.238	1.536	0.916	0.550	13.044	4.056	43.891	66.502	87.908	2.547	2.148	5.472	3.552
17.400	0.242	1.523	0.915	0.552	12.706	4.694	44.286	66.673	87.574	2.586	2.115	5.470	3.553
17.700	0.246	1.510	0.915	0.553	12.362	5.338	44.686	66.871	87.235	2.626	2.082	5.467	3.555
18.000	0.249	1.496	0.914	0.554	12.011	5.989	45.092	67.085	86.889	2.666	2.049	5.463	3.557
18.300	0.253	1.483	0.912	0.556	11.654	6.646	45.505	67.319	86.536	2.706	2.017	5.459	3.559
18.600	0.257	1.469	0.911	0.558	11.289	7.311	45.924	67.575	86.176	2.748	1.985	5.456	3.561
18.900	0.261	1.455	0.910	0.560	10.917	7.983	46.349	67.857	85.807	2.790	1.954	5.450	3.563
19.200	0.265	1.442	0.909	0.563	10.538	8.662	46.782	68.163	85.429	2.832	1.922	5.444	3.566
19.500	0.269	1.427	0.907	0.566	10.147	9.353	47.223	68.496	85.040	2.876	1.891	5.438	3.569
19.800	0.273	1.413	0.905	0.569	9.750	10.050	47.672	68.859	84.641	2.920	1.860	5.431	3.573
20.100	0.277	1.399	0.904	0.572	9.342	10.758	48.129	69.254	84.228	2.967	1.829	5.423	3.577
20.400	0.282	1.384	0.902	0.576	8.924	11.476	48.596	69.684	83.800	3.010	1.799	5.414	3.581
20.700	0.286	1.369	0.900	0.580	8.495	12.205	49.073	70.154	83.357	3.057	1.768	5.404	3.586
21.000	0.290	1.354	0.898	0.585	8.054	12.946	49.560	70.665	82.895	3.104	1.738	5.394	3.592
21.300	0.295	1.338	0.896	0.590	7.600	13.700	50.060	71.225	82.411	3.153	1.707	5.382	3.598
21.600	0.299	1.323	0.895	0.596	7.131	14.469	50.572	71.838	81.904	3.202	1.676	5.368	3.605
21.900	0.304	1.307	0.893	0.602	6.647	15.253	51.098	72.511	81.368	3.253	1.645	5.353	3.613
22.200	0.309	1.290	0.891	0.609	6.146	16.054	51.640	73.254	80.800	3.305	1.614	5.334	3.621
22.500	0.314	1.273	0.889	0.617	5.627	16.873	52.200	74.073	80.193	3.359	1.583	5.316	3.631
22.800	0.319	1.256	0.888	0.625	5.087	17.713	52.779	74.996	79.539	3.414	1.551	5.294	3.643
23.100	0.325	1.238	0.887	0.637	4.523	18.577	53.380	76.028	78.829	3.471	1.518	5.268	3.655
23.400	0.330	1.220	0.886	0.649	3.935	19.465	54.007	77.194	78.048	3.530	1.484	5.238	3.672
23.700	0.336	1.201	0.886	0.663	3.318	20.382	54.663	78.535	77.177	3.591	1.449	5.202	3.690
24.000	0.342	1.181	0.887	0.680	2.669	21.331	55.356	80.095	76.188	3.655	1.411	5.158	3.713
24.300	0.348	1.159	0.890	0.701	1.987	22.313	56.092	81.955	75.036	3.723	1.371	5.104	3.742
24.600	0.355	1.137	0.895	0.727	1.271	23.329	56.883	84.238	73.646	3.794	1.326	5.032	3.780
25.119	0.366	1.093	0.917	0.800	0.000	25.119	58.441	90.000	70.174	3.933	1.223	4.830	3.888

Table 6 Triple-Point Solutions, $M_1 = 2.4$

TRIPLE POINT SOLUTION M1 = 2.400 GAMMA = 1.400

DELTA2	P2/P01	M2	M3	M4	DELTA3	DELTA4	SIGMA2	SIGMA3	SIGMA4	P2/P1	P3/P2	P4/P1	(P4/P1)*
16.892	0.182	1.711	0.998	0.523	16.892	0.0	40.399	61.444	90.000	2.556	2.467	6.553	4.172
17.350	0.186	1.690	0.997	0.523	16.435	0.915	40.950	61.526	89.586	2.720	2.409	6.553	4.172
17.700	0.189	1.675	0.996	0.524	16.080	1.620	41.377	61.609	89.267	2.770	2.366	6.552	4.172
18.050	0.193	1.659	0.995	0.524	15.720	2.330	41.810	61.708	88.945	2.820	2.323	6.551	4.173
18.400	0.196	1.643	0.993	0.525	15.354	3.046	42.249	61.827	88.619	2.871	2.281	6.549	4.174
18.750	0.200	1.627	0.992	0.526	14.983	3.767	42.694	61.964	88.289	2.923	2.240	6.547	4.175
19.100	0.204	1.611	0.990	0.527	14.607	4.493	43.145	62.122	87.955	2.976	2.199	6.545	4.177
19.450	0.207	1.595	0.987	0.528	14.224	5.226	43.603	62.300	87.616	3.030	2.159	6.542	4.179
19.800	0.211	1.578	0.985	0.529	13.834	5.966	44.067	62.501	87.271	3.084	2.120	6.538	4.181
20.150	0.215	1.562	0.983	0.531	13.438	6.712	44.539	62.726	86.920	3.139	2.081	6.534	4.183
20.500	0.219	1.545	0.980	0.533	13.034	7.466	45.019	62.976	86.562	3.196	2.043	6.529	4.186
20.850	0.222	1.528	0.977	0.535	12.622	8.228	45.507	63.253	86.195	3.253	2.006	6.524	4.189
21.200	0.226	1.511	0.974	0.538	12.202	8.998	46.003	63.558	85.820	3.311	1.968	6.518	4.193
21.550	0.231	1.494	0.970	0.541	11.772	9.778	46.509	63.894	85.435	3.370	1.932	6.511	4.197
21.900	0.235	1.476	0.967	0.544	11.333	10.567	47.025	64.264	85.038	3.431	1.896	6.503	4.201
22.250	0.239	1.458	0.963	0.547	10.882	11.368	47.551	64.671	84.629	3.492	1.860	6.494	4.206
22.600	0.243	1.440	0.959	0.551	10.421	12.179	48.088	65.117	84.205	3.555	1.824	6.485	4.212
22.950	0.248	1.422	0.955	0.556	9.946	13.004	48.637	65.608	83.764	3.619	1.789	6.474	4.218
23.300	0.252	1.403	0.951	0.561	9.457	13.843	49.200	66.147	83.305	3.684	1.754	6.462	4.225
23.650	0.257	1.384	0.947	0.566	8.953	14.697	49.777	66.741	82.824	3.751	1.719	6.448	4.233
24.000	0.261	1.364	0.942	0.572	8.432	15.568	50.371	67.397	82.317	3.820	1.684	6.433	4.242
24.350	0.266	1.344	0.938	0.579	7.891	16.459	50.982	68.124	81.781	3.890	1.649	6.416	4.253
24.700	0.271	1.324	0.933	0.586	7.330	17.370	51.613	68.932	81.210	3.962	1.614	6.396	4.264
25.050	0.276	1.303	0.929	0.595	6.744	18.306	52.267	69.837	80.597	4.037	1.579	6.374	4.278
25.400	0.281	1.282	0.924	0.605	6.130	19.270	52.946	70.856	79.932	4.113	1.543	6.348	4.293
25.750	0.287	1.259	0.920	0.616	5.484	20.266	53.656	72.015	79.203	4.193	1.507	6.318	4.312
26.100	0.292	1.236	0.916	0.629	4.802	21.298	54.401	73.349	78.392	4.276	1.469	6.281	4.334
26.450	0.298	1.211	0.912	0.646	4.076	22.374	55.189	74.908	77.473	4.363	1.429	6.237	4.360
26.800	0.305	1.186	0.910	0.665	3.298	23.502	56.031	76.772	76.405	4.455	1.388	6.182	4.394
27.150	0.311	1.158	0.909	0.690	2.460	24.690	56.943	79.073	75.116	4.554	1.342	6.110	4.439
27.500	0.319	1.128	0.911	0.724	1.550	25.950	57.949	82.057	73.473	4.661	1.289	6.010	4.502
28.059	0.333	1.071	0.935	0.825	0.000	28.059	59.889	90.000	69.098	4.862	1.172	5.698	4.704

Table 7 Triple-Point Solutions, $M_1 = 2.6$

TRIPLE POINT SOLUTION M1 = 2.600 GAMMA = 1.400

DELTA2	P2/P01	M2	M3	M4	DELTA3	DELTA4	SIGMA2	SIGMA3	SIGMA4	P2/P1	P3/P2	P4/P1	(P4/P1)*
18.141	0.151	1.809	1.080	0.504	18.141	0.0	39.351	57.863	90.000	3.004	2.570	7.720	4.850
18.400	0.153	1.795	1.079	0.504	17.890	0.510	39.659	57.891	89.792	3.046	2.535	7.720	4.850
18.800	0.156	1.778	1.077	0.504	17.499	1.301	40.140	57.949	89.468	3.111	2.481	7.719	4.851
19.200	0.159	1.758	1.075	0.505	17.103	2.097	40.627	58.029	89.143	3.177	2.429	7.718	4.851
19.600	0.163	1.739	1.072	0.505	16.703	2.897	41.121	58.129	88.814	3.244	2.379	7.717	4.853
20.000	0.166	1.720	1.069	0.506	16.297	3.703	41.621	58.251	88.482	3.313	2.329	7.714	4.856
20.400	0.169	1.700	1.066	0.507	15.886	4.514	42.129	58.396	88.146	3.382	2.280	7.712	4.856
20.800	0.173	1.681	1.062	0.508	15.469	5.331	42.645	58.565	87.805	3.453	2.232	7.708	4.858
21.200	0.177	1.661	1.058	0.510	15.046	6.154	43.169	58.760	87.459	3.525	2.186	7.704	4.860
21.600	0.180	1.641	1.054	0.512	14.616	6.984	43.701	58.981	87.107	3.598	2.140	7.700	4.864
22.000	0.184	1.621	1.050	0.514	14.178	7.822	44.242	59.231	86.748	3.672	2.095	7.695	4.867
22.400	0.188	1.600	1.045	0.516	13.733	8.667	44.793	59.511	86.381	3.748	2.051	7.689	4.871
22.800	0.192	1.579	1.040	0.519	13.278	9.522	45.353	59.824	86.005	3.825	2.008	7.682	4.875
23.200	0.196	1.558	1.034	0.522	12.814	10.386	45.924	60.172	85.619	3.904	1.966	7.674	4.881
23.600	0.200	1.537	1.029	0.525	12.340	11.260	46.507	60.557	85.221	3.984	1.924	7.665	4.886
24.000	0.204	1.516	1.023	0.529	11.854	12.146	47.102	60.985	84.810	4.066	1.883	7.655	4.893
24.400	0.208	1.496	1.016	0.533	11.354	13.046	47.711	61.457	84.385	4.149	1.842	7.644	4.900
24.800	0.212	1.472	1.010	0.538	10.841	13.959	48.334	61.981	83.942	4.235	1.802	7.632	4.908
25.200	0.217	1.449	1.003	0.543	10.312	14.888	48.973	62.560	83.479	4.322	1.763	7.618	4.918
25.600	0.221	1.426	0.996	0.549	9.765	15.835	49.629	63.203	82.993	4.411	1.724	7.603	4.928
26.000	0.226	1.402	0.989	0.555	9.198	16.802	50.305	63.918	82.479	4.503	1.685	7.586	4.940
26.400	0.230	1.378	0.981	0.562	8.608	17.792	51.003	64.717	81.933	4.597	1.646	7.565	4.953
26.800	0.235	1.354	0.974	0.571	7.993	18.807	51.726	65.613	81.349	4.694	1.607	7.542	4.969
27.200	0.240	1.328	0.966	0.580	7.346	19.854	52.478	66.626	80.716	4.794	1.567	7.515	4.987
27.600	0.245	1.302	0.958	0.591	6.665	20.935	53.263	67.781	80.025	4.898	1.528	7.483	5.009
28.000	0.251	1.274	0.950	0.604	5.941	22.059	54.088	69.113	79.257	5.007	1.487	7.446	5.034
28.400	0.257	1.246	0.943	0.620	5.167	23.233	54.962	70.675	78.389	5.120	1.445	7.401	5.065
28.800	0.263	1.215	0.935	0.639	4.330	24.470	55.898	72.547	77.382	5.241	1.401	7.344	5.105
29.200	0.269	1.183	0.929	0.663	3.413	25.737	56.914	74.865	76.169	5.370	1.354	7.269	5.157
29.600	0.276	1.147	0.925	0.696	2.394	27.206	58.045	77.886	74.622	5.511	1.300	7.165	5.231
30.401	0.294	1.056	0.948	0.846	0.000	30.401	61.004	90.000	68.422	5.867	1.134	6.653	5.615

Table 8 Triple-Point Solutions, $M_1 = 2.8$

TRIPLE POINT SOLUTION M1 = 2.800 GAMMA = 1.400

DELTA2	P2/P01	M2	M3	M4	DELTA3	DELTA4	SIGMA2	SIGMA3	SIGMA4	P2/P1	P3/P2	P4/P1	(P4/P1)*
19.027	0.123	1.910	1.162	0.488	19.027	0.0	38.329	54.861	90.000	3.351	2.680	8.980	5.584
19.400	0.126	1.893	1.160	0.488	18.676	0.724	38.770	54.886	89.728	3.420	2.626	8.980	5.584
19.800	0.129	1.871	1.157	0.488	18.297	1.503	39.249	54.930	89.435	3.495	2.569	8.979	5.584
20.200	0.132	1.851	1.154	0.489	17.915	2.285	39.733	54.993	89.141	3.571	2.514	8.978	5.585
20.600	0.134	1.830	1.150	0.490	17.529	3.071	40.223	55.075	88.844	3.648	2.461	8.976	5.586
21.000	0.137	1.810	1.146	0.490	17.140	3.860	40.719	55.177	88.545	3.726	2.409	8.974	5.588
21.400	0.140	1.789	1.142	0.491	16.747	4.653	41.223	55.300	88.243	3.805	2.358	8.971	5.590
21.800	0.143	1.768	1.137	0.493	16.350	5.450	41.733	55.444	87.937	3.886	2.308	8.968	5.592
22.200	0.146	1.747	1.132	0.494	15.948	6.252	42.250	55.611	87.628	3.968	2.259	8.964	5.595
22.600	0.149	1.726	1.127	0.496	15.541	7.059	42.775	55.802	87.314	4.052	2.211	8.960	5.598
23.000	0.152	1.705	1.121	0.497	15.128	7.872	43.307	56.017	86.994	4.137	2.165	8.955	5.602
23.400	0.156	1.683	1.115	0.499	14.710	8.690	43.848	56.259	86.669	4.223	2.119	8.949	5.606
23.800	0.159	1.662	1.109	0.502	14.284	9.516	44.398	56.529	86.337	4.311	2.075	8.943	5.611
24.200	0.162	1.640	1.103	0.504	13.851	10.349	44.957	56.828	85.998	4.400	2.031	8.935	5.616
24.600	0.165	1.618	1.096	0.507	13.410	11.190	45.526	57.160	85.650	4.491	1.988	8.927	5.622
25.000	0.169	1.595	1.088	0.510	12.960	12.040	46.105	57.525	85.292	4.583	1.946	8.918	5.628
25.400	0.172	1.572	1.081	0.514	12.500	12.900	46.695	57.928	84.923	4.677	1.905	8.908	5.636
25.800	0.176	1.549	1.073	0.518	12.030	13.770	47.298	58.372	84.542	4.773	1.864	8.897	5.644
26.200	0.179	1.526	1.065	0.522	11.547	14.653	47.914	58.860	84.147	4.871	1.824	8.885	5.653
26.600	0.183	1.503	1.057	0.527	11.051	15.549	48.545	59.397	83.736	4.971	1.785	8.871	5.663
27.000	0.187	1.478	1.048	0.532	10.539	16.461	49.191	59.990	83.306	5.073	1.746	8.856	5.674
27.400	0.191	1.454	1.039	0.538	10.011	17.389	49.854	60.644	82.855	5.178	1.707	8.838	5.687
27.800	0.195	1.429	1.030	0.545	9.463	18.337	50.537	61.369	82.378	5.285	1.669	8.819	5.701
28.200	0.199	1.403	1.020	0.552	8.893	19.307	51.242	62.175	81.872	5.395	1.631	8.797	5.718
28.600	0.203	1.377	1.010	0.561	8.298	20.302	51.971	63.077	81.329	5.509	1.592	8.772	5.736
29.000	0.207	1.350	1.000	0.570	7.673	21.327	52.729	64.091	80.742	5.626	1.554	8.743	5.758
29.400	0.212	1.322	0.990	0.581	7.014	22.386	53.521	65.244	80.101	5.747	1.516	8.710	5.783
29.800	0.216	1.293	0.980	0.594	6.313	23.487	54.352	66.568	79.391	5.873	1.476	8.670	5.813
30.200	0.221	1.263	0.969	0.609	5.561	24.639	55.232	68.113	78.589	6.006	1.436	8.622	5.850
30.600	0.226	1.231	0.957	0.627	4.746	25.854	56.175	69.957	77.662	6.146	1.393	8.562	5.896
31.000	0.232	1.196	0.943	0.650	3.850	27.150	57.199	72.227	76.549	6.296	1.348	8.485	5.956
31.400	0.238	1.159	0.941	0.682	2.845	28.555	58.338	75.165	75.140	6.460	1.297	8.378	6.041
31.800	0.245	1.116	0.935	0.728	1.689	30.111	59.660	79.327	73.166	6.646	1.236	8.213	6.175
32.303	0.256	1.045	0.959	0.864	0.000	32.303	61.889	90.000	67.990	6.949	1.107	7.695	6.619

Table 9 Triple-Point Solutions, $M_1 = 3.0$

TRIPLE POINT SOLUTION M1 = 3.000 GAMMA = 1.400

DELTA2	P2/P0?	M2	M3	M4	DELTA3	DELTA4	SIGMA2	SIGMA3	SIGMA4	P2/P1	P3/P2	P4/P1	(P4/P1)*
19.656	0.101	2.013	1.243	0.475	19.656	0.0	37.359	52.319	90.000	3.700	2.793	10.333	6.372
20.400	0.105	1.973	1.236	0.475	18.976	1.424	38.238	52.356	89.501	3.856	2.680	10.333	6.372
20.800	0.107	1.951	1.232	0.476	18.608	2.192	38.718	52.400	89.232	3.941	2.621	10.331	6.373
21.200	0.110	1.929	1.228	0.476	18.238	2.962	39.204	52.463	88.961	4.028	2.564	10.330	6.374
21.600	0.112	1.908	1.223	0.477	17.866	3.734	39.695	52.543	88.698	4.117	2.509	10.328	6.376
22.000	0.115	1.886	1.219	0.478	17.490	4.510	40.192	52.642	88.414	4.206	2.455	10.325	6.378
22.400	0.117	1.864	1.213	0.479	17.112	5.288	40.695	52.761	88.136	4.297	2.402	10.322	6.380
22.800	0.120	1.842	1.207	0.480	16.731	6.069	41.205	52.900	87.856	4.390	2.351	10.319	6.383
23.200	0.122	1.819	1.201	0.482	16.346	6.854	41.721	53.060	87.572	4.484	2.300	10.314	6.386
23.600	0.125	1.797	1.194	0.483	15.957	7.643	42.245	53.242	87.285	4.579	2.251	10.310	6.390
24.000	0.127	1.774	1.188	0.485	15.563	8.437	42.775	53.446	86.993	4.676	2.204	10.304	6.394
24.400	0.130	1.752	1.180	0.487	15.164	9.236	43.313	53.675	86.696	4.774	2.157	10.298	6.399
24.800	0.133	1.729	1.173	0.489	14.760	10.040	43.860	53.930	86.393	4.874	2.111	10.292	6.404
25.200	0.135	1.706	1.165	0.492	14.350	10.850	44.414	54.211	86.084	4.976	2.067	10.284	6.410
25.600	0.138	1.682	1.157	0.495	13.933	11.667	44.978	54.521	85.768	5.079	2.023	10.276	6.417
26.000	0.141	1.659	1.148	0.499	13.508	12.492	45.551	54.862	85.444	5.184	1.980	10.267	6.424
26.400	0.144	1.635	1.140	0.502	13.075	13.325	46.135	55.236	85.111	5.291	1.939	10.257	6.432
26.800	0.147	1.611	1.130	0.505	12.634	14.166	46.729	55.646	84.768	5.400	1.897	10.246	6.440
27.200	0.150	1.587	1.121	0.509	12.182	15.018	47.335	56.094	84.414	5.511	1.857	10.234	6.450
27.600	0.153	1.562	1.111	0.513	11.719	15.881	47.954	56.586	84.047	5.624	1.817	10.220	6.461
28.000	0.156	1.537	1.101	0.518	11.243	16.757	48.586	57.124	83.664	5.739	1.778	10.205	6.473
28.400	0.159	1.512	1.091	0.523	10.753	17.647	49.234	57.715	83.265	5.856	1.740	10.189	6.486
28.800	0.163	1.486	1.080	0.529	10.247	18.553	49.899	58.365	82.846	5.977	1.702	10.170	6.501
29.200	0.166	1.460	1.069	0.535	9.723	19.477	50.582	59.082	82.404	6.100	1.664	10.150	6.517
29.600	0.169	1.433	1.058	0.543	9.179	20.421	51.286	59.876	81.935	6.226	1.626	10.127	6.536
30.000	0.173	1.406	1.046	0.551	8.610	21.390	52.014	60.759	81.434	6.356	1.589	10.100	6.557
30.400	0.177	1.378	1.034	0.560	8.014	22.396	52.769	61.747	80.894	6.490	1.552	10.070	6.582
30.800	0.180	1.349	1.022	0.570	7.386	23.414	53.556	62.864	80.306	6.628	1.514	10.036	6.610
31.200	0.184	1.319	1.010	0.582	6.719	24.481	54.381	64.139	79.658	6.772	1.476	9.995	6.644
31.600	0.188	1.287	0.997	0.597	6.004	25.596	55.253	65.615	78.930	6.922	1.437	9.946	6.684
32.000	0.193	1.254	0.984	0.614	5.230	26.770	56.182	67.358	78.096	7.081	1.396	9.887	6.734
32.400	0.197	1.219	0.971	0.635	4.380	28.020	57.187	69.474	77.109	7.250	1.353	9.811	6.799
32.800	0.202	1.183	0.959	0.663	3.428	29.372	58.298	72.159	75.894	7.434	1.306	9.709	6.886
33.200	0.208	1.147	0.949	0.702	2.330	30.870	59.571	75.825	74.235	7.640	1.251	9.568	7.018
33.471	0.211	1.087	0.965	0.389	0.000	33.871	62.607	90.000	67.712	8.111	1.089	8.923	7.713

Table 10 Triple-Point Solutions, $M_1 = 3.2$

TRIPLE POINT SOLUTION M1 = 3.200 GAMMA = 1.400

DELTA2	P2/P01	M2	M3	M4	DELTA3	DELTA4	SIGMA2	SIGMA3	SIGMA4	P2/P1	P3/P2	P4/P1	(P4/P1)*
20.100	0.082	2.115	1.321	0.464	20.100	0.0	36.451	50.145	90.000	4.051	2.908	11.780	7.214
20.500	0.084	2.092	1.317	0.464	19.747	0.753	36.919	50.146	89.751	4.144	2.843	11.780	7.214
21.000	0.086	2.064	1.312	0.465	19.304	1.696	37.511	50.171	89.440	4.263	2.763	11.779	7.215
21.500	0.089	2.035	1.306	0.465	18.859	2.641	38.111	50.220	89.127	4.384	2.686	11.777	7.216
22.000	0.091	2.006	1.299	0.466	18.412	3.588	38.719	50.297	88.813	4.507	2.612	11.775	7.218
22.500	0.094	1.977	1.292	0.467	17.963	4.537	39.335	50.400	88.496	4.633	2.541	11.772	7.221
23.000	0.096	1.948	1.284	0.468	17.510	5.490	39.960	50.531	88.176	4.761	2.472	11.768	7.224
23.500	0.099	1.919	1.276	0.470	17.054	6.446	40.594	50.692	87.852	4.892	2.405	11.763	7.228
24.000	0.102	1.889	1.267	0.471	16.593	7.407	41.238	50.883	87.524	5.024	2.340	11.758	7.233
24.500	0.104	1.860	1.257	0.474	16.127	8.373	41.892	51.106	87.190	5.160	2.277	11.751	7.238
25.000	0.107	1.830	1.247	0.476	15.654	9.346	42.556	51.363	86.851	5.298	2.217	11.744	7.244
25.500	0.110	1.800	1.236	0.478	15.175	10.325	43.232	51.656	86.504	5.438	2.158	11.736	7.252
26.000	0.113	1.769	1.225	0.481	14.689	11.311	43.920	51.987	86.149	5.582	2.101	11.726	7.260
26.500	0.116	1.739	1.213	0.485	14.193	12.307	44.621	52.359	85.784	5.728	2.045	11.715	7.269
27.000	0.119	1.708	1.201	0.489	13.687	13.313	45.335	52.776	85.409	5.877	1.992	11.703	7.279
27.500	0.122	1.677	1.188	0.493	13.170	14.330	46.065	53.241	85.021	6.029	1.939	11.690	7.290
28.000	0.125	1.645	1.175	0.497	12.640	15.360	46.811	53.760	84.618	6.184	1.888	11.675	7.303
28.500	0.128	1.613	1.161	0.502	12.095	16.405	47.574	54.337	84.198	6.343	1.838	11.658	7.317
29.000	0.132	1.581	1.147	0.508	11.532	17.468	48.358	54.981	83.759	6.505	1.789	11.639	7.334
29.500	0.135	1.548	1.132	0.515	10.950	18.550	49.163	55.700	83.296	6.672	1.741	11.617	7.352
30.000	0.138	1.514	1.117	0.522	10.344	19.656	49.994	56.506	82.806	6.843	1.694	11.593	7.373
30.500	0.142	1.480	1.101	0.530	9.712	20.788	50.852	57.412	82.282	7.018	1.648	11.565	7.398
31.000	0.146	1.445	1.085	0.539	9.048	21.952	51.744	58.439	81.717	7.200	1.602	11.532	7.426
31.500	0.149	1.409	1.068	0.550	8.346	23.154	52.674	59.611	81.102	7.388	1.556	11.494	7.459
32.000	0.153	1.371	1.050	0.563	7.597	24.403	53.651	60.964	80.421	7.583	1.510	11.449	7.499
32.500	0.158	1.332	1.033	0.579	6.790	25.710	54.685	62.552	79.654	7.788	1.463	11.395	7.547
33.000	0.162	1.291	1.014	0.596	5.910	27.090	55.793	64.457	78.768	8.004	1.415	11.327	7.608
33.500	0.167	1.246	0.996	0.619	4.329	29.571	56.999	66.819	77.704	8.236	1.365	11.238	7.688
34.000	0.172	1.198	0.977	0.650	3.807	30.193	58.350	69.909	76.352	8.491	1.309	11.115	7.801
34.500	0.178	1.142	0.960	0.693	2.464	32.036	59.940	74.377	74.433	8.783	1.243	10.970	7.986
35.180	0.189	1.031	0.970	0.993	0.000	35.180	63.199	90.000	67.534	9.351	1.073	10.036	8.897

Table 11 Triple-Point Solutions, $M_1 = 4.0$

TRIPLE POINT SOLUTION M1 = 4.000 GAMMA = 1.400

DELTA2	P2/P01	M2	M3	M4	DELTA3	DELTA4	SIGMA2	SIGMA3	SIGMA4	P2/P1	P3/P2	P4/P1	(P4/P1)*
20.854	0.036	2.507	1.610	0.435	20.854	0.0	33.444	43.921	90.000	5.503	3.362	18.500	11.130
21.600	0.038	2.453	1.598	0.435	20.265	1.335	34.314	43.892	89.626	5.765	3.209	18.499	11.131
22.200	0.039	2.410	1.587	0.436	19.794	2.406	35.023	43.904	89.326	5.982	3.092	18.497	11.132
22.800	0.041	2.367	1.574	0.436	19.325	3.475	35.742	43.947	89.025	6.203	2.982	18.495	11.135
23.400	0.042	2.324	1.561	0.437	18.856	4.544	36.470	44.023	88.722	6.428	2.876	18.491	11.139
24.000	0.044	2.281	1.547	0.438	18.388	5.612	37.207	44.131	88.418	6.659	2.776	18.486	11.144
24.600	0.045	2.239	1.532	0.440	17.918	6.682	37.955	44.272	88.111	6.894	2.680	18.480	11.150
25.200	0.047	2.195	1.516	0.442	17.447	7.753	38.713	44.448	87.801	7.135	2.589	18.473	11.158
25.800	0.049	2.152	1.500	0.444	16.973	8.827	39.481	44.659	87.487	7.380	2.502	18.464	11.166
26.400	0.050	2.109	1.482	0.446	16.496	9.904	40.261	44.908	87.168	7.630	2.419	18.454	11.176
27.000	0.052	2.066	1.464	0.449	16.014	10.986	41.053	45.196	86.843	7.885	2.339	18.443	11.187
27.600	0.054	2.022	1.445	0.452	15.526	12.074	41.858	45.524	86.510	8.145	2.263	18.431	11.200
28.200	0.055	1.979	1.425	0.455	15.031	13.169	42.676	45.897	86.170	8.410	2.190	18.417	11.214
28.800	0.057	1.936	1.404	0.459	14.528	14.272	43.509	46.317	85.820	8.681	2.120	18.401	11.230
29.400	0.059	1.892	1.383	0.463	14.015	15.385	44.358	46.787	85.459	8.958	2.052	18.383	11.249
30.000	0.061	1.849	1.361	0.468	13.490	16.510	45.224	47.314	85.085	9.240	1.987	18.362	11.269
30.600	0.063	1.805	1.339	0.473	12.951	17.649	46.109	47.901	84.696	9.528	1.925	18.341	11.292
31.200	0.065	1.760	1.316	0.479	12.397	18.803	47.014	48.557	84.290	9.822	1.865	18.315	11.318
31.800	0.067	1.716	1.292	0.485	11.823	19.977	47.943	49.290	83.863	10.124	1.806	18.287	11.348
32.400	0.069	1.670	1.267	0.492	11.229	21.172	48.898	50.111	83.411	10.433	1.750	18.254	11.381
33.000	0.071	1.625	1.242	0.501	10.607	22.393	49.883	51.034	82.930	10.750	1.695	18.217	11.420
33.600	0.073	1.578	1.216	0.510	9.955	23.645	50.903	52.078	82.412	11.076	1.641	18.175	11.464
34.200	0.075	1.530	1.189	0.520	9.265	24.935	51.964	53.269	81.850	11.413	1.588	18.125	11.517
34.800	0.077	1.481	1.162	0.533	8.523	26.272	53.074	54.641	81.230	11.762	1.536	18.066	11.579
35.400	0.080	1.431	1.133	0.547	7.733	27.667	54.245	56.247	80.534	12.127	1.484	17.995	11.655
36.000	0.082	1.379	1.103	0.565	6.863	29.137	55.496	58.166	79.735	12.510	1.431	17.907	11.750
36.600	0.085	1.327	1.073	0.587	5.889	30.711	56.852	60.533	78.784	12.919	1.377	17.794	11.874
37.200	0.088	1.260	1.040	0.617	4.766	32.434	58.365	63.606	77.587	13.365	1.320	17.638	12.047
37.800	0.091	1.190	1.006	0.661	3.397	34.403	60.138	67.989	75.921	13.872	1.254	17.395	12.324
38.722	0.100	1.017	0.983	0.929	0.000	38.722	64.777	90.000	67.295	15.110	1.040	15.719	14.497

Table 12 Triple-Point Solutions, $M_1 = 5.0$

TRIPLE POINT SOLUTION M1 = 5.000 GAMMA = 1.400

DELTA2	P2/P01	M2	M3	M4	DELTA3	DELTA4	SIGMA2	SIGMA3	SIGMA4	P2/P1	P3/P2	P4/P1	(P4/P1)*
20.862	0.014	2.941	1.910	0.415	20.862	0.0	30.796	39.271	90.000	7.479	3.878	29.000	17.250
21.600	0.015	2.873	1.893	0.415	20.344	1.256	31.659	39.233	89.686	7.868	3.686	29.009	17.251
22.200	0.015	2.819	1.877	0.416	19.928	2.272	32.368	39.234	89.431	8.193	3.539	28.997	17.254
22.800	0.016	2.763	1.860	0.416	19.516	3.284	33.085	39.263	89.177	8.525	3.401	28.994	17.257
23.400	0.017	2.709	1.842	0.417	19.107	4.293	33.810	39.320	88.922	8.864	3.270	28.990	17.262
24.000	0.017	2.655	1.823	0.418	18.700	5.300	34.542	39.405	88.669	9.210	3.147	28.984	17.268
24.600	0.018	2.601	1.802	0.419	18.294	6.306	35.282	39.518	88.411	9.564	3.030	28.978	17.276
25.200	0.019	2.548	1.781	0.421	17.889	7.311	36.030	39.660	88.153	9.925	2.919	28.970	17.285
25.800	0.019	2.495	1.759	0.422	17.484	8.316	36.786	39.830	87.892	10.292	2.814	28.961	17.295
26.400	0.020	2.443	1.737	0.424	17.077	9.323	37.550	40.030	87.629	10.667	2.714	28.950	17.307
27.000	0.021	2.391	1.713	0.426	16.669	10.331	38.324	40.261	87.362	11.049	2.619	28.938	17.321
27.600	0.022	2.339	1.689	0.429	16.259	11.341	39.107	40.523	87.091	11.439	2.529	28.925	17.336
28.200	0.022	2.288	1.664	0.431	15.845	12.355	39.900	40.818	86.815	11.834	2.443	28.910	17.353
28.800	0.023	2.237	1.639	0.434	15.426	13.374	40.704	41.147	86.534	12.238	2.361	28.893	17.373
29.400	0.024	2.186	1.613	0.437	15.002	14.398	41.518	41.514	86.246	12.648	2.283	28.875	17.394
30.000	0.025	2.136	1.586	0.441	14.571	15.429	42.344	42.918	85.950	13.067	2.209	28.855	17.417
30.600	0.026	2.085	1.559	0.444	14.133	16.467	43.183	42.365	85.647	13.492	2.137	28.832	17.444
31.200	0.026	2.035	1.532	0.449	13.686	17.514	44.036	42.856	85.333	13.926	2.069	28.807	17.473
31.800	0.027	1.985	1.503	0.453	13.228	18.572	44.904	43.396	85.009	14.368	2.003	28.779	17.505
32.400	0.028	1.935	1.475	0.458	12.759	19.641	45.788	43.989	84.672	14.818	1.940	28.748	17.541
33.000	0.029	1.885	1.446	0.464	12.275	20.725	46.690	44.642	84.320	15.276	1.880	28.714	17.581
33.600	0.030	1.835	1.416	0.470	11.776	21.824	47.612	45.361	83.951	15.744	1.821	28.676	17.626
34.200	0.031	1.784	1.386	0.477	11.258	22.942	48.556	46.155	83.562	16.222	1.765	28.633	17.676
34.800	0.032	1.733	1.355	0.485	10.719	24.081	49.526	47.036	83.150	16.711	1.711	28.585	17.733
35.400	0.033	1.682	1.324	0.493	10.154	25.246	50.525	48.018	82.709	17.212	1.658	28.530	17.799
36.000	0.034	1.630	1.291	0.503	9.558	26.442	51.558	49.119	82.234	17.726	1.606	28.467	17.874
36.600	0.035	1.578	1.259	0.514	8.926	27.674	52.632	50.366	81.716	18.256	1.555	28.395	17.961
37.200	0.036	1.524	1.225	0.527	8.242	28.951	53.754	51.794	81.145	18.804	1.505	28.309	18.065
37.800	0.037	1.468	1.190	0.542	7.515	30.285	54.938	53.455	80.502	19.375	1.456	28.206	18.192
38.400	0.038	1.410	1.154	0.560	6.708	31.692	56.201	55.430	79.762	19.974	1.406	28.079	18.349
39.000	0.039	1.348	1.117	0.582	5.800	33.200	57.571	57.856	78.879	20.613	1.354	27.915	18.554
39.600	0.040	1.282	1.077	0.612	4.744	34.856	59.101	60.997	77.765	21.308	1.299	27.690	18.841
40.200	0.042	1.206	1.035	0.657	3.441	36.759	60.902	65.484	76.206	22.102	1.237	27.342	19.299
41.039	0.045	1.010	0.990	0.954	0.000	41.039	65.823	90.000	67.328	24.108	1.023	24.666	23.385

Table 13 Triple-Point Solutions, $M_1 = 10.0$

TRIPLE POINT SOLUTIONS M1=10.000 GAMMA = 1.400

DELTA2	P2/P01	M2	M3	M4	DELTA3	DELTA4	SIGMA2	SIGMA3	SIGMA4	P2/P1	P3/P2	P4/P1	(P4/P1)*
19.520	0.000	4.299	2.753	0.389	19.520	0.0	25.240	30.951	90.000	21.047	5.535	116.500	68.263
20.700	0.001	4.072	2.684	0.388	18.979	1.721	26.664	31.042	89.635	23.329	4.994	116.495	68.269
21.400	0.001	3.954	2.640	0.388	18.665	2.735	27.516	31.132	89.419	24.736	4.709	116.488	68.279
22.100	0.001	3.834	2.596	0.388	18.353	3.747	28.374	31.249	89.203	26.182	4.449	116.477	68.294
22.800	0.001	3.718	2.550	0.390	18.044	4.756	29.238	31.391	88.987	27.667	4.209	116.464	68.313
23.500	0.001	3.606	2.503	0.390	17.735	5.765	30.108	31.558	88.770	29.191	3.989	116.446	68.337
24.200	0.001	3.498	2.454	0.392	17.426	6.774	30.984	31.751	88.551	30.752	3.786	116.425	68.365
24.900	0.001	3.393	2.408	0.393	17.116	7.784	31.867	31.968	88.331	32.351	3.598	116.401	68.398
25.600	0.001	3.291	2.360	0.394	16.804	8.796	32.755	32.211	88.108	33.986	3.424	116.373	68.437
26.300	0.001	3.193	2.312	0.396	16.489	9.811	33.651	32.479	87.883	35.658	3.263	116.341	68.481
27.000	0.001	3.097	2.263	0.398	16.170	10.830	34.554	32.773	87.654	37.365	3.113	116.304	68.531
27.700	0.001	3.004	2.215	0.400	15.847	11.853	35.465	33.095	87.421	39.108	2.973	116.264	68.587
28.400	0.001	2.914	2.166	0.403	15.519	12.881	36.384	33.445	87.184	40.886	2.843	116.218	68.649
29.100	0.001	2.826	2.117	0.405	15.185	13.915	37.311	33.824	86.942	42.698	2.721	116.168	68.719
29.800	0.001	2.741	2.069	0.408	14.844	14.956	38.248	34.234	86.695	44.545	2.607	116.112	68.796
30.500	0.001	2.657	2.020	0.411	14.495	16.005	39.194	34.677	86.441	46.425	2.500	116.050	68.882
31.200	0.001	2.576	1.972	0.415	14.138	17.062	40.151	35.156	86.180	48.340	2.399	115.982	68.976
31.900	0.001	2.496	1.923	0.419	13.771	18.129	41.119	35.673	85.910	50.289	2.305	115.907	69.081
32.600	0.001	2.418	1.875	0.423	13.394	19.206	42.100	36.231	85.632	52.272	2.216	115.823	69.197
33.300	0.001	2.341	1.827	0.428	13.004	20.296	43.095	36.834	85.343	54.291	2.132	115.731	69.326
34.000	0.001	2.266	1.779	0.433	12.601	21.399	44.105	37.487	85.043	56.344	2.052	115.629	69.469
34.700	0.001	2.192	1.731	0.438	12.183	22.517	45.131	38.195	84.729	58.434	1.977	115.515	69.628
35.400	0.001	2.119	1.683	0.444	11.749	23.651	46.177	38.966	84.400	60.562	1.905	115.389	69.806
36.100	0.001	2.047	1.635	0.451	11.295	24.805	47.243	39.807	84.053	62.729	1.837	115.247	70.006
36.900	0.002	1.976	1.587	0.459	10.820	25.980	48.334	40.729	83.684	64.939	1.772	115.088	70.232
37.500	0.002	1.905	1.539	0.467	10.319	27.181	49.452	41.746	83.291	67.195	1.710	114.908	70.489
38.200	0.002	1.834	1.491	0.476	9.790	28.410	50.603	42.875	82.869	69.502	1.650	114.702	70.785
38.900	0.002	1.763	1.443	0.487	9.226	29.674	51.792	44.140	82.410	71.867	1.593	114.464	71.128
39.600	0.002	1.692	1.395	0.499	8.620	30.980	53.027	45.571	81.905	74.299	1.537	114.187	71.532
40.300	0.002	1.620	1.342	0.514	7.962	32.338	54.320	47.214	81.342	76.812	1.482	113.856	72.016
41.000	0.002	1.546	1.291	0.531	7.238	33.762	55.687	49.139	80.700	79.426	1.428	113.453	72.614
41.700	0.002	1.469	1.237	0.552	6.426	35.274	57.153	51.458	79.947	82.177	1.374	112.945	73.376
42.400	0.002	1.388	1.182	0.579	5.488	36.912	58.760	54.371	79.024	85.120	1.319	112.271	74.407
43.100	0.002	1.299	1.122	0.616	4.350	38.750	60.596	58.314	77.801	88.378	1.259	111.290	75.941
43.800	0.002	1.197	1.055	0.679	2.921	40.979	62.893	64.603	75.875	92.277	1.187	109.552	78.773
44.429	0.002	1.093	0.994	0.838	0.000	44.429	67.284	90.000	67.624	99.102	1.095	99.502	98.224

Table 14 Actual Results of Iteration from Approximate Method for Estimating Mach Stem Height, $M_1 = 1.92$; $P_{o1}/P_a = 3.67$

N_{st}	Y_o	x_e	H_2	H_{3a}	H_{4a}	$\int_o^{H_{3a}}(\ldots)\, dY_{3a}$	$\int_o^{H_{4a}}(\ldots)\, dY_{4a}$	$W(Y_o)$
	0.99900	0.00105	0.00076	0.00078	0.89010	0.00009	0.08237	0.04175
	0.00100	1.04689	0.75505	0.76110	0.00089	0.08990	0.00008	-0.01086
20	0.20700	0.83101	0.59936	0.60549	0.18445	0.7128	0.01707	0.00059
	0.19645	0.84207	0.60733	0.61346	0.17505	0.07223	0.01620	0.13695×10^{-5}
	0.19642	0.84210	0.60735	0.61348	0.17502	0.07223	0.01620	0.70090×10^{-11}
	0.99900	0.00105	0.00076	0.00078	0.89010	0.00009	0.08237	0.04175
	0.00100	1.04689	0.75505	0.76138	0.00089	0.08993	0.00008	-0.01110
40	0.21059	0.82725	0.59664	0.60300	0.18765	0.07098	0.01736	0.00060
	0.19984	0.83852	0.60477	0.61113	0.17807	0.07195	0.01648	0.13036×10^{-5}
	0.19982	0.83854	0.60479	0.61114	0.17805	0.07195	0.01648	0.57496×0^{-11}
	0.99900	0.00105	0.00076	0.00078	0.89010	0.00009	0.08237	0.04175
	0.00100	1.04689	0.75505	0.76155	0.00089	0.08995	0.00008	-0.01124
100	0.21271	0.82503	0.59504	0.60153	0.18954	0.07080	0.01754	0.00061
	0.20185	0.83641	0.60325	0.60974	0.17986	0.07178	0.01664	0.12579×10^{-5}
	0.20183	0.83643	0.60327	0.60976	0.17984	0.07179	0.01664	0.50140×10^{-11}

Experimental result $Y_o = 0.20$ by A. Ferri [43].

Table 15 Actual Results of Iteration from Approximate Method for Estimating Mach Stem Height, $M_1 = 1.92$, $P_{o1}/P_a = 3.54$

N_{st}	Y_o	x_e	H_2	H_{3a}	H_{4a}	$\int_o^{H_{3a}} (\ldots)\, dY_{3a}$	$\int_o^{H_{4a}} (\ldots)\, dY_{4a}$	$W(Y_o)$
	0.99900	0.00102	0.00075	0.00077	0.88080	0.00009	0.08112	0.04055
	0.00100	1.01372	0.74682	0.75214	0.00088	0.08874	0.00008	-0.01276
20	0.23984	0.77136	0.56827	0.57367	0.21152	0.06744	0.01947	0.00062
	0.22884	0.78253	0.57650	0.58190	0.20182	0.06842	0.01858	0.20009×10^{-5}
	0.22880	0.78256	0.57652	0.58192	0.20178	0.06842	0.01858	0.19920×10^{-10}
	0.99900	0.00102	0.00075	0.00077	0.88080	0.00009	0.08112	0.04054
	0.00100	1.01372	0.74682	0.75239	0.00088	0.08877	0.00008	-0.01297
40	0.24282	0.76834	0.56605	0.57163	0.21415	0.06719	0.01971	0.00063
	0.23164	0.77968	0.57440	0.57999	0.20429	0.06819	0.01881	0.19330×10^{-5}
	0.23161	0.77972	0.57443	0.58001	0.20426	0.06819	0.01880	0.17200×10^{-10}
	0.99900	0.00102	0.00075	0.00077	0.88080	0.00009	0.08112	0.04054
	0.00100	1.01372	0.74682	0.75254	0.00088	0.08879	0.00008	-0.01309
100	0.24458	0.76655	0.56473	0.57042	0.21570	0.06705	0.01986	0.00064
	0.23330	0.77800	0.57316	0.57886	0.20576	0.06806	0.01894	0.18865×10^{-5}
	0.23327	0.77803	0.57318	0.57888	0.20573	0.06806	0.01894	0.15590×10^{-10}

Experimental result $Y_o = 0.40$ by A. Ferri [43].

Table 16 The Effect of Changing the Number of Divisions on the Initial Characteristic Line on the Calculated Mach Disc Result

M_e	P_e/P_a	N	x_{sk}	r_{sk}	x_{sk} at $r_{sk\ max}$	$r_{sk\ max}$	x_f at $r_{f\ max}$	$r_{f_{max}}$	x_{md}	r_{md}
1.5	4.0	20	1.8127	1.1523	2.8754	1.2241	3.8859	1.8961	5.4369	0.7478
		30	1.7652	1.1460	2.9067	1.2208	3.8960	1.8962	5.4216	0.7421
		40	1.6729	1.1345	2.9082	1.2206	3.8958	1.8956	5.4190	0.7383
	3.0	30	1.9097	0.9515	2.1042	0.9542	3.4187	1.6359	4.8779	0.3406
		40	1.8641	0.9503	2.1173	0.9539	3.4185	1.6359	4.8847	0.3318
	6.0	25	1.6359	1.3657	3.7906	1.6762	4.6869	2.3416	6.1909	1.3478
		40	1.4843	1.3273	3.9601	1.6695	4.7881	2.3429	6.1838	1.3444
2.0	5.0	25	2.1300	1.3192	4.6932	1.5623	6.0133	2.2995	8.2792	0.9055
		40	1.9856	1.2930	4.5528	1.5573	5.9322	2.2998	8.3509	0.8604
2.5	7.0	25	2.2450	1.4686	6.9194	2.0842	8.4816	2.8652	12.4430	1.1712
		40	2.0939	1.4322	7.0029	2.0780	8.5051	2.8736	12.5155	1.1558
	5.0	30	2.4854	1.3249	5.6870	1.6130	7.6451	2.3909	10.8680	0.6680
		40	2.3525	1.3038	5.7954	1.6099	7.5325	2.3894	11.0602	0.5718
3.0	6.0	30	2.6189	1.3929	7.8606	1.8927	9.8373	2.7064	14.9062	0.5927
		40	2.6163	1.3911	7.7557	1.8941	9.8856	2.7045	14.9046	0.5707
	7.0	20	2.7939	1.5110	8.6360	2.1330	10.3414	2.9484	16.207	0.7031
		30	2.5454	1.4592	8.3920	2.1206	10.3385	2.9421	15.8100	0.8307

REFERENCES

1. Cohen, R. S. and R. J. Seeger (Edited by), "Boston Studies in the Philosophy of Science," Ernst Mach--Physicist and Philosopher, Vol. VI, D. Reidel Publishing Co., Holland, 1970.

2. Von Neumann, J., "Refraction, Intersection, and Reflection of Shock Waves," Conference Paper on Shock Waves and Supersonic Flow, March 19, 1945, Princeton, New Jersey.

3. Polachek, H. and R. J. Seeger, "Shock Wave Interactions" in Fundamentals of Gas Dynamics, Edited by H. W. Emmons, Vol. III, Princeton University Press, 1958.

4. Powell, R. W., "Infrared Tracking," ARS Journal, Vol. 29, No. 12, December 1959, p. 973.

5. Chow, W. L. and A. L. Addy, "Interaction between Primary and Secondary Streams of Supersonic Ejector Systems and their Performance Characteristics," AIAA Journal, Vol. 2, No. 4, April 1964, p. 686.

6. Chow, W. L., "Hypersonic Rarefied Flow Past the Sharp Leading Edge of a Flat Plate," AIAA Journal, Vol. 5, No. 9, September 1967, p. 1549.

7. Bleakney, W. and A. H. Taub, "Interaction of Shock Waves," Reviews of Modern Physics, Vol. 21, No. 4, October 1949, pp. 584-605.

8. Taub, A. H., "Singularities on Shock," American Mathematical Monthly, Part II, No. 7, 61, 1954, p. 11.

9. Fletcher, C. H., A. H. Taub, and W. Bleakney, "The Mach Reflection of Shock Waves at Nearly Glancing Incidence," Reviews of Modern Physics, Vol. 23, July 1951, p. 271.

10. Clutterham, D. R. and A. H. Taub, "Numerical Results on the Shock Configuration in Mach Reflection," Proc. of Sym in Appl. Math., Vol. VI, 1953, p. 45.

11. Sternberg, J., "Triple-Shock-Wave Intersections," The Physics of Fluids, Vol. 2, No. 2, March 1959, p. 179.

12. Pack, D. C., "On the Formation of Shock-Waves in Supersonic Gas Jets (Two-Dimensional Flow)," Quarterly J. of Mechanics and Appl. Mathematics, Vol. 1, 1948, p. 1.

13. Ladenburg, R., C. C. Van Voorhis, and J. Winckler, "Analysis of Supersonic Air Jets, Part II: Interferometric Studies of Faster Than Sound Phenomena," Physical Review, Vol. 76, No. 5, 1949, p. 662.

14. Adamson, T. C. Jr. and J. A. Nicholls, "On the Structure of Jets from Highly Underexpanded Nozzles into Still Air," J. of the Aerospace Sciences, January 1959, p. 16.

15. Ashratov, E. A., "Calculations of Axisymmetric Jet Leaving a Nozzle at Jet Pressure Lower than Pressure in Medium," Fluid Dynamics (Translated from Russian), Vol. 1, No. 1, 1966, p. 113.

16. Love, E. S. and C. E. Grigsby, "Some Studies of Axisymmetric Free Jets Exhausting from Sonic and Supersonic Nozzles into Still Air and into Supersonic Streams," NACA RM L54L31, May 1955.

17. Traugott, S. C., "An Approximate Solution of the Direct Supersonic Blunt-Body Problem for Arbitrary Axisymmetric Shapes," J. of Aero-Space Sciences, Vol. 27, 1960, p. 361.

18. Belotserkovskii, O. M. and P. I. Chushkin, "The Numerical Solution of Problems in Gas Dynamics," in Basic Developments in Fluid Dynamics, (Edited by M. Holt), Vol. 1, Academic Press, 1965.

19. South, J.C.,Jr.,and P.A. Newman,"Application of the Method of Integral Relations to Real-Gas Flows Past Pointed Bodies," AIAA Journal, Vol.3, No. 9, September 1965, p. 1645.

20. Liddle, S. G. and Archer, R. D., "Transonic Flow in Nozzles using the Method of Integral Relations," J. of Spacecraft and Rockets, Vol. 8, No. 7, 1971, p. 722.

21. Howlett, L. D., "A Study of Nozzle Flow Problems by the Method of Integral Relations," Ph.D. Thesis, Department of Mechanical and Industrial Engineering, University of Illinois at Urbana-Champaign, January 1972.

22. Ames Research Staff, "Equations, Tables, and Charts for Compressible Flow," NASA Report 1135, 1953.

23. Mölder, S., "Reflection of Curved Shock Waves," ICAS Paper No. 70-11, Seventh Congress of the International Council of the Aeronautical Sciences, September 1970.

24. Tollmien, W.,"Grenzschicht-Theorie",Handb. d. Exper.-Physik IV, Part I, 1931, pp. 241-287.

25. Xerikos, J. and W. A. Anderson, "A Critical Study of the Direct Blunt Body Integral Method," Douglas Report SM-42603, December 1962.

26. Busemann, A., "A Review of Analytical Methods for the Treatment of Flows with Detached Shocks," NACA TN 1858, April 1949.

27. Thomas, T. Y., "Calculation of Curvatures of Attached Shock Waves," J. of Math. and Phy., Vol. 27, 1949, p. 279.

28. Lin, C. C. and S. I. Rubinov, "On the Flow behind Curved Shocks," J. of Math. and Phys., Vol. 27, No. 2, 1948, p. 105.

29. Conte, S. D. Elementary Numerical Analysis, McGraw-Hill Book Co., 1965.

30. Howlett, L. D. and W. L. Chow, "A Study of Nozzle and Ejector Flow Problems by the Method of Integral Relations," ME-TR-395-2, UILU-ENG 72 4002, Engineering Experiment Station, Department of Mechanical and Industrial Engineering, University of Illinois at Urbana-Champaign, June 1972.

31. Shapiro, A. H., The Dynamics and Thermodynamics of Compressible Fluid Flow, Vol. I and Vol. II, The Ronald Press Co., 1953.

32. Brown, E. F., "Compressible Flow through Convergent Conical Nozzles with Emphasis on the Transonic Region," Ph.D. Thesis, Department of Mechanical and Industrial Engineering, University of Illinois at Urbana-Champaign, 1968.

33. Gear, C. W.,Numerical Initial Value Problems in Ordinary Differential Equations, Prentice-Hall Co., Englewood Cliffs, New Jersey, 1971.

34. Lapidus, L. and J. H. Seinfeld, Numerical Solution of Ordinary Differential Equations, Academic Press, 1971.

35. Snyder, W. T., "Nonisentropic Nozzle Flow," ARS Journal, Vol. 30, No. 3, March 1960, p. 270.

36. Bryant, R.A.A., "Adiabatic Nozzle Flows," ARS Journal, Vol. 31, No. 6, June 1961, p. 828.

37. Ferguson, T. B., "Irreversible Adiabatic Nozzle Flow," ARS Journal, Vol. 32, No. 9, September 1962, p. 1389.

38. Chow, W. L. and Chang, I-Shih, "Mach Reflection from Overexpanded Nozzle Flows," AIAA Journal, Vol. 10, No. 9, September 1972, p. 1261.

39. Wang, C. J. and J. B. Peterson, "Spreading of Supersonic Jets from Axially Symmetric Nozzles," Jet Propulsion, May 1958, p. 321.

40. Eastman, D. W. and L. P. Radtke, "Location of the Normal Shock Wave in the Exhaust Plume of a Jet," AIAA Journal, Vol. 1, No. 4, April 1963 p. 918.

41. Moe, M. M. and B. A. Troesch, "Jet Flows with Shocks," ARS Journal, Mai 1960, p. 487.

42. Wecken, F., "Grenzlagen gegabelter Verdichtungsstösze," (Intersection of Forked Shocks), Z. Angew. Math. Mech., Bd. 29, Nr. 5, May 1949, p. 147.

43. Ferri, A., Elements of Aerodynamics of Supersonic Flows, The MacMillan Co., New York, 1949.

APPENDIX A

FUNCTIONS FOR EQS. (24) and (25) OF TWO-DIMENSIONAL EXTERNAL FLOW

See Fig. 13a and References [17,25].

$$A = \frac{1}{2}\left[\left(1 - v_{so}^2\right)^{1/(\gamma-1)} v_{so} - \left(1 - \omega_\varepsilon^2\right)^{1/(\gamma-1)} v_{s\varepsilon}\right] \tag{A.1}$$

$$B = \frac{\varepsilon}{2}\left(1 - v_{so}^2\right)^{[(2-\gamma)/(\gamma-1)]}\left(1 - \frac{\gamma+1}{\gamma-1} v_{so}^2\right) \tag{A.2}$$

$$C = \frac{\varepsilon}{2} K_1 \left(1 - \omega_\varepsilon^2\right)^{1/(\gamma-1)}\left\{\left[1 - \frac{2}{\gamma-1}\frac{v_{s\varepsilon}^2}{\left(1 - \omega_\varepsilon^2\right)}\right] K_3 - \frac{2}{\gamma-1}\frac{v_{n\varepsilon}\, v_{s\varepsilon}}{\left(1 - \omega_\varepsilon^2\right)} K_2\right\} \tag{A.3}$$

$$D = -\left(1 - \omega_\varepsilon^2\right)^{1/(\gamma-1)} v_{n\varepsilon}\left(1 - \frac{\varepsilon}{2}\frac{d\theta}{ds}\right) \tag{A.4}$$

$$E = \frac{1}{2}\rho_\varepsilon\, v_{s\varepsilon}\, v_{n\varepsilon} \tag{A.5}$$

$$F = K_1 \frac{\varepsilon}{2}\rho_\varepsilon\left\{v_{s\varepsilon}\left[1 - \frac{2}{\gamma-1}\frac{v_{n\varepsilon}^2}{\left(1 - \omega_\varepsilon^2\right)}\right] K_2 + v_{n\varepsilon}\left[1 - \frac{2}{\gamma-1}\frac{v_{s\varepsilon}^2}{\left(1 - \omega_\varepsilon^2\right)}\right] K_3\right\} - \frac{\varepsilon}{2}\frac{\rho_\varepsilon\, v_{s\varepsilon}\, v_{n\varepsilon}}{(\gamma-1)\phi_\varepsilon} K_4 \tag{A.6}$$

$$G = -\left[\rho_\varepsilon\, v_{n\varepsilon}^2\left(1 - \frac{\varepsilon}{2}\frac{d\theta}{ds}\right) + \frac{\gamma-1}{2\gamma}\left(1 + \frac{\varepsilon}{2R}\right)(P_\varepsilon - P_o)\right] - \frac{\varepsilon}{2}\frac{d\theta}{ds}\rho_o\, v_{so}^2 \tag{A.7}$$

where

$$K_1 = \frac{4}{\gamma+1} M_\infty \sqrt{\frac{\gamma-1}{2 + (\gamma-1) M_\infty^2}} = \frac{4}{\gamma+1}\omega_\infty \tag{A.8}$$

$$K_2 = \left[\frac{1}{2}\left(1 - \frac{1}{M_\infty^2 \cos^2 \kappa}\right) - \sin^2 \kappa\right] \cos \theta - \cos \kappa \sin \kappa \sin \theta \quad (A.9)$$

$$K_3 = \left[\frac{1}{2}\left(1 - \frac{1}{M_\infty^2 \cos^2 \kappa}\right) - \sin^2 \kappa\right] \sin \theta + \cos \kappa \sin \kappa \cos \theta \quad (A.10)$$

$$K_4 = -\frac{J}{\gamma + 1}\left[\frac{2 + (\gamma - 1) M_\infty^2 \cos^2 \kappa}{(\gamma + 1) M_\infty^2 \cos^2 \kappa}\right]^{\gamma}\left[\frac{\gamma(\gamma - 1) \tan \kappa}{2 + (\gamma - 1) M_\infty^2 \cos^2 \kappa}\right] \cdot \left[M_\infty^2 \cos^2 \kappa - 1\right]^2 \quad (A.11)^*$$

$$\phi_\varepsilon = \left[\frac{2\gamma M_\infty^2 \cos^2 \kappa - (\gamma - 1)}{\gamma + 1}\right]\left[\frac{2 + (\gamma - 1) M_\infty^2 \cos^2 \kappa}{(\gamma + 1) M_\infty^2 \cos^2 \kappa}\right]^{\gamma} \quad (A.12)$$

$$v_{s\varepsilon} = \omega_\infty\left\{\left[1 - \frac{2}{\gamma + 1}\left(\cos^2 \kappa - \frac{1}{M_\infty^2}\right)\right]\cos \theta + \left[\frac{2}{\gamma + 1} \tan \kappa\left(\cos^2 \kappa - \frac{1}{M_\infty^2}\right)\right] \sin \theta\right\} \quad (A.13)$$

$$v_{n\varepsilon} = \omega_\infty\left\{\left[1 - \frac{2}{\gamma + 1}\left(\cos^2 \kappa - \frac{1}{M_\infty^2}\right)\right](-\sin \theta) + \left[\frac{2}{\gamma + 1} \tan \kappa\left(\cos^2 \kappa - \frac{1}{M_\infty^2}\right)\right] \cos \theta\right\} \quad (A.14)$$

$$\rho = (1 - \omega^2)^{1/(\gamma-1)} \phi^{-[1/(\gamma-1)]} \quad (A.15)$$

$$P = \rho^\gamma \phi \quad (A.16)$$

$$\omega = \sqrt{v_s^2 + v_n^2} \quad (A.17)$$

and for attached shock wave, $\kappa \to \kappa_o$ as $\varepsilon \to 0$; for detached shock wave $\kappa \to 0$ as $\varepsilon \to \varepsilon_o$.

---

*In Reference [17] for axisymmetric case, J = 2. However, in the present derivation, K_4 is twice as large, that is, J = 4 for both axisymmetric and two-dimensional cases, which agrees with the results of [25].

FUNCTIONS FOR EQS. (35) and (36) OF TWO-DIMENSIONAL INTERNAL FLOW

See Fig. 13b and Reference [21].

$$A_1 = \frac{\left(1 - q_w^2\right)^{1/(\gamma-1)}\left(1 - \frac{\gamma+1}{\gamma-1} q_w^2\right)}{\left(1 + Y_w'^2\right)^{1/2}\left(1 - q_w^2\right)} \tag{B.1}$$

$$B_1 = \frac{2\left(1 - q_c^2\right)^{1/(\gamma-1)}}{\left(1 - q_c^2\right)}\left(1 - \frac{\gamma+1}{\gamma-1} q_c^2\right) \tag{B.2}$$

$$C_1 = Y_w'\left\{\frac{\left(1 - q_w^2\right)^{1/(\gamma-1)} q_w}{\left(1 + Y_w'^2\right)^{3/2}} Y_w'' - \frac{1}{Y_w}\right.$$

$$\left.\left[\frac{\left(1 - q_w^2\right)^{1/(\gamma-1)} q_w}{\left(1 + Y_w'^2\right)^{1/2}} + 2\left(1 - q_c^2\right)^{1/(\gamma-1)} q_c\right]\right\} \tag{B.3}$$

$$D_1 = Y_w'\left[2q_w\left(1 - q_w^2\right)^{[(2-\gamma)/(\gamma-1)]}\left(1 - \frac{\gamma}{\gamma-1} q_w^2\right)\right.$$

$$\left. + q_c\left(1 - q_c^2\right)^{1/(\gamma-1)}\left(1 - Y_w'^2\right)^{1/2}\right] \tag{B.4}$$

$$E_1 = Y_w' q_w\left(1 - q_c^2\right)^{[(2-\gamma)/(\gamma-1)]}\left(1 - \frac{\gamma+1}{\gamma-1} q_c^2\right)\left(1 + Y_w'^2\right)^{1/2} \tag{B.5}$$

$$F_1 = -\frac{Y_w'^2}{Y_w}\left[q_w^2\left(1 - q_w^2\right)^{1/(\gamma-1)} + \left(1 + Y_w'^2\right)^{1/2} q_w q_c\left(1 - q_c^2\right)^{1/(\gamma-1)}\right]$$

$$+ \frac{4(1 + Y_w'^2)}{Y_w}\frac{(\gamma-1)}{2\gamma}\left[\left(1 - q_c^2\right)^{\gamma/(\gamma-1)} - \left(1 - q_w^2\right)^{\gamma/(\gamma-1)}\right]$$

$$- Y_w''\left[\frac{1 - Y_w'^2}{1 + Y_w'^2} q_w^2\left(1 - q_w^2\right)^{1/(\gamma-1)} + \frac{q_w q_c\left(1 - q_c^2\right)^{1/(\gamma-1)}}{\left(1 + Y_w'^2\right)^{1/2}}\right] \tag{B.7}$$

where prime (') indicates the derivative taken with respect to the horizontal coordinate x.

APPENDIX C

CHARACTERISTIC EQUATIONS FOR NUMERICAL CALCULATION OF A STEADY SUPERSONIC FLOW FIELD

The characteristic equations for a two-dimensional or an axisymmetric flow are written as [31]:

$$\left.\frac{dr}{dx}\right|_{I,II} = \tan(\theta \mp \alpha) \tag{C.1}$$

$$\left.\frac{1}{M^*}\frac{dM^*}{d\theta}\right|_{I,II} = \mp \tan\alpha + \frac{\nu \tan^2\alpha \tan\theta}{\tan\theta \mp \tan\alpha}\frac{dr}{rd\theta} - \left.\frac{\Omega \sin^2\alpha}{\gamma(\gamma-1)}\frac{d\left(\frac{S}{c_v}\right)}{d\theta}\right|_{I,II} \tag{C.2}$$

where $\nu = \begin{cases} 0 \text{ for two-dimensional flow} \\ 1 \text{ for axisymmetric flow} \end{cases}$

$\Omega = \begin{cases} 0 \text{ for irrotational flow} \\ 1 \text{ for rotational flow} \end{cases}$

Furthermore, for an adiabatic process of a perfect gas, the change in entropy can be related to the variation of stagnation pressure through the second law of thermodynamics.

$$\frac{S_2 - S_1}{c_v} = -(\gamma - 1)\ln\left[\frac{P_{o2}}{P_{o1}}\right] \tag{C.3}$$

C.1 PRANDTL-MEYER CORNER EXPANSION

At the corner point where the expansion from state 1 to state 2 is two-dimensional and isentropic, that is, $\nu = 0$, $\Omega = 0$, the direct integration of Eq. (C.2) will give

$$\theta_2 - \theta_1\Big|_{I,II} = \mp [\omega(M_2^*) - \omega(M_1^*)] \tag{C.4}$$

where

$$\omega(M^*) = \sqrt{\frac{\gamma+1}{\gamma-1}}\ \tan^{-1}\sqrt{\frac{M^{*2}-1}{\frac{\gamma+1}{\gamma-1} - M^{*2}}} - \tan^{-1}\sqrt{\frac{M^{*2}-1}{1 - \frac{\gamma-1}{\gamma+1}M^{*2}}} \tag{C.5}$$

is the Prandtl-Meyer function.

Equation (C.4) is used to establish the flow properties of the expansion fan at the nozzle exit corner or at the location where shock intersects with the free jet boundary.

C.2 FIELD POINT PROCEDURE

As shown in Fig. C.1, points 1 and 3 are joined by a characteristic line of family I and points 2 and 3 are joined by a characteristic line of family II. Points 1 and 3 are known, and point 3 is to be determined. Equations (C.1) and (C.2), when written in finite difference forms, give

$$\frac{r_3 - r_1}{x_3 - x_1} = \tan(\bar{\theta}_{13} - \bar{\alpha}_{13}) \tag{C.6}$$

$$\frac{r_3 - r_2}{x_3 - x_2} = \tan(\bar{\theta}_{23} + \bar{\alpha}_{23}) \tag{C.7}$$

$$\frac{1}{\bar{M}_{13}^*}\frac{M_3^* - M_1^*}{\theta_3 - \theta_1} = -\tan\bar{\alpha}_{13} + \frac{\nu \tan^2\bar{\alpha}_{13}\tan\bar{\theta}_{13}}{\tan\bar{\theta}_{13} + \tan\bar{\alpha}_{13}}\frac{r_3 - r_1}{\bar{r}_{13}(\theta_3 - \theta_1)}$$

$$+ \frac{\Omega \sin^2\bar{\alpha}_{13}}{\gamma(\theta_3 - \theta_1)} \ln\left[\frac{P_{o3}}{P_{o1}}\right] \tag{C.8}$$

$$\frac{1}{\bar{M}^*_{23}} \frac{M^*_3 - M^*_2}{\theta_3 - \theta_2} = \tan \bar{\alpha}_{23} + \frac{\nu \tan^2 \bar{\alpha}_{23} \tan \bar{\theta}_{23}}{\tan \bar{\theta}_{23} + \tan \alpha_{23}} \frac{r_3 - r_2}{\bar{r}_{23} (\theta_3 - \theta_2)}$$

$$+ \frac{\Omega \sin^2 \bar{\alpha}_{23}}{\gamma(\theta_3 - \theta_2)} \ln \left[\frac{P_{o3}}{P_{o2}}\right] \qquad (C.9)$$

where Eq. (C.3) has been applied. The bar superscript indicates that an average value is to be taken.

In the small characteristic grid shown in Fig. C.1, if the streamline passing through point 3 intersects line $\overline{12}$ at point s, the coordinates of point s can be found from the geometric relation of the intersection of two straight lines, $\overline{12}$ and $\overline{s3}$. Hence,

$$x_s = \frac{r_2 - r_3 + x_3 \tan \theta_s - x_2 \tan \beta}{\tan \bar{\theta}_s - \tan \beta} \qquad (C.10)$$

$$r_s = r_2 - (x_2 - x_s) \tan \beta \qquad (C.11)$$

The flow angle and stagnation pressure at point s can, then, be approximated by using linear interpolation.

$$\theta_s = \theta_2 + (\theta_1 - \theta_2) \frac{r_s - r_2}{r_1 - r_2} \qquad (C.12)$$

$$P_{os} = P_{o3} = P_{o2} + (P_{o1} - P_{o2}) \frac{r_s - r_2}{r_1 - r_2} \qquad (C.13)$$

where $P_{os} = P_{o3}$, because point 3 and point s are on the same streamline and have the same entropy.

The iterative solution of the simultaneous equations, Eqs. (C.6), (C.7), (C.8), and (C.9), with the help of Eqs. (C.10), (C.11), (C.12), and (C.13), will furnish the unknown flow variables at point 3.

To begin with an iterative solution, the property at point 1 is

usually used as the average value between points 1 and 3, and that at point 2 is used between points 2 and 3. However, Eqs. (C.8) or (C.9) will blow up when points 1 or 2 are on the axis of symmetry. This difficulty can be avoided through the following modification: Referring to Fig. C.2, when point 2 is on the axis of symmetry, and introducing

$$\lim_{\substack{r_2 \to 0 \\ \theta_2 \to 0}} \frac{\tan \bar{\alpha}_{23} \tan \bar{\theta}_{23}}{\tan \bar{\theta}_{23} + \tan \bar{\alpha}_{23}} \frac{1}{r_{23}} = \lim_{\substack{r_2 \to 0 \\ \theta_2 \to 0}} \frac{\tan \bar{\theta}_{23}}{\left(\frac{\tan \bar{\theta}_{23}}{\tan \bar{\alpha}_{23}} + 1 \right) r_{23}}$$

$$\simeq \frac{\theta_{23}}{r_{23}} \equiv \frac{\theta_3}{r_3} \qquad \text{(C.14)}$$

because $\lim_{\substack{r_2 \to 0 \\ \theta_2 \to 0}} \tan \bar{\theta}_{23} \simeq \bar{\theta}_{23}$

Equation (C.9) becomes

$$\frac{M_3^* - M_2^*}{\bar{M}_{23}^*} = \theta_3 (1 + \nu) \tan \bar{\alpha}_{23} + \Omega \frac{\sin^2 \bar{\alpha}_{23}}{\gamma} \ln \left(\frac{P_{o3}}{P_{02}} \right) \qquad \text{(C.15)}$$

which is used to replace Eq. (C.9) for the special case when point 2 is on the axis of symmetry.

C.3 CONSTANT PRESSURE JET BOUNDARY POINT PROCEDURE

As shown in Fig. C.3, points 1 and 3 are on the same free jet boundary without intersecting with shock discontinuity, and points 2 and 3 are joined by a characteristic line of family II. Points 1 and 2 are known, and point 3 is to be calculated.

The slope of the jet boundary between points 1 and 3 is given by

$$\frac{r_3 - r_1}{x_3 - x_1} = \tan \bar{\theta}_{13} \qquad \text{(C.16)}$$

On the constant pressure jet boundary

$$M_3^* = M_1^* \tag{C.17}$$

and, since free jet boundary is also a streamline,

$$P_{o3} = P_{o1} \tag{C.18}$$

Therefore, Eqs. (C.7), (C.9), and (C.15), plus conditions (Eqs. (C.17) and (C.18)) can be solved for x_3, r_3, and θ_3.

C.4 AXIS POINT PROCEDURE

If point 3 is at the intersection of a characteristic line and the axis of symmetry as shown in Fig. C.3 and points 1 and 3 are joined by characteristic curve of family I. Points 1 and 2 are known, and point 3 is to be determined.

Since points 2 and 3 are on the same axis streamline,

$$P_{o3} = P_{o2} \tag{C.19}$$

Also, on the axis of symmetry

$$\theta_3 = 0, \quad r_3 = 0 \tag{C.20}$$

Therefore, Eqs. (C.6) and (C.8) can be used to solve for two unknowns, M_3^* and x_3.

C.5 DOWNSTREAM POINT OF A SHOCK WAVE

Downstream of a shock wave, the points 1 and 2 are known; point 3 just behind the shock wave is to be determined. Referring to Fig. C.5, points 2 and 3 are joined by characteristic line of family II. In front of the shock wave, the flow is nonuniform and the flow properties are known.

The slope of the shock wave between points 1 and 3 is given by

$$\frac{r_3 - r_1}{x_3 - x_1} = \tan \bar{\xi}_{13} \tag{C.21}$$

where

$$\bar{\xi}_{13} = \frac{(|\sigma_1| + \theta_{1\infty}) + (|\sigma_3| + \theta_{3\infty})}{2} \tag{C.22}$$

Deflection angle δ_3 and stagnation pressure P_{o3} are readily available from oblique shock wave equations whenever the shock wave angle σ_3 is assumed known during the iteration process (Note: $\theta_3 = |\delta_3| + \theta_{3\infty}$).

Equations (C.21), (C.7), and (C.9), together with the oblique shock wave relations, are sufficient to determine the unknowns, x_3, r_3, M_3^*, θ_3, and P_{o3} at point 3.

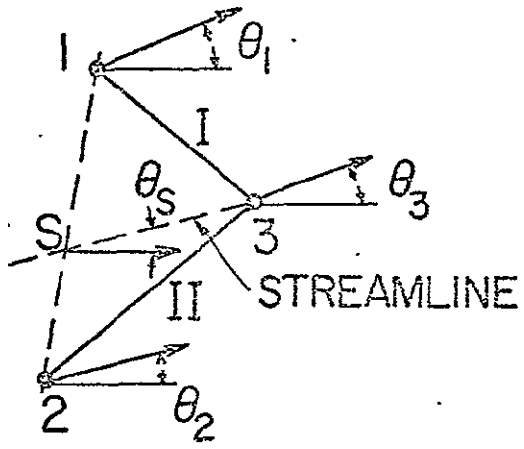

Figure C.1 Field Point

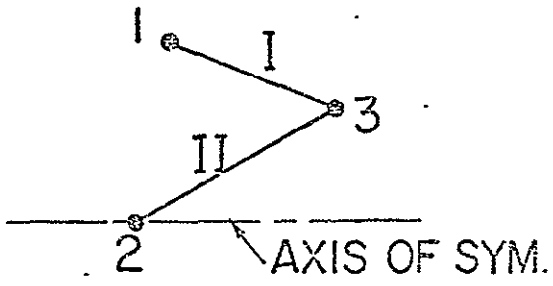

Figure C.2 Field Point with Point 2 on Axis of Sym.

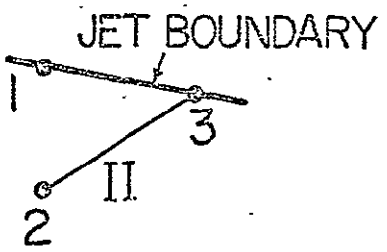

Figure C.3 Jet Boundary Point

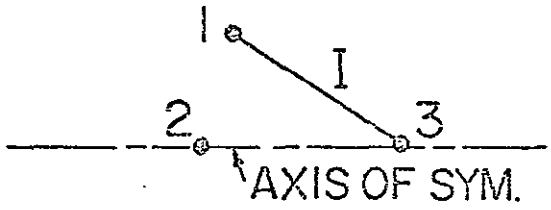

Figure C.4 Axis Point

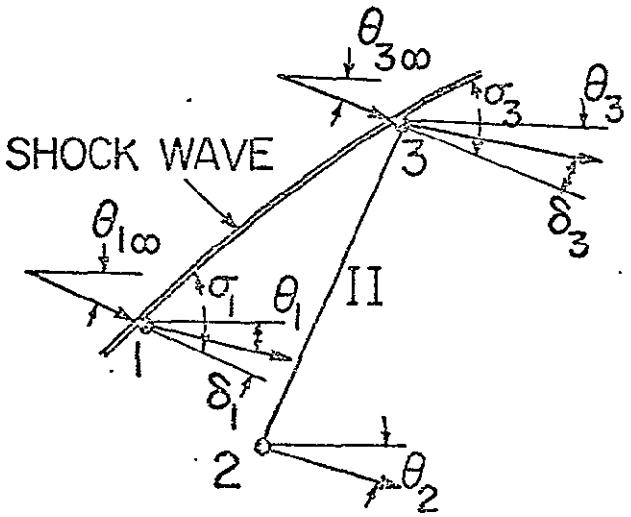

Figure C.5 Downstream Point of a Shock Wave

VITA

I-Shih Chang was born on [redacted], in [redacted] The Republic of China. He received his primary education at Pan-Chiao Elementary School and his secondary education at Chien-Kuo Middle School in Taipei. He entered Taiwan Provincial Taipei Institute of Technology in 1960 and graduated in 1965. He ranked first in mechanical engineering of the National High Grade and Engineer Examination of The Republic of China and was awarded the Professional Mechanical Engineer Licence by the government of The Republic of China in 1965. After serving a one-year tour of duty as a reserve officer in the Chinese Navy, he worked as a teaching assistant at Taipei Institute of Technology from July 1966 to January 1968. He entered the University of Kansas at Lawrence, Kansas, in February 1968, held a research assistantship in the summer of 1968, and was awarded the degree of Master of Science in Mechanical Engineering by the University of Kansas in 1969. He enrolled at the University of Illinois at Urbana-Champaign in September 1969 and held a research assistantship sponsored by the National Aeronautics and Space Administration, Lewis Laboratory in Cleveland, Ohio, for four years.

With Professor W. L. Chow, he co-authored a paper entitled "Mach Reflection from Overexpanded Nozzle Flows" which appeared in AIAA Journal, Vol. 10, No. 9, September 1972.

He is a member of the all-university honor society, Phi Kappa Phi.